Geological Survey of Israel
Ministry of Energy

Evaluating climate effects over long-term salts accumulation in hyperarid soils using stochastic modeling

Lior Siman Tov

Report GSI/04/2021

Jerusalem, Febuary 2021

32 Yeshayahu Leibowitz St. Jerusalem 9692100, Israel

Cover picture:
Late Pleistocene (~70 Ka) reg soil profile at Shehoret stream alluvial fan, southern Negev. A clear and well-developed gypsic horizon (By) is observed at depth of 10 - 30 cm. The control of soil properties, climatic factors, and time on gypsum concentration and depth of accumulation were studied in this research. Mature reg profiles like this one can be instrumental for inferring the paleoclimate of the region. Modeling of gypsum concentration and accumulation depth suggests that during the late Pleistocene (70-10 ka), mean annual rainfall and sulfate concentration in rainfall in the southern Negev were higher than today. Photo by Uri Shaanan.

Back cover:
Early Holocene (~13 Ka) surface at Ze'elim stream alluvial fan, Judean Desert, near the southwestern shore of the Dead Sea. This relatively young surface demonstrates poorly developed desert pavement and contain low amount of pedogenic gypsum in the reg soil profile. These profiles were developed under climate conditions that are similar to current conditions and were used in this study to calibrate the gypsum accumulation model. Photo taken by Lior Siman-Tov.

Cover design: Tirza Tzuberi

Geological Survey of Israel
Ministry of Energy

Evaluating climate effects over long-term salts accumulation in hyperarid soils using stochastic modeling

Lior Siman-Tov

This thesis was submitted in partial fulfillment of the requirements for the degree of "Master of Science" to the senate of the Hebrew University of Jerusalem.

The study was carried out under the supervision of:

Dr. Onn Crouvi, Geological Survey of Israel.

Prof. Efrat Morin, The Hebrew University of Jerusalem.

Report GSI/04/2021 Jerusalem, February 2021

Abstract

Hyperarid (< 80 mm yr^{-1}) soils in hot deserts are characterized by accumulations of soluble salts (gypsum and halite) in diagnostic horizons as a result of limited water availability. In most desert terrains, the source for pedogenic gypsum and halite is atmospheric dust and rainwater. The interplay between climatic properties such as frequency and intensity of rain events, rainfall composition, dust flux, and evaporation rates, govern the depth and concentration of these salts, but the effects of these properties on the accumulation of pedogenic salts were never quantified. Up to date, only empirical correlations between annual rainfall and pedogenic salt horizons are available. Better understanding of these relationships can improve our estimation of regional paleoenvironmental and paleoclimate conditions.

The goals of this study are to: 1) simulate long-term gypsum accumulation in soils, 2) quantify the effect of climatic factors, dust flux, hydraulic soil parameters and time, over pedogenic gypsum accumulation and 3) estimate the most likely climatic scenarios that led to the formation of the diagnostic gypsic horizon developed in late Pleistocene (22.9 – 62.5 Ka) abandoned alluvial fan surfaces in the hyperarid Negev desert, southern Israel. To achieve these goals, I constructed a compartment model that simulates gypsum accumulation in soil and tests its sensitivity to various changes in the long-term climate properties. The model predicts gypsum content and depth of accumulation in the soil profile over thousands of years and more. The input parameters are stochastically simulated rainstorms, potential evapotranspiration (PET), dust flux, and sulfate concentration in rainwater, at daily time steps. The model was calibrated using data of Holocene (10.3 – 13.5 Ka) soil profiles developed on stable alluvial fans in the hyperarid Negev, with the assumption that the climate during the Holocene was not much different than today in terms of rainfall properties and PET (i.e., mean annual rainfall < 80 mm and annual PET of 2000 – 2300 mm yr^{-1}). Sensitivity analysis indicates that gypsum accumulation is highly sensitive to mean annual rainfall and sulfate concentration in rainwater, and less sensitive to annual dust flux and PET. Synthetic gypsum profiles were calculated using different climate scenarios and compared to late Pleistocene soils. Results suggest that (a) gypsum accumulation in late Pleistocene soils cannot occur simply by extending current climate conditions for a much longer duration. (b) The plausible climate scenarios for the late Pleistocene must include additional rain input (mean annual rainfall 1.5 – 2.0 times than today) and increased sulfate concentration in rainwater (2.0 – 2.5 times than today) to successfully reconstruct the observed accumulated gypsum in mature (22.9 – 62.5 Ka) soil profiles.

Acknowledgements

I would like to acknowledge and express my gratitude for the funding that was provided by the Geological Survey of Israel and the Institute of Earth Sciences for my education at the Hebrew University of Jerusalem; I am most appreciative of my advisors Dr. Onn Crouvi and Prof. Efrat Morin who have provided me with this opportunity to further my education, have offered encouragement and advice throughout this period, with tremendous patience and extraordinary attention to details. Special thanks to Dr. Francesco Marra, Dr. Ravid Rosenzweig, and Dr. Itay J. Reznik for contributing my research from their fields of expertise. To Dr. Rivka Amit for her contribution to my understanding of the fascinating world of the Israeli soils. And to Prof. Yehouda Enzel, the master of words, for simplifying my chaotic thoughts.

I am additionally thankful to my friends and colleagues from the institute of earth sciences in the Hebrew university who supported me along the way and more importantly, lighten my daily life during my studies. To my committee members, Prof. Alon Angert and Dr. Nadav Lansky.

I also would like to thank my family, friends, and colleagues for the constant support and encouragement over the last two years. Lastly, I would like to thank my wife, Hila who supported and encouraged me in moments of hardship.

Table of content

List of figures

List of tables

1. Introduction

Hyperarid (<80 mm yr^{-1}) soils in hot deserts are characterized by accumulations of soluble salts horizons such as halite and gypsum, as a result of limited water availability (Dan et al., 1982; Eswaran and Zi-Tong, 1991; Nettleton et al., 1982). In most desert terrains, pedogenic salts are derived from atmospheric dust and soluble ions in rainwater (Gerson et al., 1985). Therefore, climate properties such as rainfall, evaporation and dust flux govern the depth and concentration of pedogenic salts in soil horizons. However, only few studies quantified the link between climate properties and gypsum accumulation, focusing merely on mean annual rainfall (Dan and Yaalon, 1982; Marion, 1994; Marion et al., 1985; Retallack, 2005; Retallack and Huang, 2010). Other factors such as potential evapotranspiration (PET), dust flux, rainwater composition, temporal change in soil hydraulic properties and annual rainfall dispersion, have not been tested for their effect on gypsum distribution in the soil column. Here, I offer to model long-term (10 – 63 Ka) gypsum accumulation in desert soils while considering overlooked factors to better understand gypsum accumulation rates with time and the climatic thresholds for its accumulation. Quantifying the relations between climate and salts accumulation, can improve determining regional mean paleoenvironmental conditions and paleoclimate.

1.1 *Pedogenic gypsum in reg soils and their paleoclimate significance*

Gypsum ($CaSO4{\cdot}H2O$) is common in aridisols, saline and alkaline soils, and in irrigated soils; gypsum-rich soils are globally distributed mainly in semiarid to hyperarid regions (e.g., the southern Negev of Israel, Middle East, China, Africa, Australia, and the Southwestern United States) (Eswaran and Zi-Tong, 1991; Nettleton et al., 1982). Soils with gypsic horizon are estimated to cover 2.01 million km^2 worldwide (Eswaran and Zi-Tong, 1991). In the Negev desert, pedogenic gypsum accumulates in reg soils that develop on stable alluvial fans composed of coarse gravelly alluvium (Amit and Gerson, 1986; Amit and Yaalon, 1996; Dan and Yaalon, 1982). These soils are permeable and well-drained (Gerson et al., 1985; Gerson and Amit, 1987). The rough gravely surface of the alluvial fan traps airborne dust that accumulates under the evolving desert pavement. Pedogenic gypsum accumulates upon infiltration and evaporation of rainwater containing Ca^{2+} and SO_4^{2-} ions. These ions originate from both gypsum dust particles and rainwater. With time, reg soils displays an increase in gypsum concentration, and a diagnostic By horizon develops (Figure 1). Concurrently to gypsum accumulation in the soil profile, the surficial gravels undergo physical weathering and a desert pavement gradually forms; The pavement induces plugging, high runoff yield, and a decrease of dust trapping efficiency (Greenbaum, 1986). Dust accumulates within the upper part of the soil (Vesicular A horizon and gravel-free B horizon), increasing the fraction of fine materials (< 2 mm) with time (Amit et al., 1993; Amit and Gerson, 1986). Diagnostic horizons, pavement cover, texture and gravel composition are indicators for soil maturity and can be instrumental for soil age estimation; absolute dating of these soils chronosequences using Optically Stimulated Luminescence (OSL), validated these time dependence processes and put them in an absolute timeframe (Porat et al., 2010).

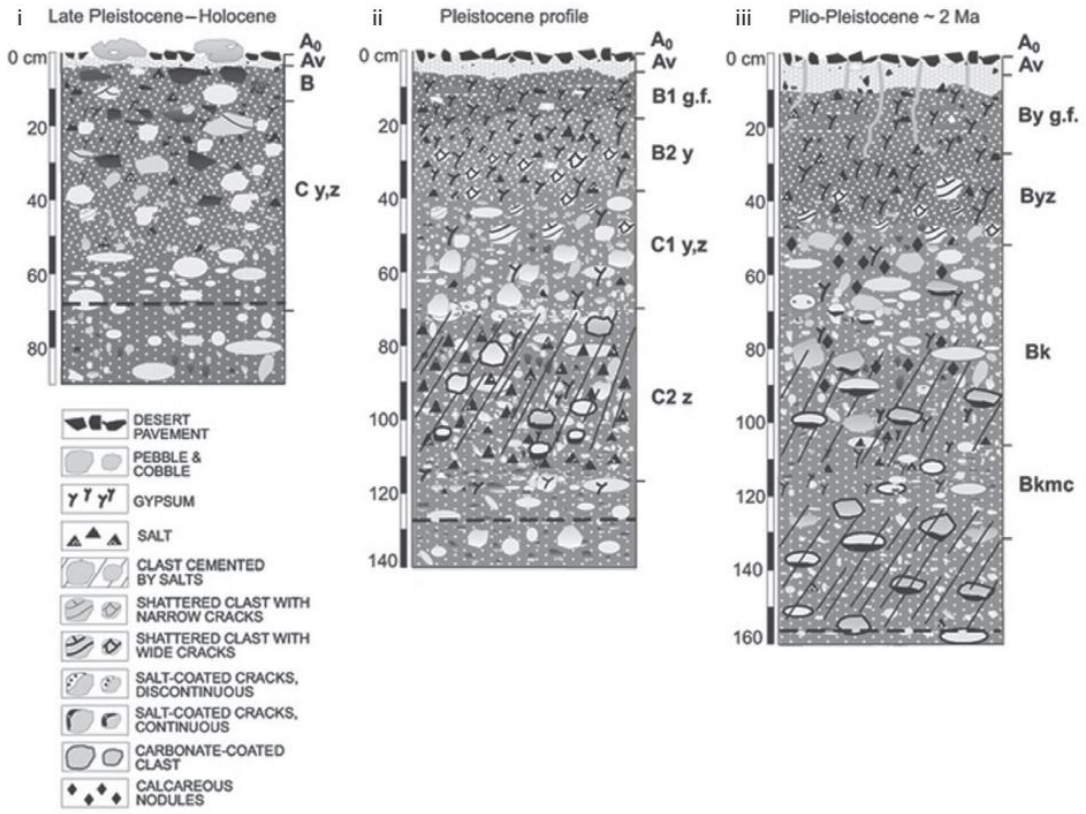

Figure 1: Reg soil chronosequence in southern Israel. Gypsic By horizon gradually forms as gypsum concentration increases with time. Gravel free Av horizon thickens as airborne dust infiltrates the surface. Gravel shattering and accumulation of fine materials increases the soil profile thickness. Concurrently, desert pavement developes on the surface. (Taken from Amit et al.,2017).

Gypsum is well preserved in reg soils in comparison to salts of higher solubility such as halite and potassium chloride (the solubility of gypsum is 2.0–2.5 g/l at 25 °C, much less than the one for halite 360 gr/l at 25°C and potassium chloride 339.7 gr/l at 25°C). The depth of gypsic (By) horizon was found to be correlated with mean annual rainfall; this correlation is used to estimate paleo-precipitation using paleosols (Retallack and Huang, 2010). In other cases, spatial occurrence of pedogenic gypsum was used as a proxy for aridification (Amit, Simhai, et al., 2011). Currently, gypsic-salic reg soils in the Negev form under hyperarid climate (< 80 mm yr^{-1}), whereas under more humid conditions (> 80 mm yr^{-1}), the presence of vegetation encourages the formation of calcic horizons. Amit et al. (2006) showed that gypsic-salic reg soils are found on > 200 Ka surfaces in the southern Negev that lack any sign of calcic horizons, and suggested that since the late Pliocene to early Pleistocene, hyperaridity prevailed over southern Negev. Later study found calcic horizons buried under gypsic-salic reg soils of the Paran plains located in the southern Negev; The calcic paleosol was dated to 2-1 Ma, when the climate favored pedogenic carbonate accumulation; only since 1 Ma the climate changed to its hyperarid state (Amit, Simhai, et al., 2011).

Although the current hyperarid Negev remained so since the late Pliocene, it is still possible that mean annual rainfall was higher than today (Enzel et al., 2008). Studies conducted in other regions of the Negev, suggest a wetter climate in the area during the late Pleistocene. Speleothems formed in the central Negev (current mean annual rainfall of 30 – 150 mm) point toward humid intervals at 142-109 Ka with estimated annual rainfall of 300-350 mm (Vaks et al., 2010); Evidence of ancient waterbodies existed in the southern Negev and southern Jordan during the late Pleistocene (70-12 Ka), sustained by wetter conditions (Ginat

et al., 2018). Studies of the lake Lisan water level also suggest an increased rainfall in the Dead Sea basin, which partly includes the hyperarid Negev Sea (Bar-Matthews et al., 1997, 2003; Sorin et al., 2010; Stein, 2001; Vaks et al., 2003, 2006). These studies imply towards a relatively humid late Pleistocene climate in the Negev, albeit a regional paleorainfall estimation for the southern and east Negev is not available. A more accurate scenario for this region can be derived by studying the accumulation depth and concentration in the soil profile, instead of relaying merely on spatial occurrence.

1.2 *Dust and rainfall as sources of pedogenic gypsum*

Pedogenic gypsum in reg soils is an intrusive material and have an atmospheric origin, either as solid matter or dissolve in rainfall. Dust transports sulfates, chlorides, and carbonates which are later accumulate on the surface and precipitate in the presence of rainfall. During most of the late Pleistocene, dust was transported to the Negev from two main sources: (1) distal sources in the North African and Arabian deserts (Ganor, 1975; Ganor and Foner, 1996; Yaalon and Ganor, 1979), and, (2) proximal sources such as Wadi El-Arish in northern Sinai, the Mediterranean shelf exposed during periods of low sea level (Gerson and Amit, 1987), and sand dunes that advanced into the Sinai and Negev deserts during the late Pleistocene (Crouvi et al., 2008). According to samples collected during dust storms in the Negev area, the overall mineralogical composition of non-clay dust particles is 35-45% quartz, 30-40% calcite, 10-20% dolomite and 5-10% feldspar where gypsum content is low (< 1%) (Ganor, 1975).

Crouvi et al. (2017) and Amit et al (2011), showed that proximal dust started to accumulate in the Negev at ~200 Ka; with highest dust mass accumulation rates during the last glacial (marine oxygen isotope stages (MIS) 2–4; 70–10 Ka). An abrupt decrease in these rates occurred towards the Holocene. The high dust accumulation rates during the last glacial period (LGP) coincides with the high gypsic concentration found in late Pleistocene (62.5 – 27 Ka) reg soils. However, this correlation has not been thoroughly investigated, and the higher concentration of gypsum in late Pleistocene soils compared to young, Holocene (10.3 - 13.5 Ka) soils is attributed mainly to accumulation with time (i.e., and not to change in climate, dust, rainwater composition, etc.) (Amit et al., 1993; Amit and Gerson, 1986).

An additional source for soluble ions is rainwater. Rain chemical composition is determined by marine sources such as sea spray, and nonmarine sources such as dust and anthropogenic activity (Singer, 1994). Rainwater composition in areas far away from the sea (e.g. southern Israel), are characterized by a high concentration of major ions (Na, K, Ca, Mg, Cl, SO_4), mainly due to dilution and high dust availability (Herut et al., 1995, 2000). Sulfate in rainwater can have various origins such as sea salt (NaCl and Na_2SO_4), terrestrial dust ($CaSO_4$) and SO_2 oxidation in the form of H_2SO_4 (Legrand et al.,1988). Sulfate in rainwater should be therefore taken into account when quantifying the input of soluble ions.

1.3 *Long-term modeling of salts accumulation in soils*

Modelling salts accumulation in soils has been previously attempted to accurately assess the role of selected factors over the process. Two modeling approaches are often used to model solute transfer in soils: (1) A physical approach that evaluates salts concentration as a function of time by solving water flow equations (Bresler, 1967; Bresler and Hanks RJ, 1969; Suarez and Šimůnek, 1997; Warrick et al., 1971; Zeng et al., 2014). (2) A conceptual approach that represents the soil profile as a 1D vertical sequence of compartments of pre-defined dimensions; each compartment is characterized by soil properties, chemical composition, and water content (Arkley, 1963; Marion, 1994; Marion et al., 1985; Mcfadden et al., 1991; McFadden and Tinsley, 1985).

Physically-based models are commonly used to analyze water movement and solutes transport in soils; these models are designed and applied for solving short term transport, spanning from seconds to days. In addition, numerous soil parameters such as hydraulic conductivity, diffusion constant, soil porosity, air entry value, etc., are required for solving the diffusion and advection functions. To model long-term (thousands years and more) climate influence over water and solute transport in soil, a conceptual, 1D compartment model is more appropriate. Since the age of mature reg soils is more than 60 Ka, the model must be able to calculate numerous iterations in a reasonable time, with an intra annual resolution, and a daily time scale. Furthermore, estimation of constantly changing soil parameters is highly inaccurate for long time durations. Considering these constraints, conceptual models that require simple calculations and fewer soil parameters are more preferable in approaching the long-term modeling of salts accumulation.

Arkley (1963) was one of the first to introduce a process–based conceptual model that calculated water movement in soil. McFadden and Tinsley (1985) used this approach to simulate Ca translocation and $CaCO_3$ precipitation in soils. Marion et al. (1985) implemented a compartment model (CALDEP) which calculates calcite accumulation following daily rainfall and evaporation. While its predecessors used deterministic rainfall models that repeated the same pattern each year, CALDEP incorporates a stochastic weather generator (WG) to better represent extreme rainfall events. The model was later improved to the CALGYP model, which also included gypsum accumulation (Marion, 1994).

The above-mentioned models took a simple approach to redistribute water within the soil compartments based on hydrological properties. According to this approach, rainwater infiltrates the soil and reaches a final wetting depth (WD) determined by the soil water holding capacity (WHC). WHC is calculated as the difference between the WHC parameters of residual water content and field capacity. Residual water content is the lower limit of soil water content and signifies the minimal amount of water available for evaporation and/or root uptake. It can be calculated using a water retention curve measured for a soil sample in the lab, or by using the soil texture (Schaap et al., 2001). Field capacity is the water content at a semi steady state, where soil suction head equals to the gravimetric head leading to decreased downward water flux. Field capacity is a problematic term and general definition remained undetermined, however it can be theoretically derived from water retention curve (WRC) (Lehmann et al., 2008). As WD is determined by the WHC, sampling soil water profile after a known amount of water infiltrated the soil can also be used to determine field capacity at a site, this approach was taken by Marion (1994; 1985).

Despite the success of these models in simulating pedogenic salt accumulation, there is an uncertainty in their analyses due to variability in soil and weather properties. For example, these models assume a constant dust accumulation rate with time. In addition, these models have not fully calibrated their soil and weather parameters, and have never been tested outside of Southwestern USA. Paleoclimate reconstruction using these models is simplistic with few predetermined scenarios (McFadden and Tinsley, 1985). Here I suggest to follow and improve the CALGYP model, testing a wide range of parameters and implying this model to the hyperarid soils of Israel.

1.4 *Modeling rainfall and evaporation using weather generators*

A wide variety of point-scale WGs are used to supply climate data that include rainfall, PET and temperature on a given time scale and for a single station. On a daily time scale, at a site, rainfall WGs often use Markov chains (Richardson, 1981) or semi-empirical distribution of wet/dry spells (Semenov and Brooks, 1999). Rain depth is then determined from probability distributions that represent natural rainfall data sets. Rain

depth distributions are generally skewed to the right so the Weibull, gamma, or exponential distributions often get chosen for this purpose (Dunn, 2004; Marani and Ignaccolo, 2015; Marra et al., 2018).

Extreme events can have a great influence on geomorphological and pedogenic processes in arid areas (Amit et al., 2010), therefore, generating these events by WG is vital, yet not trivial giving their low-frequency. A new approach for describing extreme events considers them as the right tails of the distributions of all ordinary events (Marani and Ignaccolo, 2015). Recently, extreme daily rainfall in the Eastern Mediterranean was successfully simulated as Weibull distribution right tail equivalent (Marra et al., 2019).

Evaporation is another important factor in modeling the accumulation of evaporitic minerals, however, modeling evaporation is rather complicated due to a large number of spatial and temporal dependent parameters. Evaporation processes can be categorized into potential and actual, where the PET is a measure for the amount of evapotranspiration that would occur if sufficient water is available. Actual evapotranspiration (AET) is the actual amount of water taken from the surface as a result of evaporation and transpiration. A common way of evaluating PET is by employing the Penman equation (Penman, 1948), which requires meteorological parameters that are frequently measured by meteorological stations. AET can be derived from PET as a function of current soil water content (Garfunkel, 1998; Marion et al., 1985; Thornthwaite, 1948). Tsakiris (1988) suggested a stochastic model for generating daily PET series based on calculated Penman – Monteith values from meteorological data of a specific station. This method is based on calculating the probabilities of deviation from the mean monthly PET for four types of days in relation to rainfall occurrence and applying them for generating a daily PET series. Here I suggest to develop a point stochastic WG which uses the above mentioned methods. The WG will be able to simulate the current climate in the study area with the ability to alter specific rainfall characteristic and examine their affect over pedogenic gypsum accumulation.

2. Research goals

The overall aim of the research is to quantify the effect of climatic properties and time on the accumulation of pedogenic gypsum in hyperarid reg soils.

Specifically, the goals of the study are to:

1. Develop a simplified soil compartment model for simulating long-term water transport and gypsum dissolution/accumulation, and to link it with a point stochastic weather generator that produces the necessary climatic data for the simulation.
2. Quantify the effect of climatic factors, dust flux, hydraulic soil parameters and time, over pedogenic gypsum accumulation.
3. Estimate the most likely climatic scenarios that led to the formation of the diagnostic gypsic horizon developed during the late Pleistocene (22.9 – 62.5 Ka) in abandoned alluvial fan surfaces in the hyperarid Negev.

3. Study sites and data

The study area is the dry part of the hyperarid region of Israel, characterized by mean annual rainfall < 50 mm. Reg soil chronosequences from two sites were used for model calibration and evaluation (Figure 2): (1) Ze'elim stream alluvial fan, located in the Judean Desert near the southwestern shore of the Dead Sea. (2) Shehoret stream alluvial fan, located in the southern Arava near Elat. Soil water profiles from Evrona stream alluvial fan (6 km north of Shehoret site), were used to calibrate the soil parameters. The sites differ by mean annual rainfall, annual PET and mean annual number of rain days (Table 1). Soil data collected by Amit (1993) at both sites were used for model calibration and validation (Table 2).

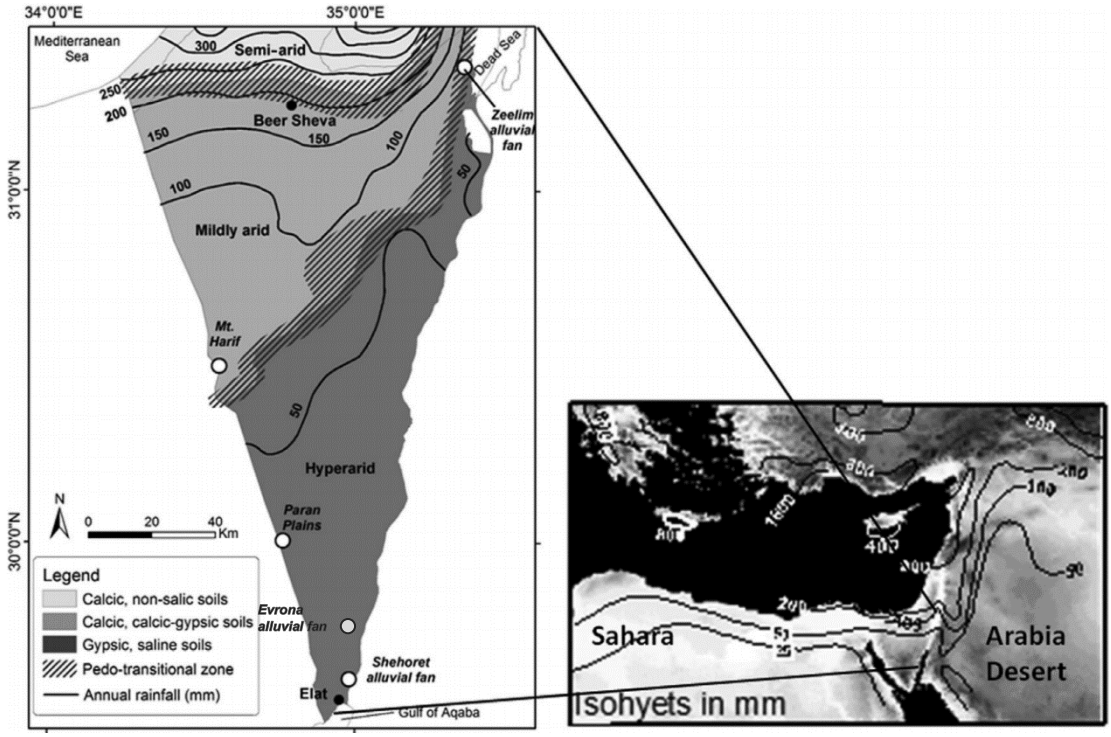

Figure 2: Soil association map of the Negev desert, annual rainfall distribution and regional location map of the Negev Desert. gypsic soils develop in the hyperarid region (after Amit et al. 2011).

Table 1: Mean rainfall properties from Elat and Sedom meteorological stations provided by the Israel Meteorological Service (IMS). A Weibull daily rain distribution defined by scale and shape parameters is given for each station.

Site name, Meteorological station	Mean annual rainfall [mm]	Mean annual wet day depth [mm]	Mean annual number of wet days per year	Mean annual PET [a] [mm]	Mean annual temp. [°C]	Station ID	Period	Weibull distribution parameters scale, shape	constraints on Weibull parameters [b] α, C
Ze'elim, Sedom	39	2.6	15.0	2300	23	337000	[1969,2018]	1.6/0.6	0.2, 0.5042
Shehoret, Elat Evrona, Elat	18	1.9	9.6	2100	25	347700	[1949,2019]	1.3/0.5	0.2, 0.4257

a PET is calculated using the Penman – Monteith equation, in accordance with FAO-56 standard which does not accommodates for the lack of vegetation in the study area. Daily PET data is available for the last 9 years in Sedom and 18 years in Elat.

b Constraints (see Eq. 6) were calculated based on an approximated model for all meteorological station in southern Israel (Marra et al., 2020)

Ze'elim alluvial fan was deposited after lake Lisan level finally decreased at the end of the late Pleistocene (~25 Ka). Since then, the sublacustrine delta was gradually carved by cut and fill terraces and reg soils began to develop. The alluvial fan sediments are composed mainly of limestone, dolomite, and chert with a minor amount of fine earth (Amit et al., 1993). The terraces ages ranges from the end of late Pleistocene (22.9 Ka) to early Holocene (10.3 Ka), established using OSL dating (Porat et al., 2010). Halite accumulation is minimal whereas gypsic horizons are observed at 30-70 cm depth with gypsum concentration that ranges from 4 [meq/100 g soil < 2 mm] in young profiles to 300 [meq/100 g soil < 2 mm] in mature profiles (Amit et al., 1993). Desert pavement is poorly developed and a thin (0.5 cm) vesicular A horizon is apparent. The lower horizons are dominated by high gravel content (~60% in volume).

Shehoret alluvial fan is composed of limestone, chert, sandstone, schist and diorite (Amit et al., 1993; Gellman et al., 2018). The terraces ages ranges from the middle of late Pleistocene (~62.5 Ka) to the very end of late Pleistocene (~13.5 Ka; here this youngest terrace will be considered as of early Holocene age) (Porat et al., 2010). The mature profiles are thick (80-120 cm) with well-defined soil horizons. The surface consists of well-developed, smooth pavement; the B horizons are gravel-free and reach a depth of 5-20 cm. Gypsum is accumulated at depths of 10-30 cm and reaches a concentration of 500 [meq/100 g soil < 2 mm]. High halite content is observed at a depth of 70 cm and deeper (Amit et al., 1993). Young profiles are thin (40 cm) and horizons are poorly developed. Desert pavement is poorly developed. Gypsum is accumulated at depths of 5-35 cm and reaches a concentration of 300 [meq/100 g soil < 2 mm]. The lower horizons in all terraces are dominated by high gravel composition (~60%-80%).

Table 2: Measured gypsum profiles and OSL ages from Shehoret, Evrona, and Ze'elim alluvial fans. Soil profiles are taken from Amit (1993). OSL ages are taken from (Porat et al., 2010). Soil hydraulic parameters are calculated using fine material texture and corrected for bulk samples using the gravel fraction (explained in the method section).

Profile name	Surface	OSL age [Ka]	Horizon	Top [cm]	Base [cm]	Gypsum [meq/100 g soil <2mm]	Sand [wt%]	Silt [wt%]	Clay [wt%]	Gravel >2mm [% vol]	Field capacity [$cm^3\ cm^{-3}$]	Residual w. content [$cm^3\ cm^{-3}$]	Gypsum [meq/100 g soil bulk] *
Ze'elim, ZEL11	12	10.3 Holocene	Av	0	0.5	0.4	32.5	49.3	18.2	0	0.22	0.06	0.4
			B	0.5	6.5	3.8	59.0	39.2	1.8	60	0.08	0.02	1.5
			C	6.5	45	14.8	68.2	29.8	2.0	60	0.08	0.02	5.9
Ze'elim, ZEL1	1	22.9 late Pleistocene	Av	0	0.5	2.8	78.0	18.0	3.9	0	0.18	0.05	2.8
			Bg,f	0.5	1.5	2.5	67.8	29.7	3.3	60	0.08	0.02	1.0
			C1	1.5	30	14.5	27.3	16.97	2.3	60	0.07	0.02	5.8
			C2	30	55	87.0	18.1	69.6	12.3	60	0.09	0.03	34.8
			S	55	80	34.3	67.2	25.3	7.6	60	0.08	0.02	13.7
Ze'elim, ZEL2	1	22.9 late Pleistocene	Av	0	0.5	0.5	70.5	23.6	5.9	0	0.21	0.04	0.5
			B	0.5	1.5	1.0	74.7	19.0	5.1	0	0.18	0.05	1.0
			C1a	1.5	15	1.4	67.3	29.8	3.0	60	0.10	0.02	0.5
			C1b	15	20	2.2	36.5	45.8	17.8	60	0.11	0.03	0.9
			C1c	20	30	12.2	44.8	43.1	12.1	60	0.11	0.03	4.9
			C1d	30	40	11.4	81.8	16.7	1.5	60	0.09	0.02	4.5
			C1e	40	50	34.7	50.9	42.0	7.1	60	0.10	0.02	13.9
			C1f	50	70	80.4	15.5	69.3	15.2	60	0.11	0.03	32.2
Shehoret T1-10	Qa3	13.5 Holocene	Av	0	0.5	2.7	58.0	33.2	8.8	10	0.19	0.04	2.4
			Bw	0.5	1.5	3.3	36.5	41.7	21.8	70	0.07	0.02	1.0
			ClY	1.5	20	7.5	90.3	7.4	2.3	70	0.04	0.02	2.3
			c2	20	40	8.3	93.2	4.2	2.6	80	0.03	0.01	1.7
Shehoret T1-9	Qa3	13.5 Holocene	Al	0	3	3.9	74.7	19.7	5.5	20	0.17	0.03	3.1
			A2	3	6	5.1	68.0	23.2	8.8	50	0.10	0.02	2.6
			Bw	6	8	7.8	63.5	24.8	11.8	20	0.17	0.03	6.2
			Clzy	8	28	8.2	85.4	10.0	4.6	60	0.07	0.02	3.3
			c2z	28	40	8.4	88.7	11.1	0.2	70	0.04	0.02	2.5
Shehoret T2-10	Qa2	27.0 late Pleistocene	Al	0	0.2	3.0	64.7	26.9	8.4	10	0.19	0.04	2.7
			Clv	0.2	40	39.1	73.5	20.2	6.3	70	0.06	0.01	11.7
			C2Y	40	70	14.4	85.7	13.5	0.8	85	0.02	0.01	2.2
			C3Y	70	95	10.6	89.0	9.9	1.1	85	0.02	0.01	1.6
			c4	95	100	34.3	89.3	10.5	0.2	90	0.01	0.01	3.4
Shehoret T1-1	Qa1	62.5 late Pleistocene	Av	0	3	4.3	55.3	32.7	12.0	0	0.21	0.04	4.3
			Blgf	3	10	3.0	78.9	14.6	6.6	0	0.18	0.05	3.0
			B2y	10	20	377.5	56.4	40.2	3.4	80	0.04	0.01	75.5
			BUY	20	40	147.4	87.1	11.0	1.9	20	0.10	0.04	117.9
			Clyz	40	60	103.9	87.3	10.5	2.3	60	0.05	0.02	41.6
			C2zmy	60	150	123.0	81.7	18.2	0.2	80	0.04	0.01	24.6
			c3z	150	250	144.1	77.6	22.1	0.3	60	0.07	0.02	57.6
Shehoret T2-1	Qa1	62.5 late Pleistocene	Av	0	2	5.5	49.3	38.7	12.0	0	0.22	0.06	5.5
			BlgP	2	23	202.0	71.0	28.7	0.4	0	0.18	0.05	202.0
			BUY	23	43	367.3	60.7	38.8	0.5	70	0.06	0.01	110.2
			Clyz	43	83	141.7	74.7	21.6	3.7	70	0.05	0.01	42.5
			C2Z	83	118	17.1	88.3	9.1	2.6	80	0.03	0.01	3.4
Sheoheret1	Qa1	62.5 late Pleistocene	Av	0	0.5	2.3	49.9	42.8	7.3	0	0.21	0.04	2.3
			Bg,f	0.5	15	262.6	49.0	44.2	7.1	0	0.21	0.04	262.6
			B2cs	15	30	536.7	90.5	8.3	1.2	60	0.04	0.02	214.7
			Ccs,sa	30	55	164.2	87.0	10.9	2.2	60	0.04	0.02	65.7
			C1sa	55	80	17.0	82.5	15.7	1.4	60	0.05	0.01	6.8
			C2sa	80	90	38.0	91.0	8.5	0.6	60	0.04	0.02	15.2
			Sedimen	90	120	6.9	95.0	4.0	1.0	60	0.04	0.02	2.7
Sheoheret3	Qa1	62.5 late Pleistocene	Av	0	0.5	1.7	47.8	45.4	6.8	0	0.21	0.04	1.7
			bg,f	0.5	8.5	335.8	57.7	40.7	1.6	0	0.21	0.04	335.8
			B2cs	8.5	20	129.6	91.5	7.2	1.3	0	0.13	0.05	129.6
			C1cs.sa	20	28	49.9	88.5	9.8	1.7	60	0.04	0.02	20.0
			C2cs.sa	28	44	27.2	87.8	9.9	2.3	60	0.04	0.02	10.9
			C3sa	44	70	135.3	76.1	18.9	5.0	60	0.05	0.01	54.1
			C4sa	70	80	12.5	89.4	7.3	3.3	60	0.04	0.02	5.0

** This value was calculated in this study based on the gypsum [meq/100 g soil <2mm] and the gravel content see Eq.31.*

4. Methods

The methodology of this study included three main steps:

1. Constructing a compartment model that simulates gypsum accumulation in soil and testing its sensitivity to various climate properties. The model predicts gypsum content and depth of accumulation in the soil profile over thousands of years on a daily basis. The input data include stochastically simulated rainfall, PET, dust flux, and sulfate concentration in rainwater, at daily time steps. The model was calibrated and tested using data of three Holocene (10.3 – 13.5 Ka) soil profiles (ZEL11, T1.10, T1.9; Table 2), assuming that the climate during the Holocene was not much different than today.
2. Conducting sensitivity analyses to evaluate how a change in each factor affects the rate of accumulation, depth of pedogenic gypsum and the total concentration of gypsum in the soil profile.
3. Running numerous sets of input parameters and altered climate scenarios with the calibrated model to reconstruct the most likely climate conditions that led to the formation of the well-developed gypsic horizons (ZEL1, T1.1, T2.1, Shehoret1, Shehoret3; Table 2) that characterize mature, late Pleistocene reg soils in the study area.

The model is composed of (1) a weather generator responsible for stochastically creating the daily rain and PET series, (2) a soil compartment model responsible for water balance and chemical equilibrium calculations (Figure 5). Two additional modules were activated only for the late Pleistocene soils: (3) field capacity and (4) runoff modules that address the changes in time of mature (10.3 – 13.5 Ka) soil and surface properties (see below). Each stage of the model evaluation focuses on soil water or gypsum profiles. In the first stages, WHC parameters related to water distribution are calibrated, and in the second stage, gypsum sources parameters are calibrated using measured soil profiles (Figure 3):

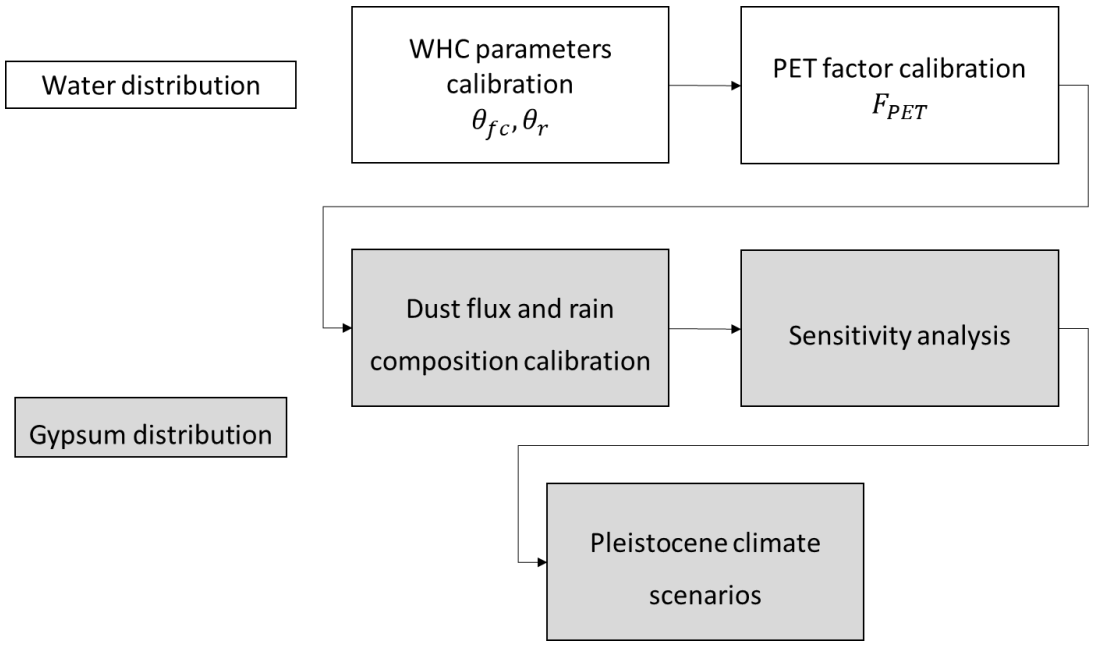

Figure 3: Model flow chart. Stages related to water distribution in the soil appear in white boxes. Stages related to gypsum distribution appear in grey boxes..

Table 3: Input parameters used by the model. Each parameter is used for different module and the value is a given or acquired after calibration. Some parameters can be compared to values from the literature.

Parameter	Units	Relevant module	Source	Value	Estimated values from published studies
Duration	[years]	Compartment	Table 2	Vary according to soil data 10300-62500	-
Soil profile depth	[cm]	Compartment	Table 2	100 Holocene 150 Pleistocene	-
Profile area	[cm^2]	Compartment	Marion, 1985	1	
Compartment thickness	[cm]	Compartment	Marion, 1985	5	-
Field capacity θ_{fc}	[$cm^3\ cm^{-3}$]	Water	Calibrated	0.1	0.19 (Loessial soil after Horowitz, 2019)
Residual water content θ_r	[$cm^3\ cm^{-3}$]	Water	Amit, 1990	0.01	0.02 (Loessial soil after Horowitz, 2019)
PET factor F_{PET}	[-]	Water	Calibrated	1.2	0.6 (Loessial soil after Horowitz, 2019)
Annual dust flux *	[g $m^{-2}\ yr^{-1}$]	Chemical	Calibrated	5	2-6 (fine materials in measured profiles)
Gypsum in dust	[%]	Chemical	Ganor,1975	1	-
SO4 in rainwater *	[mg l^{-1}]	Chemical	Calibrated	10	20 measured for 67 rain days in central Negev (Herut, 2000)
Ca in rainwater	[mg l^{-1}]	Chemical	Calibrated	35	35 measured for 67 rain days in central (Herut,2000)
Mean annual rainfall *	[mm]	WG	IMS	Elat 18 Sedom 39	-
Mean annual number of wet days*	[-]	WG	IMS	Elat 9.6 Sedom 15	-
Mean annual PET *	[mm]	WG	IMS	Elat 2100 Sedom 2300	-

* *Parameter also compose a late Pleistocene climate scenario.*

4.1 *Weather generator*

Point-scale WG is used to stochastically construct simulated time series of daily rainfall and PET with statistical properties representing the measured data of a meteorological station. The WG uses Markov chains and empirical distribution of wet/dry spells (Richardson, 1981; Semenov and Brooks, 1999) to determine the occurrence of rain events and PET value.

4.1.1 *Sequences of Wet/Dry days*

Three probabilities are calculated for each Julian day index: (1) conditional probability of a wet day after a wet day (WAW), (2) conditional probability of a wet day after a dry day (WAD). The probabilities are calculated as follows:

$$PWAW_i = \frac{WAW_i}{Wet_{i-1}} \quad (1)$$

$$PWAD = \frac{WAD_i}{n - Wet_i} \quad (2)$$

Where i is the Julian day index (1:365), n is the number of years in the sample, Wet_i is the number of occurrences of a wet days during day i among the sampled years, WAW_i is the number of occurrence of wet days during day i with the condition of a previous wet day and WAD_i is the number of occurrence of wet days during day i with the condition of a previous dry day. These probabilities are then smoothed using

a double convolution of 50 and 40 days windows for the first and second convolutions. For modified climate scenarios, altering the number of annual rain days can be achieved by introducing a factor to the probability of wet days attributed to each Julian day.

4.1.2 *Rain depth of wet days*

Rain depth is determined from a Weibull probability distribution, which successfully simulates the Eastern Mediterranean hyperarid climate, characterized by a low frequency of events (Marra et al., 2018). The distribution density function is defined as follows:

$$f(x;\lambda,\kappa) = \begin{cases} \frac{\kappa}{\lambda}\left(\frac{x}{\kappa}\right)^{\kappa-1} \cdot e^{-\left(\frac{x}{\lambda}\right)^{\kappa}}, & x \geq 0 \\ 0\,, & x < 0 \end{cases} \quad (3)$$

Where k is the shape parameter and λ is the scale parameter. Shape and scale parameters for Elat and Sedom stations are estimated using the Simplified Metastatistical Extreme Value (SMEV) (Marra et al., 2019) formulation over the measured data set. Using both the empirical rain day distribution and the station Weibull parameters, one can simulate rain day occurrences and depth.

To evaluate the effect of different climate properties on the model simulations, modification in weather properties is required. This modification is achieved by changing the Weibull distribution parameters. Altering mean daily rain depth is done by intervening with the scale and shape parameters. An empirical relation between these parameters is derived for a single station using meteorological data from a local group of stations (Marra et al., 2020). The relation serves as a local constraint on the intensity distribution of rain events and allows to define it using the mean intensity I:

$$f(x;\lambda,\kappa) = f(x;\mathrm{I}) \quad (4)$$

$$\lambda \cdot \Gamma\left(1+\frac{1}{\kappa}\right) = \mathrm{I} \quad (5)$$

$$\kappa = \alpha \cdot log\lambda + C \quad (6)$$

The distribution definition is reduced to one degree of freedom in Eq. 4 as λ and κ are estimated by the mean of the distribution (Eq. 5) and a logarithmic relation described in Eq. 6 where α and C are empirically determined. The mean of the distribution is the mean annual rainy day depth (i.e., mean annual rainfall divided by the mean annual number of rainy days). Applying the calculated Weibull distribution and the wet day probability factor to the WG yields a modified rain series.

4.1.3 *PET simulation*

Evaporation category based on day type (DAD/Wet/DAW) and Julian index (i.e., 1095 categories) is assigned for every day in the generated series. Mean and standard deviation (SD) of daily PET values were calculated from measured data at an IMS station for each category and normal distribution functions were fitted for each category. PET values for the generated series were sampled from these probabilities according to the relevant category. Altering the annual PET value for modified climate scenarios is done by introducing a factor to the calculated daily PET and evenly increase or decrease it for the entire series.

4.1.4 *Series construction*

The series was constructed by assigning a random variable between 0 and 1 for every day and then comparing it to the calculated Wet/Dry probabilities (Figure 4). A PET value was assigned to each simulated day according to its category. For wet days, the daily rain amount was acquired using random values of a

Weibull distribution with specified scale and shape parameters (Table 1). Each series is characterized by mean annual rainfall, mean number of annual rain days, mean annual PET and mean annual rainy day depth.

By definition, stochastic models incorporate random components and provide different outputs for a given input parameters set, the range of these possible results can be defined as the stochastic uncertainty. For the purpose of this study, results for a given input were reported as the mean of 100 calculations with a stochastic uncertainty component.

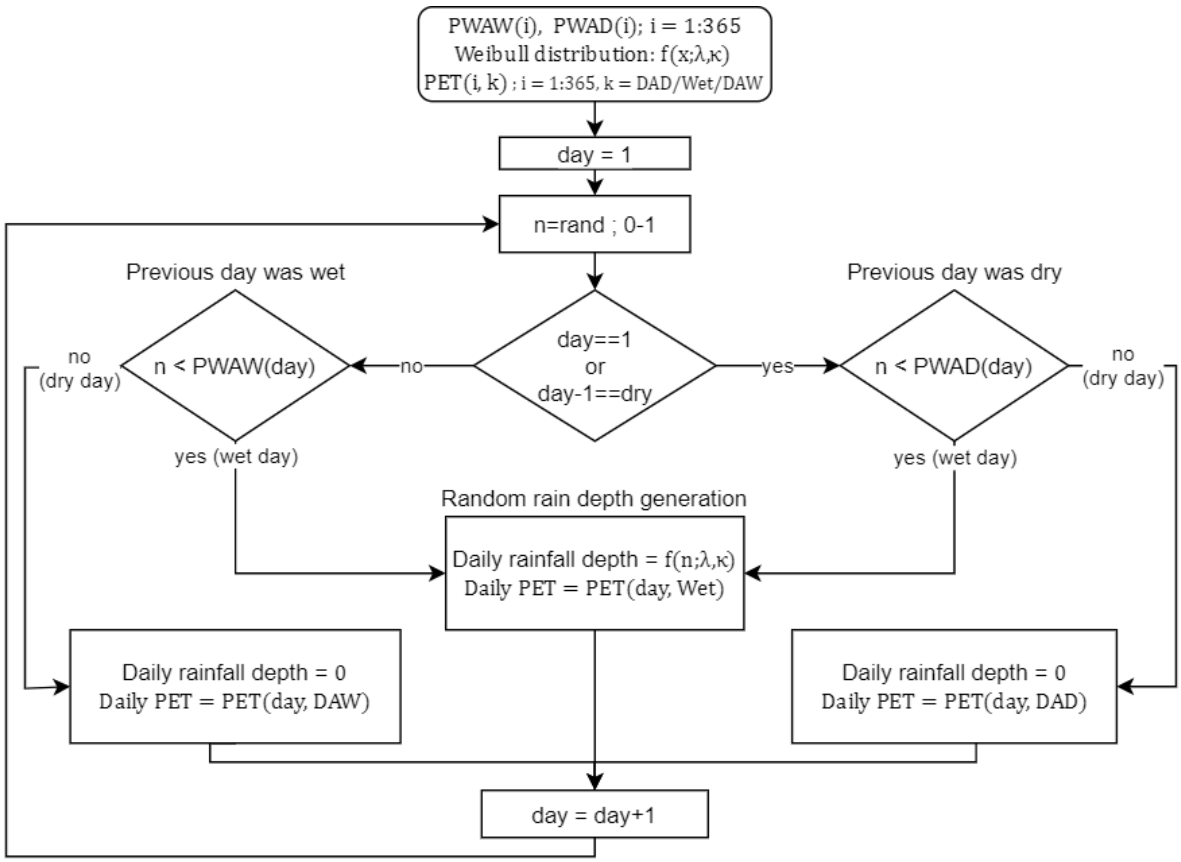

Figure 4: The weather generator scheme for 1 year of synthetic data generation. The input is the conditioned probabilities for rainfall, the weibull distribution, and the PET values for each day type and julian index. The first day is dry by choice and a uniform random value between 0 and 1 is generated for each following day, to determined weather the current day is wet or dry. In the case of a wet day, rainfall depth is randomly generated from the given weibull distribution. PET value is determined according to the current day category.

4.2 *Compartment model*

4.2.1 *Soil water balance*

The one-dimensional flow model consists of a soil column divided into several compartments of predefined thickness (5 cm in this study) and surface area of 1 cm^2. The input data for the model are the generated daily rainfall and PET series (Figure 5). AET is calculated for each day in accordance with soil water content applying the linear relation between AET and PET used by Marion et al. (1985) and further developed by Horowitz (2019) as described in eq. 7:

$$AET = F_{PET} \cdot \begin{cases} PET, & TotalMoisture > WHCindex \cdot TotalWHC \\ \frac{TotalMoisture}{TotalWHC} \cdot PET, & TotalMoisture \leq WHCindex \cdot TotalWHC \end{cases} \quad (7)$$

$$TotalWHC = \sum_{i=0}^{T.M.depth} WHC_i \cdot 5[cm^3]$$

$$WHC_i = \theta_{fc_i} - \theta_{r_i}$$

WHC here is the water holding capacity of each compartment and is given in volumetric water content units [cm3 cm-3], as are the θ_{fc} (field capacity) and θ_r (residual water content). $T.M.depth$ is the maximal effective depth for evapotranspiration processes, ranges from 100-150 cm. $TotalWHC$ is the sum amounts of WHC given in [cm^3]. $TotalMoisture$ is the sum amounts of existing water given in [cm^3]. $WHCindex$ =0.546 (Marion et al., 1985) is the point in WHC range, at which AET turns from being energy limited (i.e., controlled by the atmospheric demand, AET=PET), to soil water limited. The AET value is multiplied by a factor, F_{PET}, to accommodate with variables which are not considered by the PET calculation such as the lack of vegetation. Note that the values of θ_{fc} and F_{PET} were found through the calibration of the water module (see 4.3.1).

Rainfall depth, dust and soluble ions are added to the first compartment each day. Water that exceeds the compartment's θ_{fc} is transferred to the compartment below. Soluble ions are transferred according to the ratio of excess water. After distributing water and soluble ions downward, water is subducted from the compartments to represent the evaporation process: starting from the uppermost compartment and going down, the excess water above the θ_r was summed until it equaled the daily computed AET (Eq. 7). At the end of each day, the chemical equilibrium module determines the gypsum accumulation in accordance with the water content at each compartment.

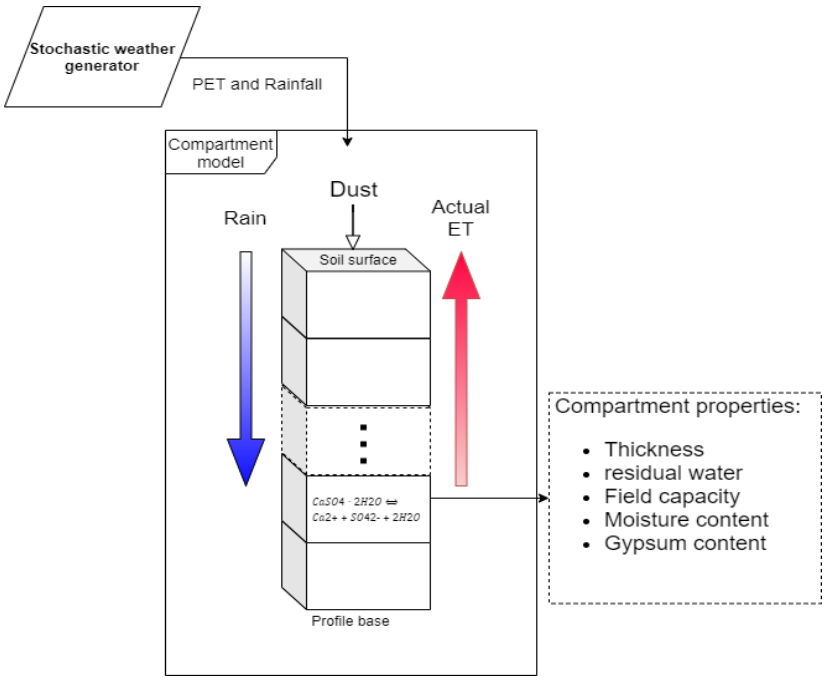

Figure 5: A schematic diagram of the water redistribution process in soil compartment model. Rain Infiltrates to the soil and distributed according to the hydrological properties of the compartments. Water evaporate each day according to the generated daily PET and calculated AET. Gypsum equilibrium is calculated daily for each compartment (Modified after Marion et al., 1985).

4.2.2 *Chemical module*

The chemical submodule calculates whether gypsum precipitation or dissolution occurs according to the current concentration of soluble ions. Calculations were performed at each iteration and for each compartment, to determine the distribution of salts through the simulated soil profile. The reaction is expressed by:

$$CaSO_4 \cdot 2H_2O \Leftrightarrow Ca^{2+} + SO_4^{2-} + 2H_2O \quad (8)$$

The saturation state of a solution with respect to gypsum can be expressed as:

$$\Omega = \frac{IAP}{K_{sp}(T)} = \frac{a_{Ca^{2+}} \cdot a_{SO_4^{2-}} \cdot a_{H_2O}^2}{\left(a_{Ca^{2+}} \cdot a_{SO_4^{2-}} \cdot a_{H_2O}^2\right)_{eq}} \quad (9)$$

Where IAP is the ion activity product, a_i is the activity of species i, K_{sp} is the equilibrium constant as a function of the temperature. Ω is the degree of saturation, where $\Omega > 1$ defines a supersaturated solution, and $\Omega < 1$ is an undersaturated solution. Equilibrium between the components of Eq. 8 is defined when $\Omega = 1$. Activity is defined as follows:

$$a_i = C_i \cdot \gamma_i \quad (10)$$

Where C_i is the concentration of species i and γ_i is the ion activity coefficient for species i.

The ion activity coefficients were calculated using the Davis equation (Davies and Shedlovsky, 1964) along with the Debye-Hückel and is given by:

$$log\gamma = -A(T)z_i^2 \cdot \left(\frac{\sqrt{I}}{1+\sqrt{I}} - 0.3I\right) \quad (11)$$

where A is a constant which depends on the temperature and I is the ionic strength:

$$A = 0.4918 + 6.6098 * 10^{-4}T + 5.0231 * 10^{-6} * T^2 \quad (12)$$

$$I = 0.5 \sum C_i z_i^2 \quad (13)$$

Where T is temperature and z is the ionic valance. Plugging the results of Eq. 12-13 to Eq. 11 yields the ion activity coefficient needed for the ion activity described in Eq. 10.

Calculation of the number of moles needed to be transferred between the gypsum and the soluble ions to reach equilibrium is performed by calculating the number of moles required to bring Eq.10 to equilibrium, all in terms of ion activity:

$$\Omega = 1 = \frac{(a_{Ca^{2+}} - x) \cdot (a_{SO_4^{2-}} - x)}{K_{sp}} \quad (14)$$

where x is the number of moles needed to reach equilibrium. Isolating x in Eq. 14 yields:

$$x^2 - x\left(a_{Ca^{2+}} + a_{SO_4^{2-}}\right) + \left(a_{Ca^{2+}} * a_{SO_4^{2-}} - K_{sp}\right) = 0 \quad (15)$$

$$x_{1,2} = -\left(a_{Ca^{2+}} + a_{SO_4^{2-}}\right) \pm \sqrt{\left(a_{Ca^{2+}} + a_{SO_4^{2-}}\right)^2 - 4 * \left(a_{Ca^{2+}} * a_{SO_4^{2-}} - K_{sp}\right)}$$

Eq. 15 is a polynomial with two solutions, the solution x which generates non-negative concentrations is chosen.

This module assumes the following:

- Temperature has little effect on the equilibrium constant k_{sp} in the range between 15 and 35 ˚C (Reznik et al., 2009). Since soil temperatures in the study area do not change substantially during day and night cycles (Amit et al., 1993), the temperature is assumed to be constant (25ºC).
- Only thermodynamic constraints were taken into account, neglecting reaction kinetics. i.e., an undersaturated solution has to reach equilibrium by instantly dissolving solid gypsum. A supersaturated solution has to precipitate gypsum instantly to reach equilibrium.

4.2.3 *Runoff module*

With time, desert pavement gradually develops on the alluvial fan surfaces and induces runoff and plugging (Amit and Yaalon, 1996; Gerson et al., 1985; Gerson and Amit, 1987). In field experiments, Greenbaum (1986; 2020) quantified the runoff ratio (the ratio between the amount of rain that does not infiltrate the soil, i.e., runoff, and the amount of total rain) for three different rain intensities (Table 4); these experiments were conducted on four different alluvial fan surfaces that differ in their desert pavement maturity (i.e., time). As the model developed in this study uses daily rain rather than short-duration rain intensity, a new relationship between daily rain and daily runoff was derived.

Table 4: runoff ratio (%) for various rainfall intensities from alluvial surfaces of different ages in Evrona stream. After (Greenbaum et al., 2020)

Surface age [Ka]	14 mm hr^{-1}	40 mm hr^{-1}	76 mm hr^{-1}
106	17.5	30.7	67.4
31	8.2	14.1	48.7
10	1.9	10.4	40.1
~0	-	-	12.0

Relation between runoff ratio and intensity was assumed to be linear since no other relation was suggested by Greenbaum (2020). Also, the number of the experiments is low and available data are scarce, therefore uncertainties are expected to be high. For this reason, the module is tested for its overall effect over the model results in section 5.4.

Linear models were approximated for three surfaces of different ages using the data collected in a series of rainfall experiments conducted over reg soil surfaces of different ages (Table 4):

$$r_{106ka} = 0.0082i + 0.03; R^2 = 0.96 \quad (16)$$

$$r_{31ka} = 0.0067i + 0.05; R^2 = 0.94 \quad (17)$$

$$r_{10ka} = 0.0082i + 0.10; R^2 = 0.88 \quad (18)$$

Where i is the rain intensity given in [mm/hr] and r is the estimated ratio between runoff amount and total rainfall depth in [mm mm^{-1}] over a surface of a specific age.

These models were used to calculate the daily runoff generated using measured 10 minutes rain data in Elat and Sedom stations. Three linear models were approximated (Figure 7):

For Elat station:

$$dro_{106ka} = 0.111 \cdot drf; R^2 = 0.68 \quad (19)$$
$$dro_{31ka} = 0.070 \cdot drf; R^2 = 0.68 \quad (20)$$
$$dro_{10ka} = 0.060 \cdot drf; R^2 = 0.68 \quad (21)$$

For Sedom station:

$$dro_{106ka} = 0.067 \cdot drf; R^2 = 0.58 \quad (22)$$
$$dro_{31ka} = 0.045 \cdot drf; R^2 = 0.58 \quad (23)$$
$$dro_{10ka} = 0.035 \cdot drf; R^2 = 0.58 \quad (24)$$

Where drf is the daily rainfall in [mm] and dro is the calculated daily runoff [mm] over a surface of a specific age. Using the slopes of Eq. 19-24, another linear model based on 3 points was calculated to relate surface age to slope:

For Elat station:

$$\beta = 5 \cdot 10^{-7} \cdot age + 0.0522; R^2 = 0.99 \quad (25)$$

For Sedom station:

$$\beta = 3 \cdot 10^{-7} \cdot age + 0.0333; R^2 = 0.99 \quad (26)$$

Where age is the surface age [yr] and β is the slope coefficient of Eq. 19-24. β is the slope coefficient in the equation of the form presented in Eq. 22-24:

For Elat station:

$$dro(age, drf) = (5 \cdot 10^{-7} * age + 0.0522) * drf \quad (27)$$

For Sedom station:

$$\mathrm{d}dro(age, drf) = (3 \cdot 10^{-7} * age + 0.0333) * drf \quad (28)$$

Where dro is the daily runoff [mm] age is the surface age [yr] given at model runtime according to the iteration number. drf is the daily rainfall [mm] given at model runtime according to the daily rainfall depth supplied by the WG. The three main steps of the process are visualized for the case of Elat station (Figure 6). Desert pavement over Holocene surfaces is poorly developed and has little effect over runoff ratio (Table 4), therefore the module was activated when the simulated profile age exceeds 10 Ka. An example of Eq. 27 behavior is visualized for few surfaces ages, the difference between the ages is represented by the slopes (Figure 7). The plot demonstrates the slight effect of the surface age on the correlation between runoff and daily rainfall.

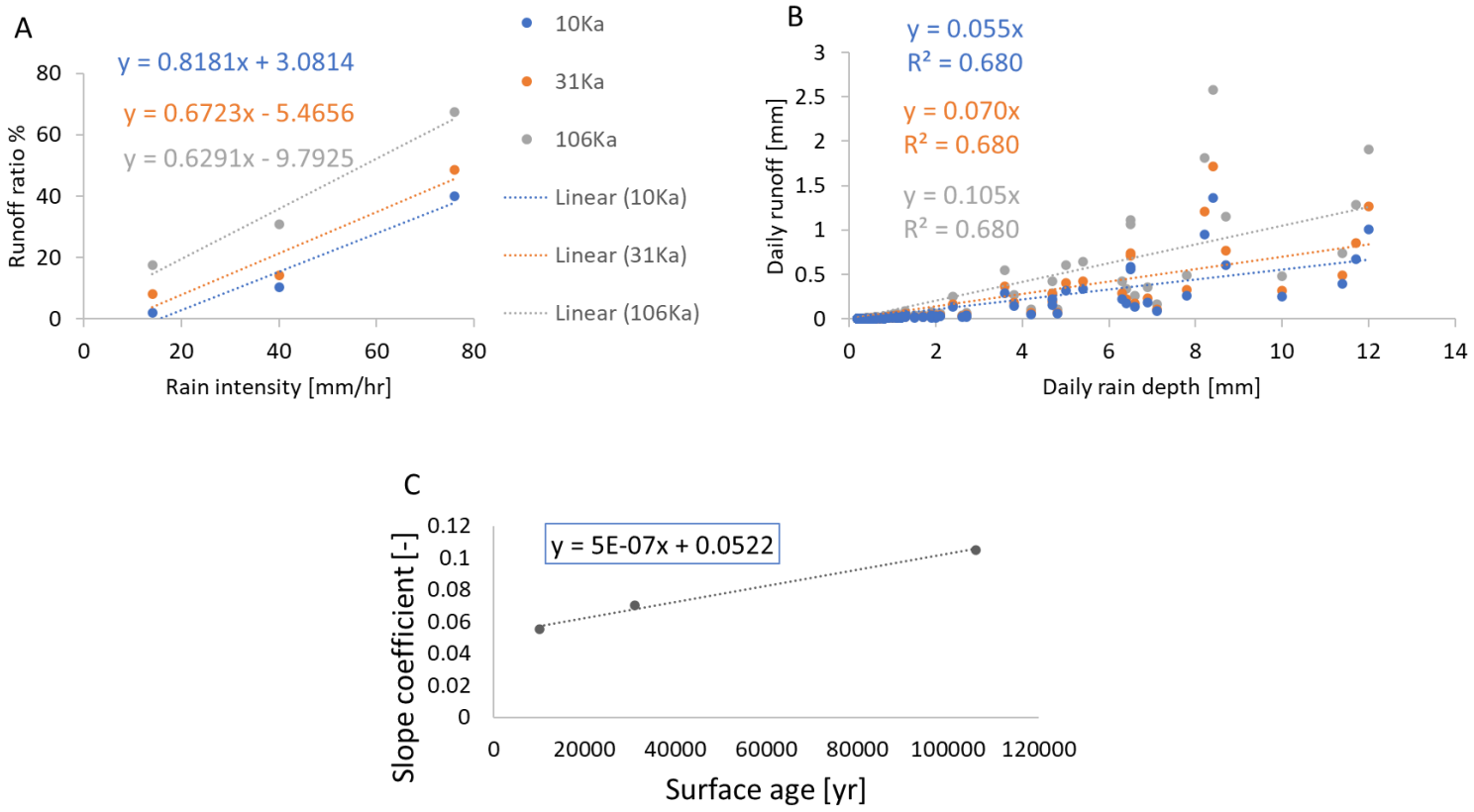

Figure 6: Building the runoff module: (A) runoff ratio as function of intensity (Eq. 16-18), date taken from Greenbaum 2020 (Table 4). (B) daily runoff as function of daily rain depth in Elat station (Eq.19-21). (C) slope coefficient as function of surface age (Eq.27). See text for more details.

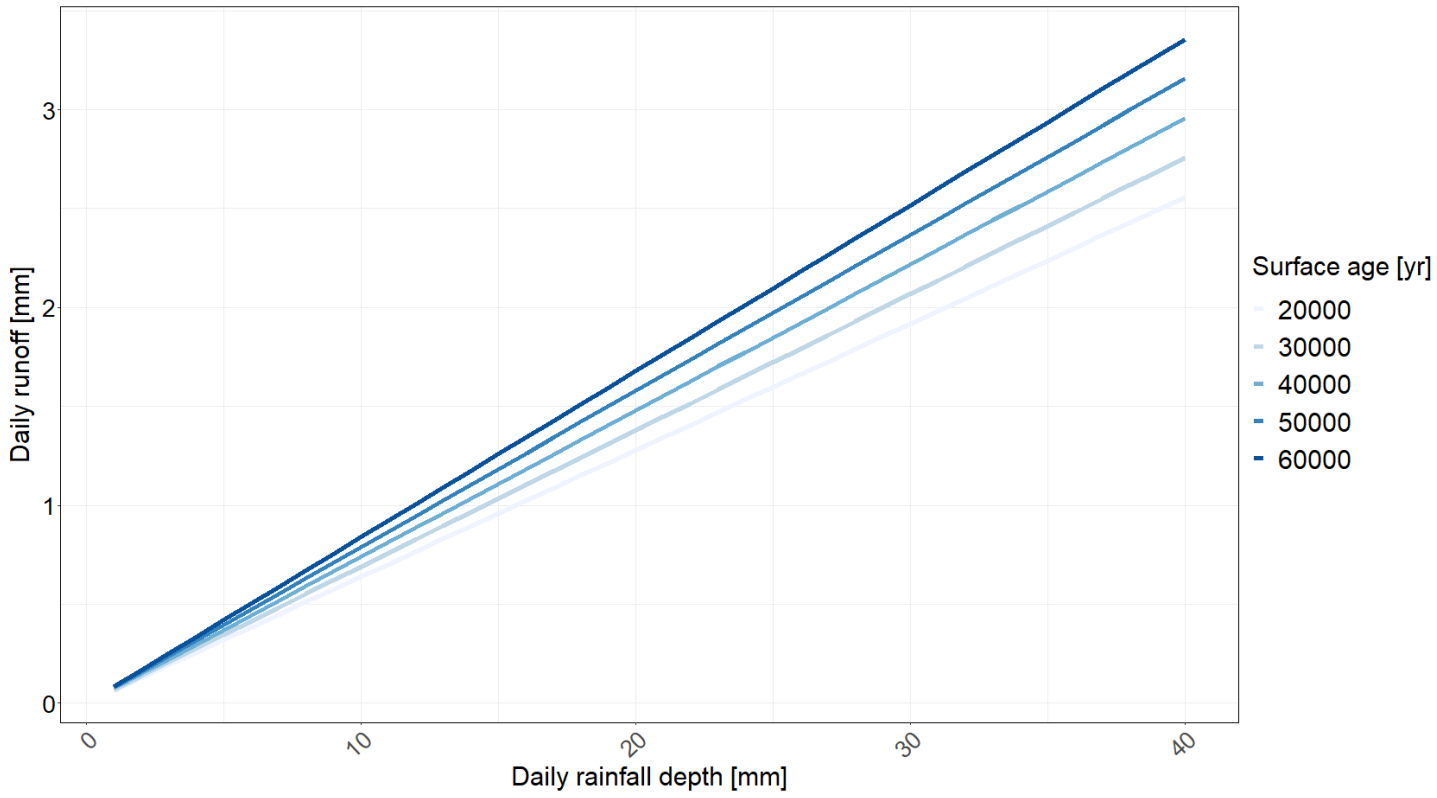

Figure 7: Daily runoff as a function of daily rainfall depth for surfaces of different ages based on Eq.27 , using meteorological data from Elat station.

4.2.4 *Field capacity module*

The field capacity (θ_{fc}) of the upper soil gradually increases with time as dust is being accumulated, forming the Av horizon underneath the desert pavement; This process gradually progresses to deeper parts of the soil resulting in a gravel free horizon at the upper part of the soil. In mature profiles (62.5 Ka) this gravel free horizon reaches a thickness of ~20 cm its texture resembles loess soils characterized by field capacity of $\theta_{fc} = 0.19$ (T. Horowitz, 2019). A linear field capacity module was developed to simulate this process by gradually increasing θ_{fc} as a function of the synthetic soil profile age, i.e., the model runtime. The module starts when the synthetic age is 10 Ka, until it reaches 63 Ka – at that point field capacity of 0.19 is assumed in the upper 20 cm of the soil. The module starts with increasing the field capacity in the top most compartment; When the upper value has been reached, the same process starts in the compartment below (Figure 8).

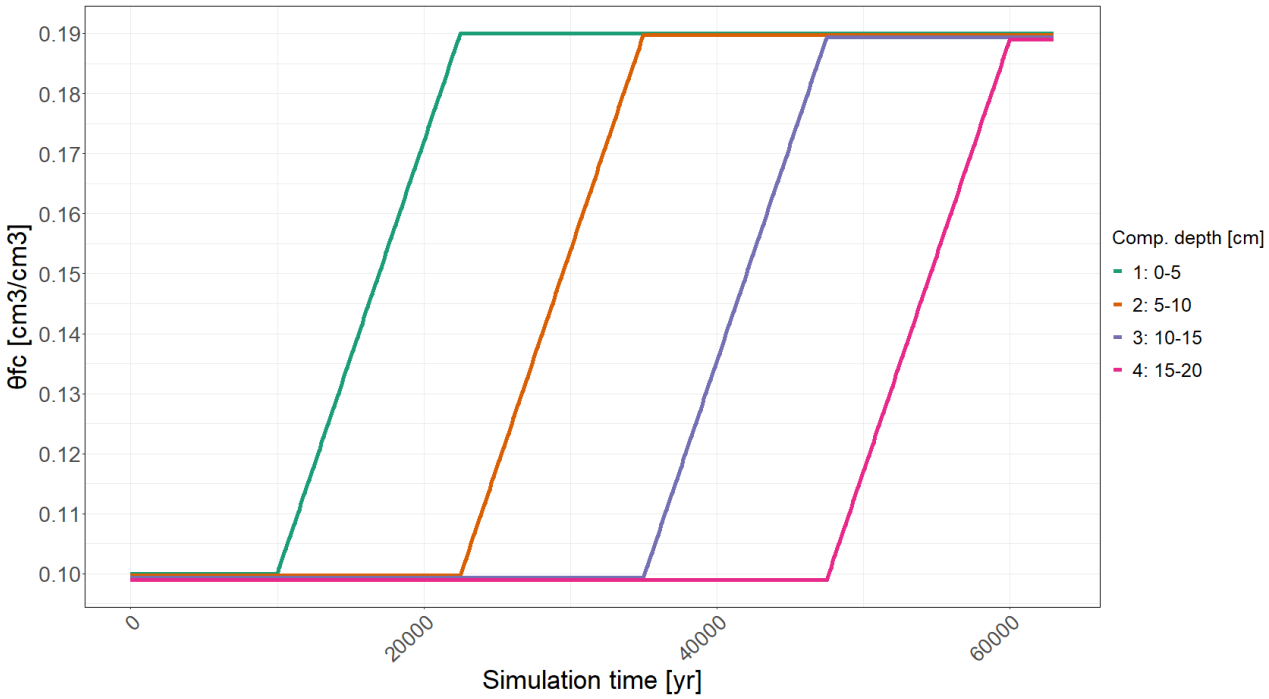

Figure 8: The field capacity module that gradually increases the field capacity within the upper soil (see text).

4.3 *Model calibration*

The first stage of the calibration process focused on soil parameters and evaporation factors using measured soil water profiles from Holocene reg soils at both sites. The second stage focused on gypsum related parameters of sulfate concentration in rainwater and annual dust flux.

4.3.1 *Soil parameters and evaporation factor*

Residual water content (θ_r) was estimated using soil water curves of Holocene reg soils measured during the summer at Ze'elim site (Amit, 1990). Soil parameters were considered identical for profiles of the same age at both study sites. Field capacity (θ_{fc}) is difficult to quantify due to its complexity. However, it is highly correlated with WD. Measurements conducted on Holocene reg soil in Evrona report the WDs immediately after several simulated rainfall experiments. The same rainfall depth values were inserted into the compartment model using a range of possible θ_{fc} values (0.01 – 0.30 cm^3 cm^{-3} with 0.01 interval);

compartment thickness was set to 1 cm to support the high resolution of the soil water samples. Root-mean-square-deviation (RMSD) was calculated for all the experiments as the deviation from the observed and the calculated WD:

$$RMSD_{\theta_{fc}} = \sqrt{\frac{\sum_{i=EV1}^{EV5}(WD_i(\theta_{fc},\dots) - WDe_i)}{5}} \quad (29)$$

Where EV1-EV5 are the number of experiments, $WD_i(\theta_{fc})$ is a WD calculated with a tested value and WDe_i is the experiment results.

Table 5: Infiltration experiments conducted over alluvial surfaces of Holocene age in Evrona alluvial fan. WD was measured after a sprinkling experiment. After (Greenbaum, 1986).

profile	Sprinkled rainfall amount (mm)	WD (cm)
EV1	4.3	4.5
EV2	4.2	5.5
EV3	3.8	3.5
EV4	3.5	5
EV5	3.2	4

To validate the calibration process, θ_r and θ_{fc} were calculated using the ROSETTA software (Schaap et al., 2001) based on soil texture. The program input is the gravel, silt and clay fraction of the soil fine material (< 2mm) and the outputs are the van Genuchten parameters (n and α) (van Genuchten, 1980) and the saturated and residual water content (θ_s and θ_r). θ_{fc} is then calculated using the soil water retention curve (Assouline and Or, 2014) and corrected to include the permeable gravel fraction:

$$\theta_{fc\,(<2mm)} = \theta_r + (\theta_s - \theta_r) \cdot \left[1 + \left(\frac{n-1}{n}\right)^{1-2n}\right]^{\left(\frac{1-n}{n}\right)} \quad (30)$$

$$\theta_{fc} = \theta_{fc\,(<2mm)} \cdot (1 - Gf) \quad (31)$$

Where Gf is the observed volumetric gravel fraction, θ_r and θ_{fc} are calculated for each measured horizon (Table 2).

F_{PET} was estimated using sampled soil water profile measured in Holocene reg soils from Ze'elim site following recorded rain events (Table 6). Rainfall depths equal to the recorded values, were inserted to the model using a range of possible F_{PET} values (0.1-3.0 with 0.1 interval), and PET values were supplied by the WG according to the month when the measurements were taken. RMSD score was calculated as the deviation from the observed and the calculated WD. Since soil measurements were given as gravimetric whereas the model uses volumetric measures, the following conversion was used:

$$\theta_v\left[\frac{cm^3_{water}}{cm^3_{dry\,soil}}\right] = \frac{\frac{m_{water}}{\rho_{water}}}{\frac{m_{soil}}{BD}} = \frac{BD\left[\frac{g}{cm^3}\right]}{\rho_{water}\left[\frac{g}{cm^3}\right]} \cdot \frac{m_{water}[g]}{m_{dry\,soil}[g]} = \frac{BD\left[\frac{g}{cm^3}\right]}{1\left[\frac{g}{cm^3}\right]} \cdot \theta_g\left[\frac{g_{water} - g_{dry\,soil}}{g_{dry\,soil}}\right] \quad (32)$$

Where θ_g and θ_v are the gravimetric and volumetric soil content respectively, ρ_{water} is water density (1 g cm^{-3}) and BD is the bulk density. BD was set to BD = 1.33 g cm^{-3}, this value was used by Amit (1990) for similar calculation during the work on reg soils in the study area.

Table 6: Soil water content measurements were taken after recorded rain events in ZEL11 profile at Ze'elim alluvial fan. Water values were given in gravimetric content and converted to volumetric using Eq. 32.

Sampling date	Rainfall depth [mm]	Sampling time [h] after rain event	Sample top depth [cm]	Water in soil [g/g]	Water in soil [$cm^3\ cm^{-3}$]
7.2.1988 (Amit, 1990)	21	48	0 10 20 30 40	0.03 0.02 0.02 0.02 0.01	0.04 0.03 0.03 0.03 0.01
12.3.2020 (this study)	14	72	0 10 20 30 40	0.02 0.04 0.01 0.00 0.01	0.03 0.06 0.01 0.00 0.01

4.3.2 *Sulfate concentration in rainwater and annual dust flux*

Sulfate (SO_4^{2-}) concentration in rainwater and annual dust flux were calibrated using measured gypsum profiles from both Ze'elim and Shehoret Holocene soils. The range of tested sulfate values was 0 – 20 mg l^{-1} with 0.1 mg l^{-1} interval. For annual dust flux, the tested values range was 0 – 10 g m^{-2} yr^{-1} with 0.1 g m^{-2} yr^{-1} interval. During the early stages of soil formation (i.e., Holocene), gypsum is spread along the soil profile with no distinct gypsic horizon (Amit et al., 1993). Thus, the simulated gypsum profiles were compared to the measured ones based only on the mean gypsum concentration over the profile. Mean gypsum concentration is given by:

$$\overline{gyp}\left[\frac{meq}{100g\ soil}\right] = \frac{\sum_{i=1}^{Max.Horizon} gyp_i\left[\frac{meq}{100g\ soil<2mm}\right]\cdot th_i[cm]}{\sum_{i=1}^{Max.Horizon} th_i[cm]} \quad (33)$$

Where $Max.horizon$ in the total number of horizons in measured profiles or compartments in simulated profiles. gyp_i is the gypsum concentration in the compartment/horizon, th_i is the compartment/horizon thickness (constant value of 5 cm for simulated profiles).

Gypsum concentration in measured profiles is calculated for the fine fraction of the soil sample (< 2 mm). Compartments in the simulated profiles can be considered as 5 [cm^3] of gravel free soil composed of homogeneous fine material (< 2 mm). Correction of the measured concentration is therefore required for comparing simulated and measured profiles:

$$gyp_i\left[\frac{meq}{100g\ soil\ bulk}\right] = gyp_i\left[\frac{meq}{100g\ soil<2mm}\right]\cdot(1-Gf) \quad (34)$$

Where Gf is the observed volumetric gravel fraction as appear in Table 2.

The WG supplied the stochastic rain series according to the location of the measured profile to be compared, and computation time was set to the OSL age of the profile (10.3 Ka in Zel11, 13.5 Ka in T1.9 and T1.10). Each combination of the calibrated parameters was tested for each measured profile and for 100 repetitions to minimize the stochastic uncertainty. RMSD score was calculated for each combination of the parameters as the deviation between the observed and measured mean gypsum concentration:

$$RMSD_{DF,SO4} = \sqrt{\frac{\sum_{p=1}^{p=3}\sum_{i=1}^{100}(S_{p,i}(D_p,\theta_{fc},\theta_r,F_{PET},DF,SO4,\dots)-O_p)}{300}} \quad (35)$$

Where DF is annual dust flux g m^{-2} yr^{-1}, SO4 is sulfate concentration in rainwater mg l^{-1}, p is the Holocene profile number, i is the repetition number, $S_{p,i}$ is a calculation for each profile and repetition, D_p is the age

of the observed profile and O_p is the mean gypsum concentration in the profile $\left[\frac{meq}{100g\ soil}\right]$. 300 samples are ultimately calculated. The error for the OSL ages is neglected since the stochastic uncertainty incorporates it. The validity of this assumption was strengthened in and discussed the results section.

4.4 *Sensitivity analyses*

To evaluate the effect of soil and climate parameters on total gypsum concentration and depth of maximal gypsic content (i.e. the depth of the gypsic horizon) in simulated profiles, sensitivity analysis was conducted following two separate procedures.

4.4.1 *Local sensitivity to calibrated parameters*

To evaluate the local sensitivity of the mean gypsum concentration and gypsic horizon depth to field capacity, residual water content, sulfate concentration in rainwater, and annual dust flux, the model was supplied with a rainfall and PET series representing the current climate in Elat and Sedom. The model was tested with parameters modified to ±20% of their calibrated values, with soil profile thickness of 100 cm. To overcome the stochastic uncertainty, 100 calculations were conducted for every parameter modification. Each result was compared to a reference result calculated with unmodified parameters and with identical rainfall/PET series. To minimize the effects of pedogenic processes, soil hydrology alteration and climate change, the computation duration was set to 10 Ka (Holocene). The relative sensitivity of a parameter is calculated as follow:

$$S_i^r = \frac{M(Z_i+\Delta Z_i)-M(Z_i)}{\mathrm{M(Z_i)}} \cdot \frac{Z_i}{\Delta Z} \quad (36)$$

Where S_i^r is the relative sensitivity of parameter i, M is the model, Z_i is the calibrated value of parameter i and ΔZ_i is the difference from the calibrated parameter (i.e., $\pm\ Z_i \cdot 0.2$). This value is calculated for each parameter and for both output values of mean gypsum concentration and gypsic horizon depth.

4.4.2 *Sensitivity to climate properties*

To evaluate the sensitivity of the mean gypsum concentration and gypsic horizon depth to mean annual rainfall, mean number of annual rain days and PET, the model was supplied with modified rainfall/PET series. The calibrated parameters were set to their reference values and soil profile thickness was set to 100 cm. Each of the climate related parameters was tested separately by calculating gypsum profiles using a wide range of possible values: for mean annual rainfall the tested values were 0 – 100 mm with 1 mm interval, for mean annual rain days the tested values were 1 – 30 with 1 day interval, for annual PET the tested values were 900 – 2400 mm with 300 mm interval. Each value was tested 100 times to neglect stochastic uncertainty.

4.5 *Late Pleistocene scenarios*

To estimate the climate properties that led to the formation of the late Pleistocene reg soils (22.9 Ka in Ze'elim and 62.5 Ka in Shehoret), the model was tested with numerous, stochastically-generated rain and PET series, modified from the current climate as a basis. Mature profiles were calculated in two steps to incorporate both late Pleistocene and Holocene conditions: (1) A modified scenario was used for the first 12.9 Ka and 53 Ka of computation time duration in Ze'elim and Shehoret respectively. (2) A Holocene scenario of calibrated values and recent climate properties was used for the last 10 Ka of the computation time. The cluster of simulated gypsum profiles calculated using these various climate scenarios differ by mean annual rainfall, number of rainy days, annual PET, dust flux and sulfate concentration in rainwater.

Each parameter examined for a range of potential values (Table 7) and each combination of parameters is supplied to the model as a scenario. The simulated gypsum profiles of each scenario were subsequently compared to the gypsum profiles observed in mature surfaces.

Table 7: Scenarios parameters and range of tested values. Intervals appear in brackets.

Mean annual rainfall (mm)	Mean number of wet days per year	Mean annual PET (mm)	Sulfate concentration in rainwater (mg l^{-1})	Annual dust flux (g m^{-2} yr^{-1})
10:100 (10)	1:18 (2)	1200:2400 (400)	8:24 (2)	1:31 (10)

To test the model results, several late Pleistocene soils were used. Based on these soils, a mean gypsum concentration was calculated and a range for gypsic (Bmy/By) horizon was set for a given surface/age (Table 8). Scenarios were estimated according to the success rate in yielding profiles which exhibit gypsum concentration in the range of the observed value ± 10% and gypsic horizon depth within the range of the observed depth. Each scenario was tested 100 times to reduce the stochastic uncertainty. The range of potential values tested for each parameter is extremely broad at first to disqualify out of range parameters. After several batches of calculation, the range was reduced and tested values resolution increased. The final set of scenarios was eventually simulated 100 times to find the most likely scenarios.

Table 8: Gypsum properties for late Pleistocene surfaces. By depth range is the top and bottom of the shallowest and deepest By horizons in the surface, respectively. The mean gypsum content is the mean of all the soil horizons

Site	Surface	OSL age [yr]	Profiles	Bmy/By Depth [cm]	Mean gypsum [meq/100 g bulk]
Ze'elim	1	22900	ZEL1 ZEL2	30-70	17.3± 2
Shehoret	Qa1	62500	T1.1 T2.1 Shehoret1 Shehoret3	10-20	70± 7

5. Results

5.1 *Weather generator*

The WG produced daily rainfall and PET series simulates the current climate conditions at both study sites. The examined rainfall properties are wet days probability, distribution of annual rainfall depth and number of annual wet days. Examined PET properties are mean daily PET and daily PET distribution. 1500 simulated series of 60 years duration are aggregated to evaluate the median value and uncertainty. Daily PET distribution appears bi-modal as the two modes represent winter and summer. The simulated climate properties are overall in good agreement with the observed data (Figure 9).

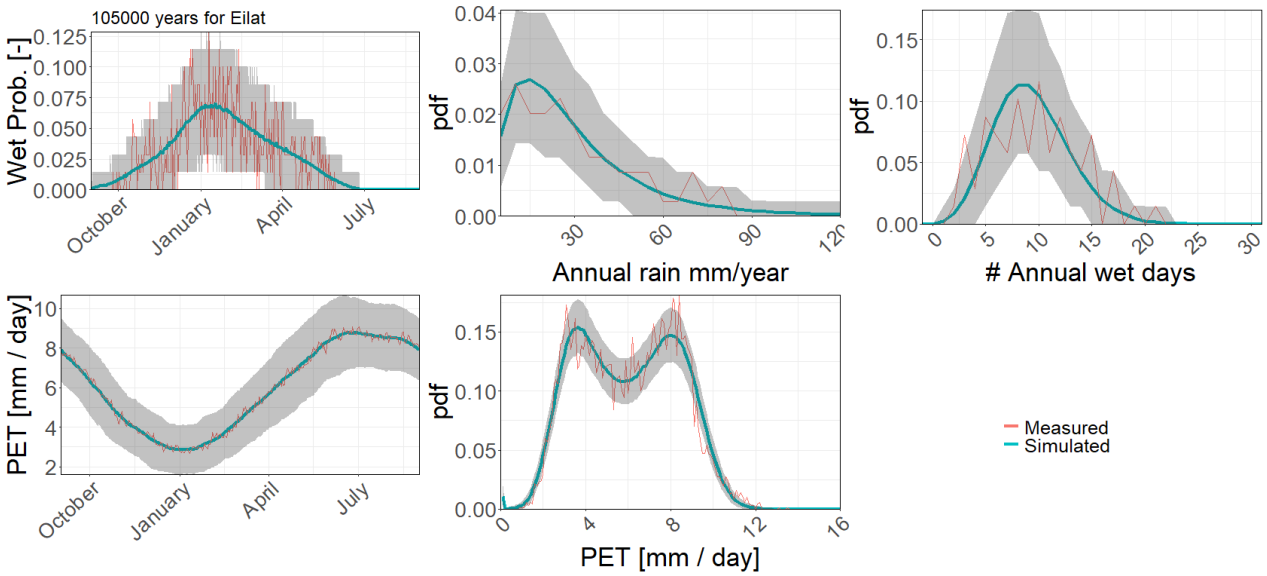

Figure 9: 1500 simulated series of 70 years duration (overall 105,000 years) are aggregated and compared to the IMS measured series of 70 years (1949-2019) for Elat station. The simulated green curve represents the median value of the simulated series. The gray area represents the 5% and 95% uncertainty range from the median. The orange curve is the measured data supplied by the IMS.

5.2 *Calibration*

5.2.1 *Water-related parameters*

Water curves measured during the summer indicate that $\theta_r = 0.010 \frac{g_{water}}{g_{soil}}$. This value was converted to volumetric water content of : $\theta_r = 0.013 \frac{cm^3}{cm^3}$ using Eq. 32 with bulk density value of $BD = 1.33$ (Figure 10). The calibration procedure of field capacity yield a value of $\theta_{fc} = 0.1 \frac{cm^3}{cm^3}$ with the minimal RMSD score (Figure 11).

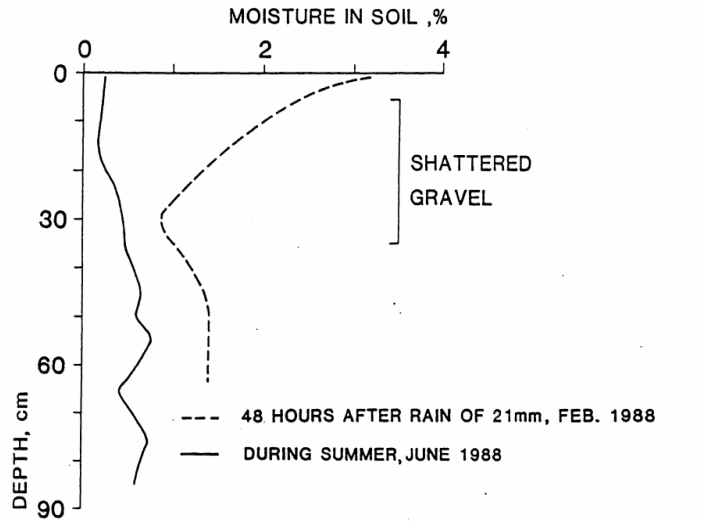

Figure 10: Volumetric water content measured in Holocene reg soils in Ze'elim (Amit, 1990). *Summer measurements represent the residual water content that equals to ~1% =* $0.010 \frac{g_{water}}{g_{soil}}$.

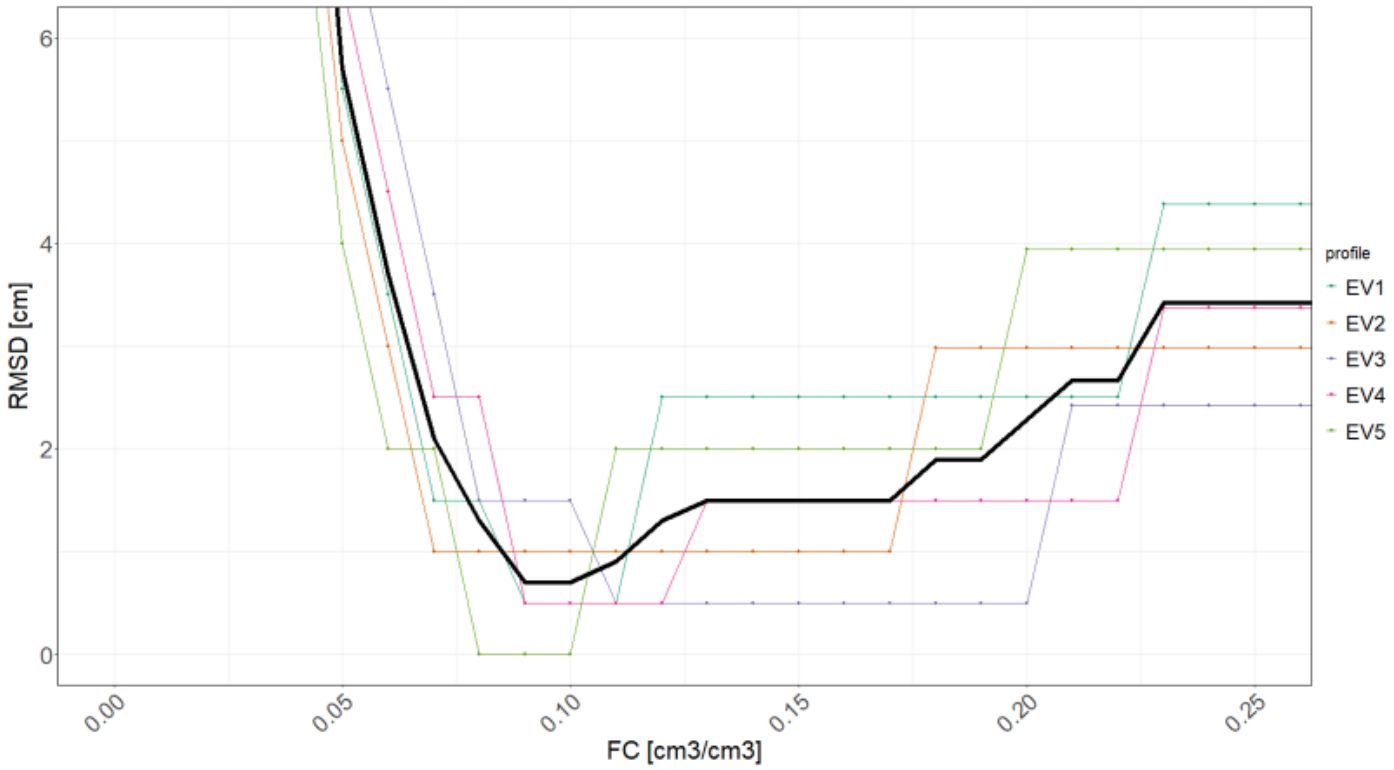

Figure 11: Calibration of field capacity using wetting depth values measured in Holocene soils in Evrona after recorded rain events. Mean value is presented in black. The lowest RMSD is for field capacity of 0.1 cm³ cm⁻³.

Estimation of soil parameters based on soil texture was calculated for every horizon of the measured profiles. The mean values of θ_{fc} and θ_r for Holocene soil profiles from both study sites are compared to the calibrated values and are in general agreement (Table 9).

Table 9: Calibrated values compared to values calculated using soil texture properties.

Parameter	**Calibrated values [cm³ cm⁻³]**	**Average calculated values [cm³ cm⁻³]**	**Percentage difference* [%]**
θ_r	0.013	0.018±0.013	28%
θ_{fc}	0.100	0.105±0.062	5%

(*) $\frac{calibrated-calculated}{calculated} * 100$

The calibration procedure resulted in $F_{PET} = 1.2$ (Figure 12). This result suggests that the AET values, calculated according to PET values generated by the WG, are underestimated, and should be increased by 20%.

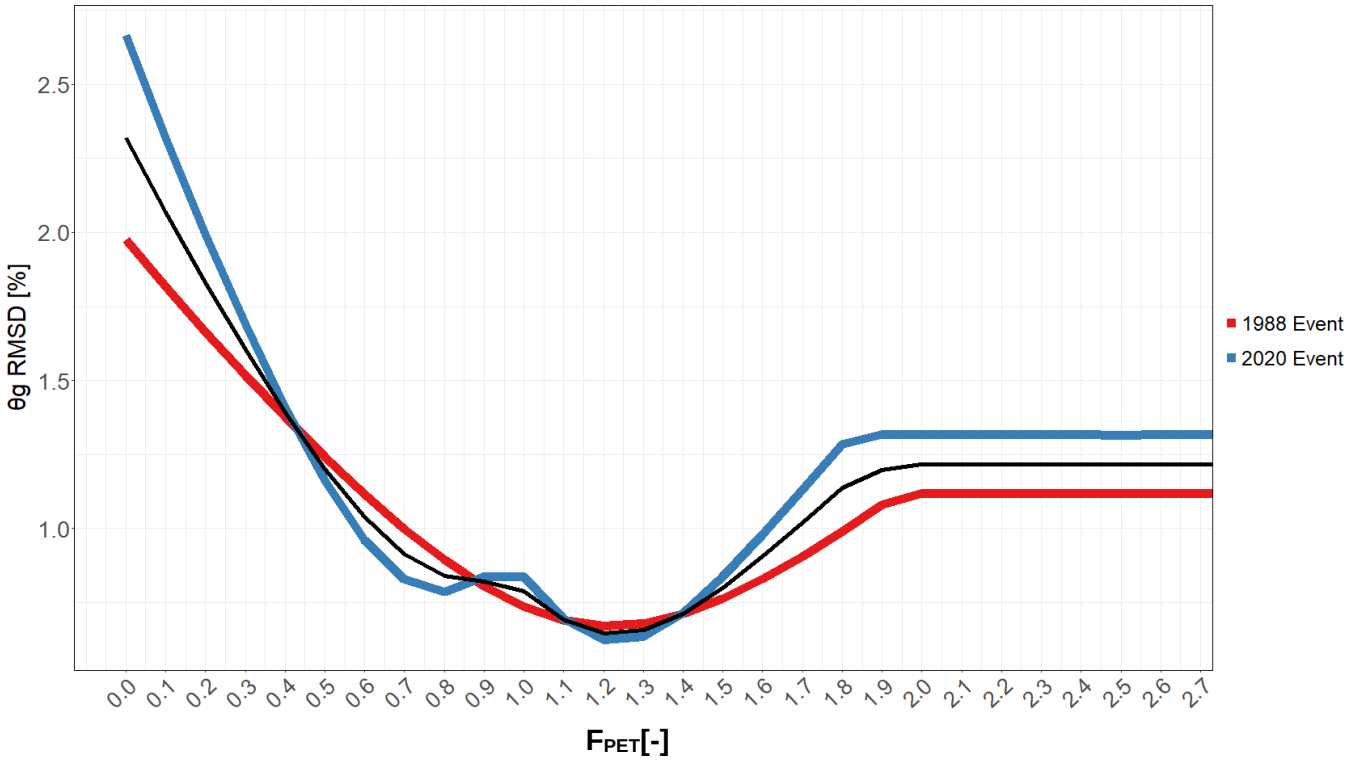

Figure 12: Calibration of the factor of evaporation using two water profiles measured few days after a recorded rain event in Holocene reg soils in Ze'elim. The black curve is the mean value. The lowest RMSD is for F_{PET} of 1.2.

5.2.2 *Gypsum parameters*

The calibration procedure using measured Holocene reg soils results in optimal values of 10 mg l^{-1} for sulfate concentration in rainwater and 2.5 g m^{-2} yr^{-1} for annual dust flux (Figure 13). The response surface demonstrates that the target function of mean gypsum concentration (Eq. 33) is not sensitive to annual dust flux, whereas it is highly sensitive to sulfate concentration in rainwater.

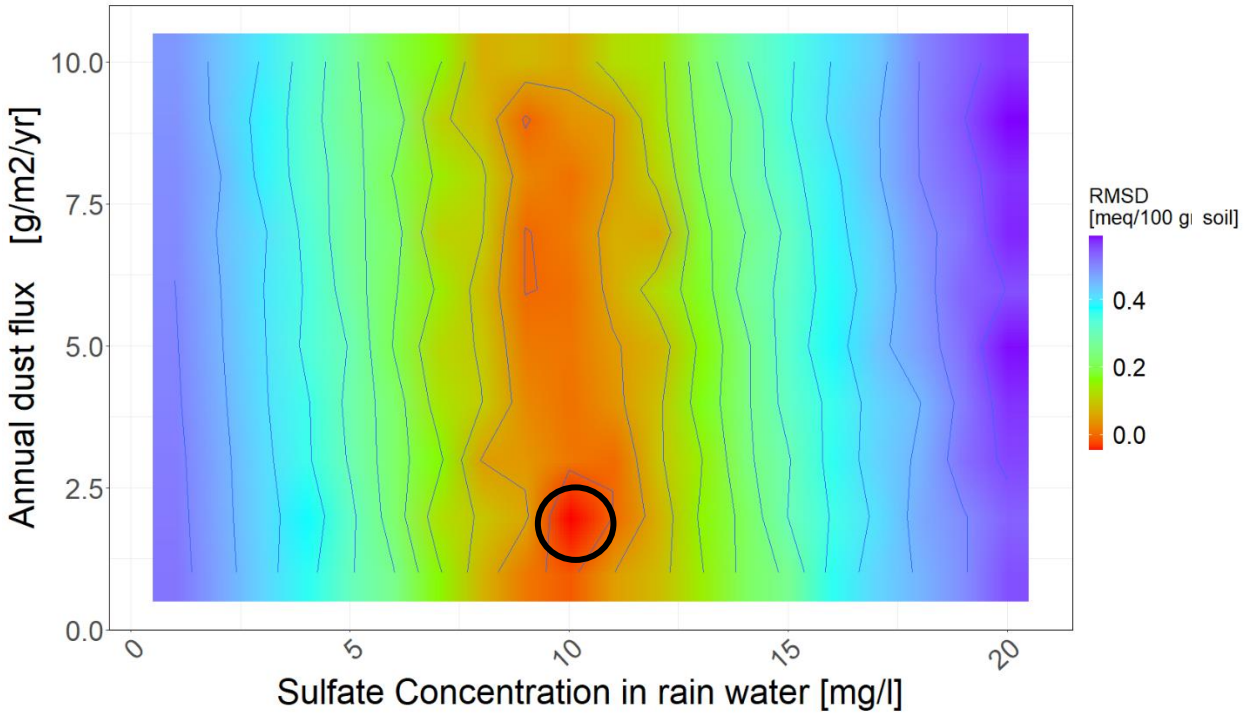

Figure 13: Response surface for calibration of annual dust flux and sulfate concentration in rainwater, based on gypsum profiles measured from Holocene reg soils (ZEL11, T1.10, T1.9). Red colors represent a good approximation to the measured surfaces; The lowest RMSD surrounded by a black circle is for annual dust flux of 2.5 $g\ m^{-2}\ yr^{-1}$ and sulfate concentration in rainwater of 10 mg l^{-1}.

5.3 *Local sensitivity analyses*

Local sensitivity analyses for soil parameters, sulfate concentration in rainwater and annual dust flux, indicate that gypsum mean concentration and accumulation depth are very sensitive to sulfate concentration in rainwater: increase in sulfate concentration lead to an increase in mean gypsum concentration and to deeper accumulation of gypsum. Field capacity greatly affect gypsum accumulation depth (higher field capacity leads to deeper accumulation depth) but has limited effect on the mean gypsum concentration. is inversely proportional to gypsic horizon depth (Figure 14). All other examined properties do not seems to greatly influence gypsum concentration and depth.

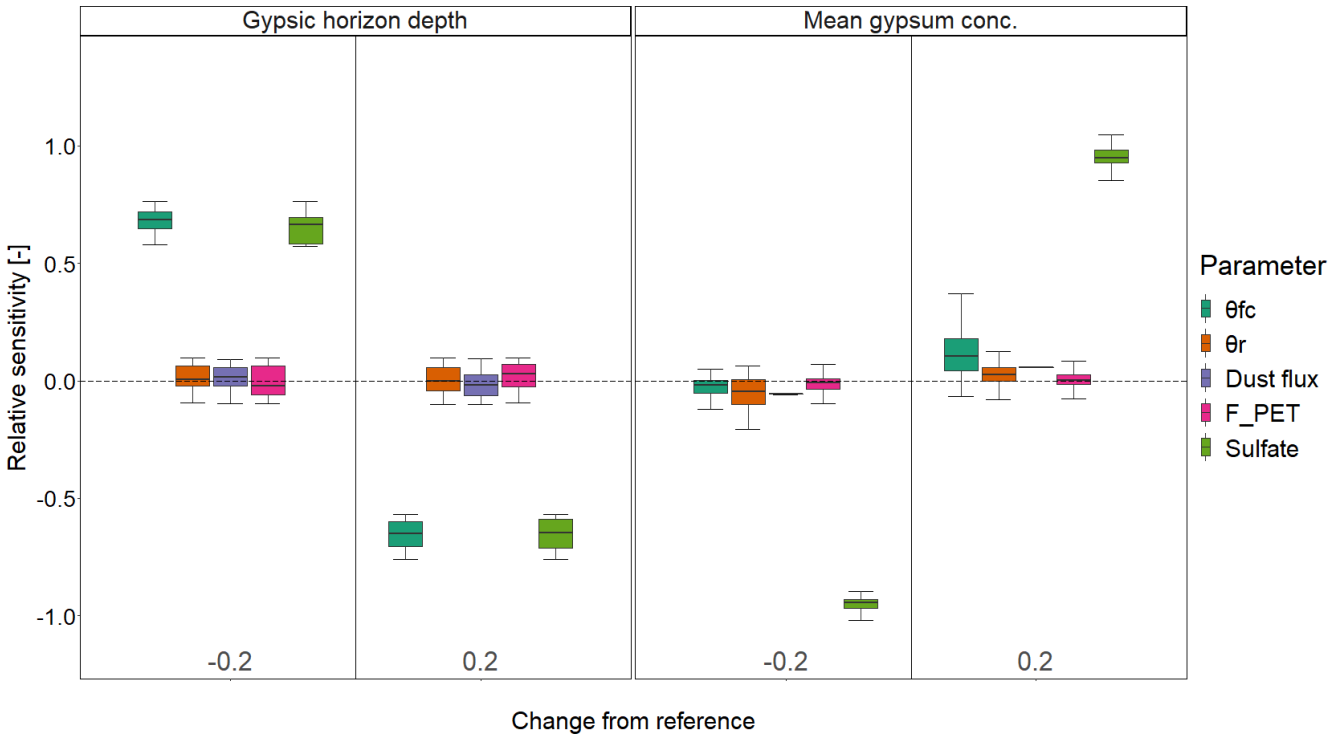

Figure 14: Relative sensitivity of soil and dust related parameters with the range of change of +0.2 or -0.2 (±20%) from the calibrated parameters. Boxplots of the 95% uncertainty range (i.e., the difference between the 97.5% and the 2.5% quantiles) of relative sensitivity for each parameter. The black line in each boxplot marks the median, the boxes lower and upper border represent the 25% and 75% quartiles, respectively, the whiskers mark the minimum and maximum values, unless these values exceed $1.5 \cdot IQR$ *(inter quartile range – the distance between lower and upper quartiles). Each box represents 100 comparisons between results generated with modified parameters and results generated with calibrated parameters.*

An increase in annual rain depth will lead to a higher mean gypsum concentration in the profile. However, exceeding a threshold value of rain (in this case, 300 mm yr^{-1}) leads to an extensive downward water transport in the soil column and pronounced deep leaching of gypsum from the soil column. The threshold value depends on the thickness of the modeled soil profile (in this case, 100 cm); for thicker soils, the threshold will increase, and vice versa. Higher mean annual rainy day depth also leads to an increased depth of gypsic horizon (Figure 15). Local sensitivity was tested for several PET values, the results indicate that gypsic horizon depth is located in shallower depths as annual PET increases (Figure 16).

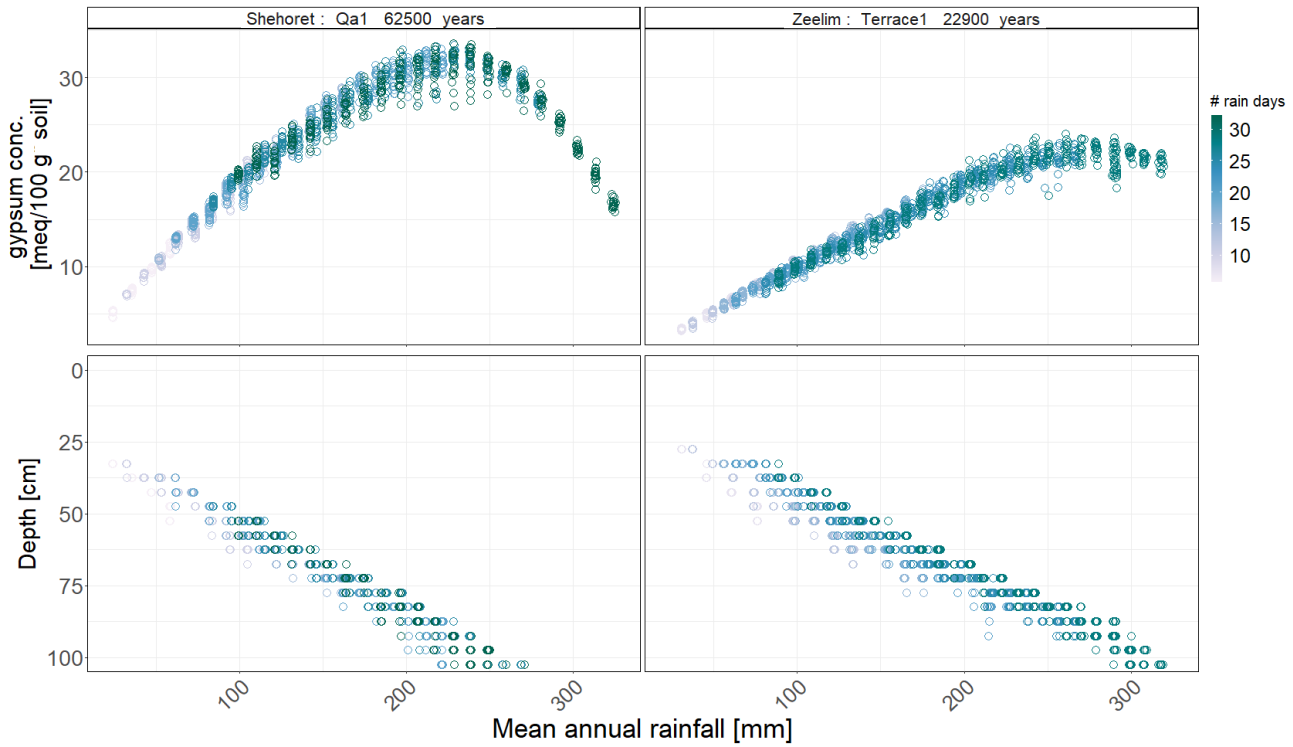

Figure 15: Sensitivity analysis for mean annual rainfall and rain event depth. Gypsum concentration and depth increases as more water is supplied by rainfall while further increase leads to dissolution and downward washing. Note that for a given annual rainfall less rain days will result in increased depth, i.e., gypsic horizons deepens as rain event depth increases.

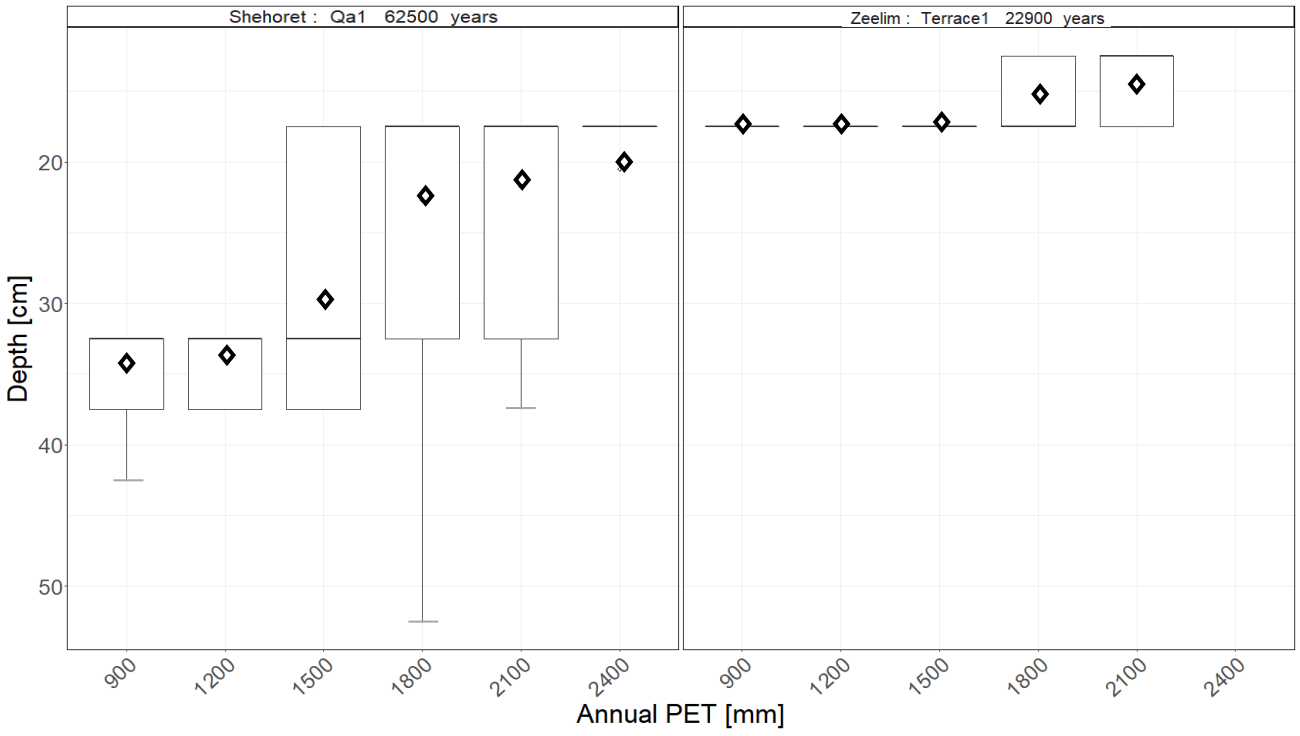

Figure 16: Local sensitivity analysis for annual PET in both regions. Boxplots of the 95% uncertainty of gypsic horizon depth for different annual PET values (see figure 14 for elaborated explanation on boxplots). Diamonds represent the mean value. Since the calculated depth is in 5 cm resolution the mean value better represents the difference between results for different PET values. Note that gypsic horizon depth shallows as the annual PET increases.

5.4 *Gypsum accumulation rate*

Mean annual rainfall and sulfate concentration in rainwater are the most influential parameters. The model was used to quantify the effect of these two properties on the gypsum accumulation rate (Figure 17A). 1000 years of gypsum accumulation using a range of values for sulfate concentration in rainwater and modified climate series with different mean annual rainfall. The series was modified after the Holocene rain series in Elat in a similar process used to receive the results for the sensitivity analysis. Gypsum accumulation rate as a function of mean annual rainfall and the total amount of sulfate that infiltrates the soil (both from rainwater and dust) is presented in Figure 17B. The features of these figures are further discussed in 6.5.

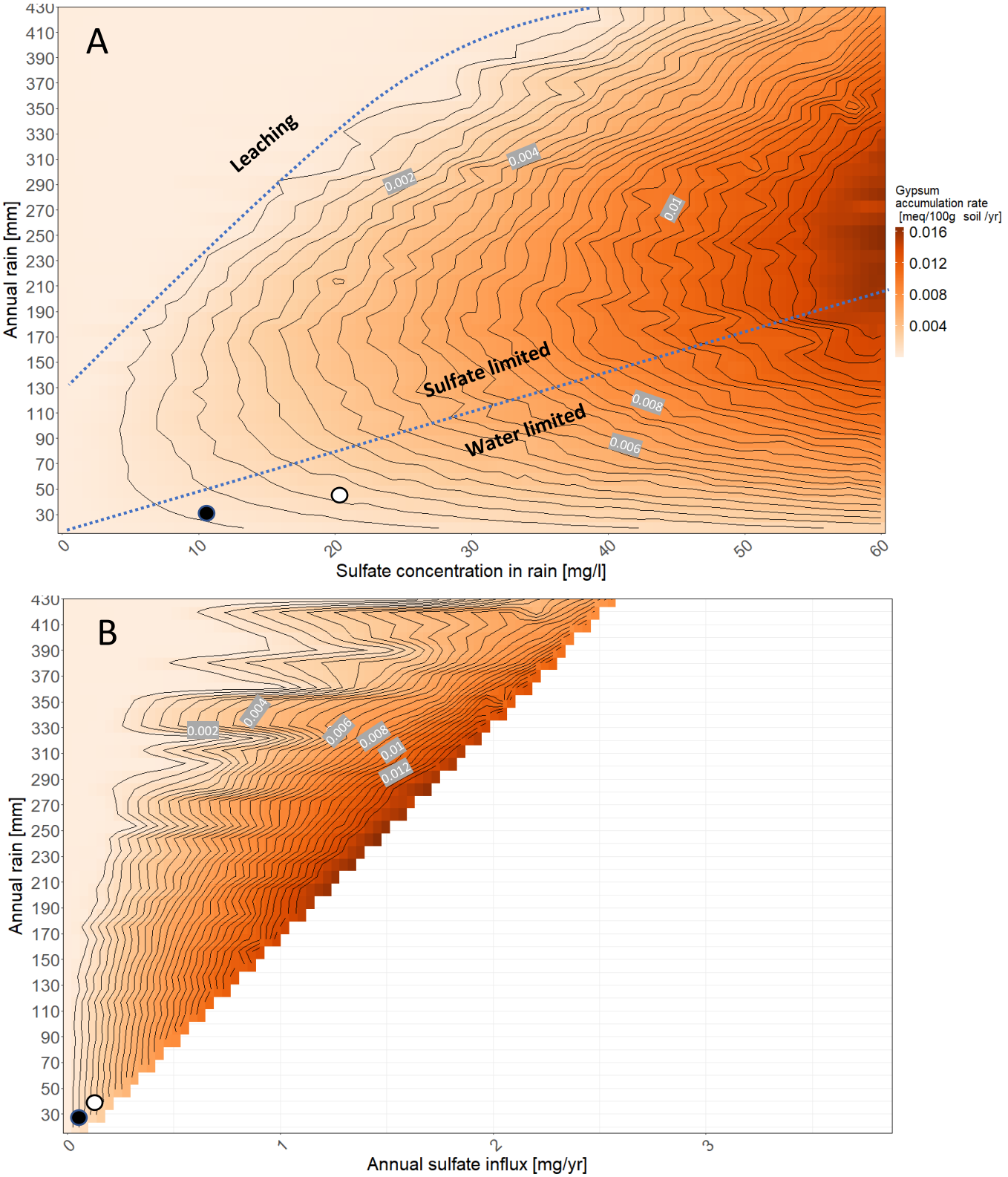

Figure 17: Gypsum accumulation rate as a function of mean annual rainfall and (A) sulfate concentration in rain . (B) as figure A but with actual amount of sulfate infiltrating the soil. 1000 years calculation was tested for each combination of the two parameters, using the parameters calibrated for Holocene profiles, and without including the field capacity and runoff modules. The black circle indicates the accumulation rate expected in the the study site under current climate conditions. The empty circles indicate the rate expected for a possible late Pleistocene scenario described in section 5.5.

5.5 *Late Pleistocene profiles*

Gypsum profiles of late Pleistocene soil were calculated with the runoff and field capacity modules (Figure 18). The runoff module lowers the amount of water entering the soil with time (and hence the gypsum flux) and reduces gypsum mean concentration. The field capacity module yields a shallower gypsic horizon as WHC increases; Increase in field capacity also slightly increases the gypsum content in the soil; The combinations of the modules yields a shallower gypsic horizon and reduces the concentration of gypsum in the soil profile.

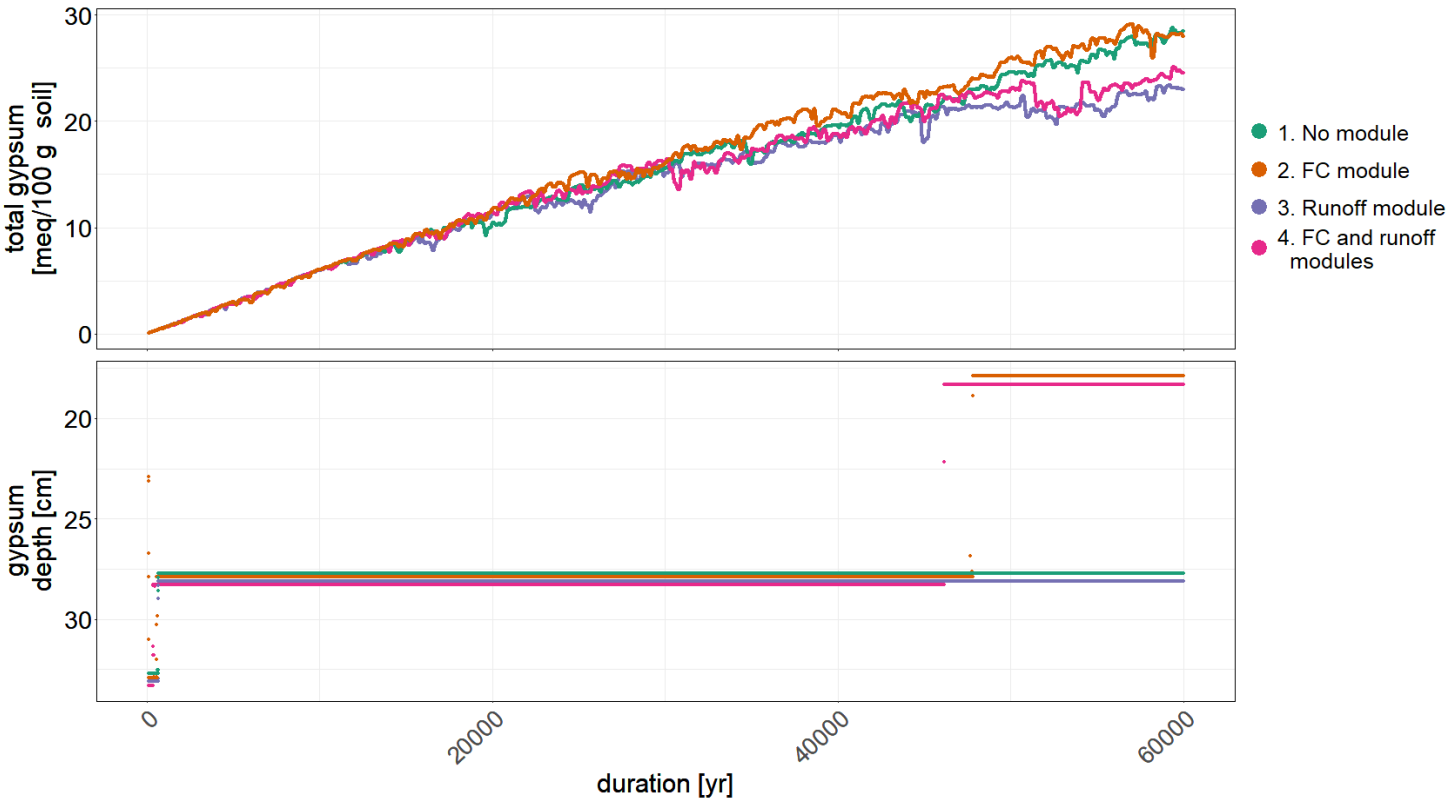

Figure 18: Effect of field capacity and runoff modules over gypsum accumulation. Modules integration results in reduction of gypsum concentration and shallowing the gypsic horizon depth. Each curve was calculated using modified rainfall series of 40 mm yr^{-1} , 10 annual wet days and sulfate concentration of 20 g l^{-1} . Soil column height was set to 100 cm.

Running the calibrated model with current (Holocene) climate conditions for 62.5 Ka, generated a gypsum profile that is very different than the measured one (late Pleistocene profile T2.1 in Shehoret site), with much lower mean gypsum concentration and a deeper maximal gypsic horizon (Figure 19). The sensitivity analyses imply that higher mean annual rainfall and/or higher sulfate concentration in rainwater are required to reach the observed gypsum concentration.

The simulated profiles that fall within the range of gypsum depth and concentration observed in mature late Pleistocene reg soils in the study area are considered to represent plausible climate scenarios. Due to the stochastic uncertainty, each scenario was simulated 100 times and estimated by the number of successful forecasting, i.e., generate a profile that falls inside the desired range (Figure 20).

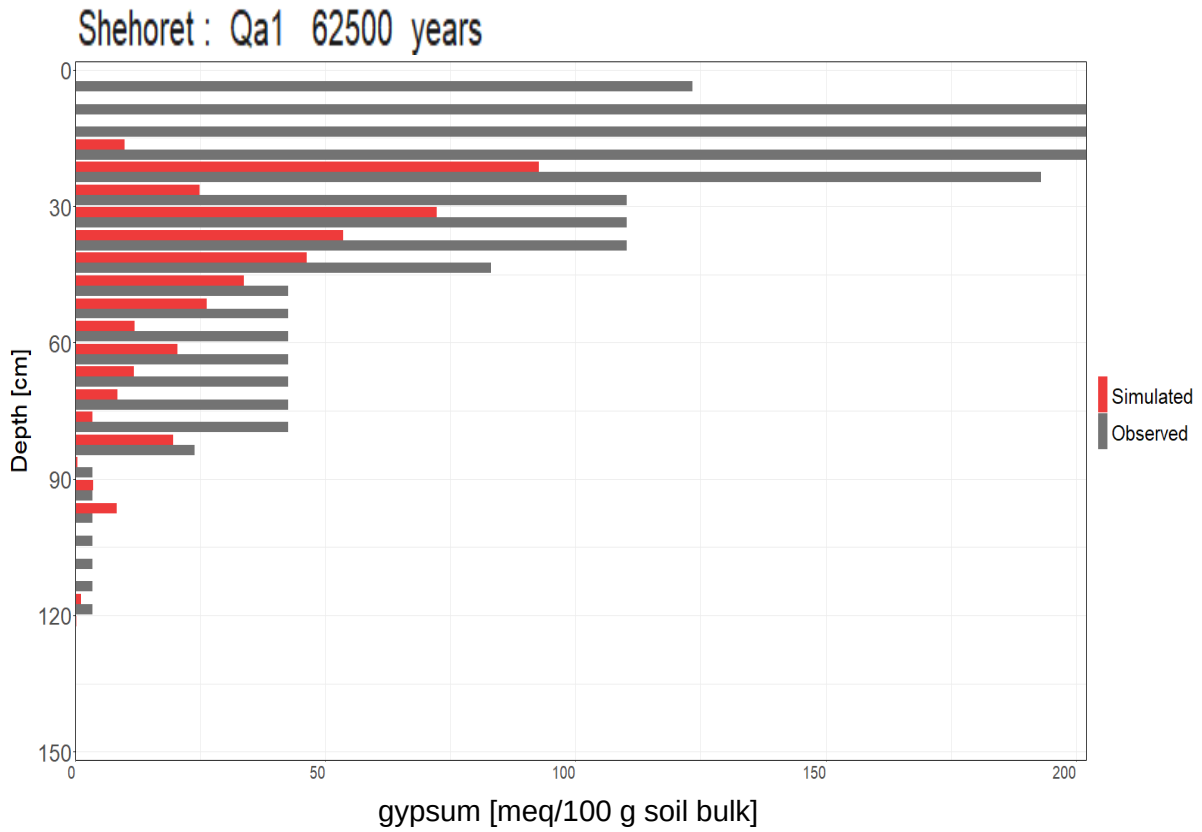

Figure 19: Simulated gypsum profile for 62.5 Ka with current climate in Elat and parameters calibrated for Holocene profiles. The concentration of the observed profile is corrected for gravel content. Note how the simulated profile differ from the measured one for 62.5 Ka surface.

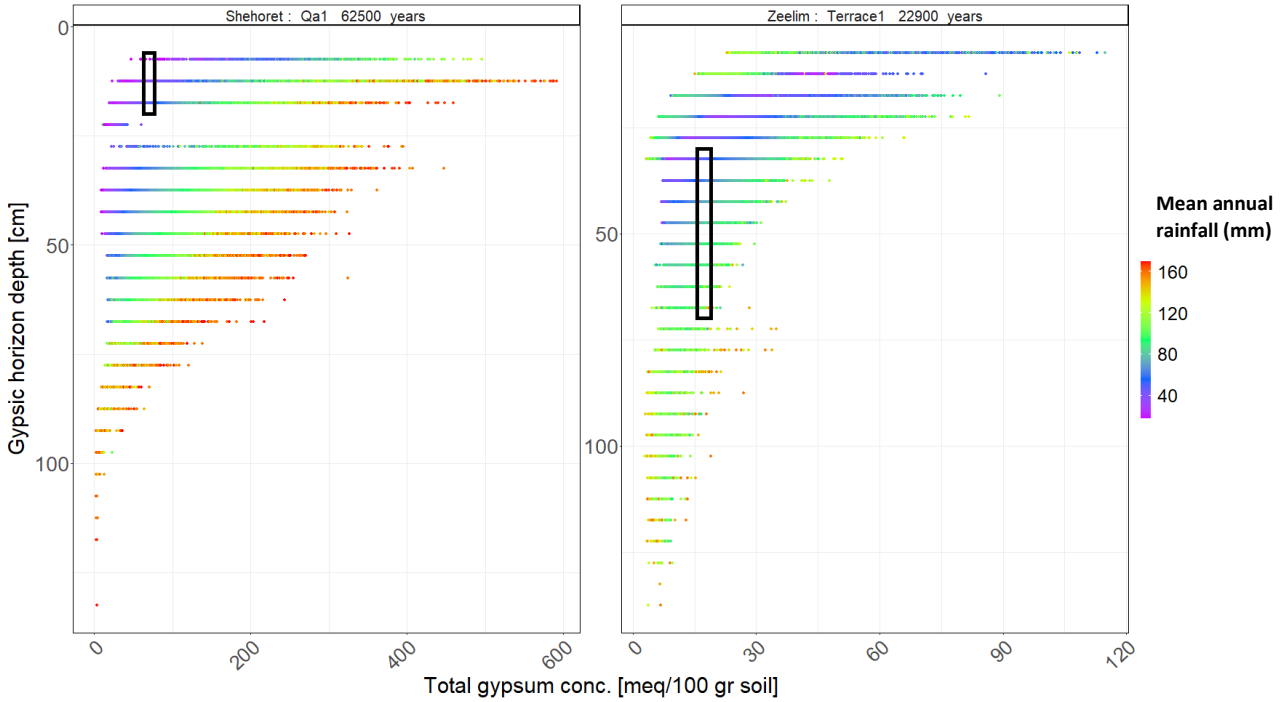

Figure 20: Computations cluster for both study sites. Black square indicates the measured range of gypsum concentration and gypsic horizon depth. Gypsum concentration range is the average value of the horizons in each profiles (T1-1, T2-1, Sheoheret1 and Sheoheret3 for Shehoret Qa1 ; ZEL1 and ZEL2 for Ze'elim Terrace 1) ± 10%. Gypsic depth range is the difference between the shallowest and deepest By horizon of the profiles at each surface.

The late Pleistocene scenarios for Ze'elim (22.9-10 Ka) and Shehoret (62.5-10 Ka) that were found plausible with high success rates were aggregated by the composing parameters (Figure 21 A, B). For each parameter, the discussed range of possible values is between the 25% and the 75% percentiles, denoted in the plot as the inter quartile range (IQR). The possible values of mean annual rain ranges from 40 to 50 mm in Shehoret and 40 to 60 mm in Ze'elim. These ranges are much higher than the current mean annual rainfall (18 and 39 mm, respectively) and are relatively narrow compared to the entire range of possible values (10 - 120 mm yr^{-1}). A relatively narrow range is also demonstrated for the mean annual rain days and sulfate concentration in rainwater. However, PET and dust flux are dispersed over the tested range and therefore exhibit less accurate estimations. Results also indicate that 5 to 15 annual rain days are estimated for Shehoret, and 5 to 16 annual rain days are estimated for Ze'elim. In Shehoret, the most likely sulfate concentration in rainwater range from 15 to 25 mg l^{-1}, much higher, than the calibrated value (Holocene) of 10 mg l^{-1}. Sulfate concentration in Ze'elim remains unchanged. A wide range of annual dust flux is feasible, however, most of the aggregated scenarios include dust flux higher than the current 2.5 g m^{-2} yr^{-1}, as suggested by the median value.

Since few of the examined parameters are expected to be correlated, a correlation matrix complements the range of values found for each parameter (Figure 21 C, D). High positive correlation between mean annual rain and mean annual rain days, suggests that both parameters should increase to maintain the desired gypsic horizon depth. A strong negative correlation between sulfate concentration in rainwater and mean annual rainfall is expected since gypsum concentration was found to be highly sensitive to both parameters. Negative correlation between dust flux and sulfate concentration in rainwater is also expected since both contribute to the gypsum accumulation, however, the relatively low correlation value follows the reduced effect of dust flux over gypsum accumulation. PET is not well correlated with other parameters, though negative correlation with sulfate concentration in rainwater shows that both parameters affect gypsum accumulation, an observation that concords with the PET sensitivity analysis.

The scenario with the highest confidence level was tested 500 times, the range of results is plotted against the range of gypsic depth and concentration observed in the terrace at the study area (Figure 22). All the computations were run for a duration of 63000 ± 6000 years, to include the error on the OSL ages. Results indicate that the OSL error is neglectable compared to the dispersion generated by the stochastic rain series.

Table 10: Scenarios for Shehoret and Ze'elim that exhibit >= 90% and >= 85% success rate, respectively.

Region	OSL age (Ka)	Sulfate concentration in rainwater (mg l^{-1})	Annual dust flux (g m^{-2} yr^{-1})	Mean annual rainfall (mm)	Mean annual number of wet days per year	Annual PET (mm)	Success rate (%)
Shehoret	**62.5**	20	20	41.9	13.2	2590	100
		24	30	30.1	8.8	2600	99
		24	20	39.8	8.7	1730	99
		22	30	40.2	8.8	2600	98
		22	10	41.9	13.2	2590	98
		24	30	40.7	10.9	1300	98
		24	30	39.2	6.8	1300	98
		22	30	38.7	4.9	2170	97
		20	30	41.9	13.2	1290	97
		18	20	51.9	13.2	2590	97
		16	30	53.4	15.6	2580	97
		18	10	53.4	15.6	2580	97
		20	20	48.8	6.7	2170	97
		24	20	40.7	10.9	1300	96
		24	10	39.8	8.7	2160	96
		24	20	39.8	8.7	2160	96
		24	1	41.7	13.2	1290	96
		22	30	40.2	8.8	2160	96
		20	30	41.9	13.2	1720	96
		20	30	41.9	13.2	2160	96
		24	10	39.2	6.8	2600	95
		22	20	40.2	8.8	2600	95
		22	10	41.9	13.2	1720	95
		20	20	41.9	13.2	2160	95
		18	30	41.9	13.2	2590	95
		22	10	41.9	13.2	1290	94
		22	20	41.9	13.2	1290	94
		20	20	41.9	13.2	1720	94
		20	10	41.9	13.2	2590	94
		18	20	53.4	15.6	1720	94
		18	1	53.4	15.6	2580	94
		24	10	39.2	6.8	2170	94
		18	30	48.8	6.7	2600	93
		22	20	40.8	10.9	1300	93
		22	20	40.8	10.9	2160	93
		22	1	41.9	13.2	1720	93
		18	30	41.9	13.2	2160	93
		22	1	41.9	13.2	2590	93
		20	1	51.9	13.2	2590	93
		22	30	38.7	4.9	1740	93
		24	20	39.0	4.8	1300	93
		24	20	39.2	6.8	1300	93
		24	10	39.2	6.	1740	93
		24	20	39.2	6.8	1740	93
		24	1	39.2	6.8	2600	93
		24	20	39.8	8.7	1300	93
		24	10	39.8	8.7	1730	93
		20	30	40.8	10.9	2590	92
		22	10	40.8	10.9	2590	92
		22	20	40.8	10.9	2590	92
		22	30	39.6	6.8	1730	92
		22	30	40.2	8.8	1730	92
		22	20	40.2	8.8	2160	92
		24	10	40.7	10.9	1730	91
		24	1	40.7	10.9	2160	91
		24	30	30.1	8.8	2160	91
		22	30	40.8	10.9	1300	91
		20	10	41.9	13.2	2160	91
		22	1	41.9	13.2	2160	91
		18	30	51.9	13.2	1720	91
		18	20	51.9	13.2	2160	91
		16	30	51.9	13.2	2590	91
		18	10	53.4	15.6	2150	91
		24	10	40.7	10.9	2590	90
		22	30	40.8	10.9	2160	90
		18	30	50.8	10.9	2590	90
		24	1	39.2	6.8	2170	90
		24	10	39.8	8.7	2600	90
		18	30	48.8	6.7	2170	90
		20	10	51.9	13.2	1720	90
		20	1	53.4	15.6	1290	90
		20	1	53.4	15.6	1720	90
Ze'elim	**22.9**	10	30	39.7	8.8	1520	94
		10	20	46.8	13.8	1520	91
		10	1	56.2	15.6	2280	91
		10	10	47.5	12.1	2280	90
		8	30	56.1	13.8	2280	90
		10	10	56.3	15.6	2280	90
		8	30	56.6	15.7	2280	89
		8	20	56.5	15.7	2280	89
		8	30	56.5	15.7	1900	88
		10	30	39.7	8.8	1910	88
		8	30	56.2	13.8	1900	88
		10	10	57.0	12.1	1900	87
		8	20	65.0	15.5	2280	87
		10	30	38.7	10.5	1140	87
		10	20	48.4	10.4	2290	87
		10	20	47.4	12.1	1900	87
		8	30	46.8	13.8	1900	87
		12	20	32.4	5.3	1910	86
		12	1	48.4	10.4	1900	86
		10	30	40.9	7.1	2290	85
		10	30	32.5	5.3	2290	85

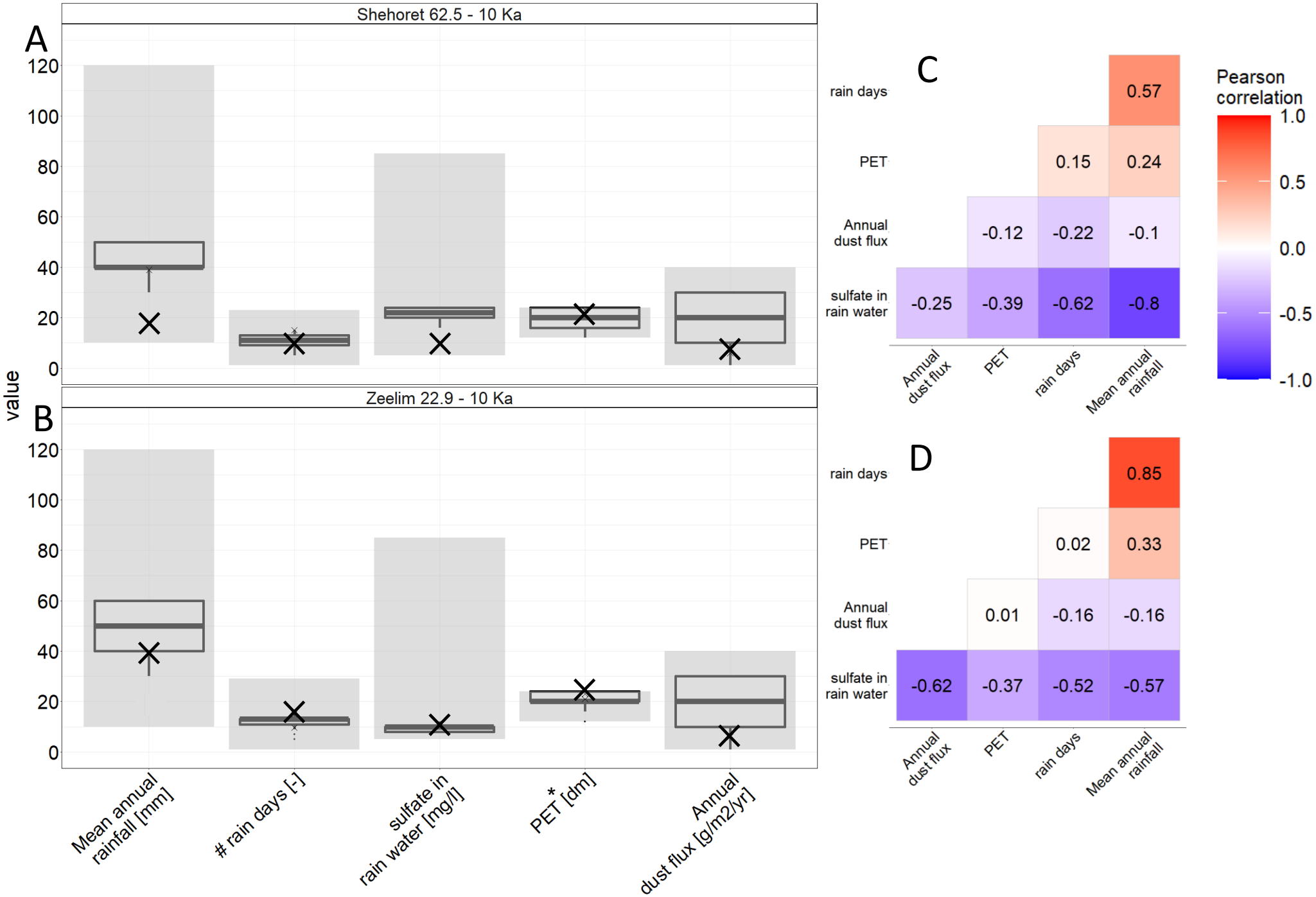

Figure 21: The most likely values of different cliamte and soil parameters that prevailed during the late Pleistocene (62.5 – 10 Ka for Shehoret, 22.9 – 10 Ka for Ze'elim) based on the best fitting scenarios. (A,B) . Boxplots of the 95% uncertainty of the value of each parameter in the most likely scenarios (see figure 12 for elaborate explanation on boxplots). The total range of tested values is indicated by the gray area. Current measured climate values and Holocene calibrated values appear as X (C,D) Pearson correlation for scenario parameters for both study sites. (*) Annual PET is denoted in Decimeters (10^2 mm) for comparison purpose.

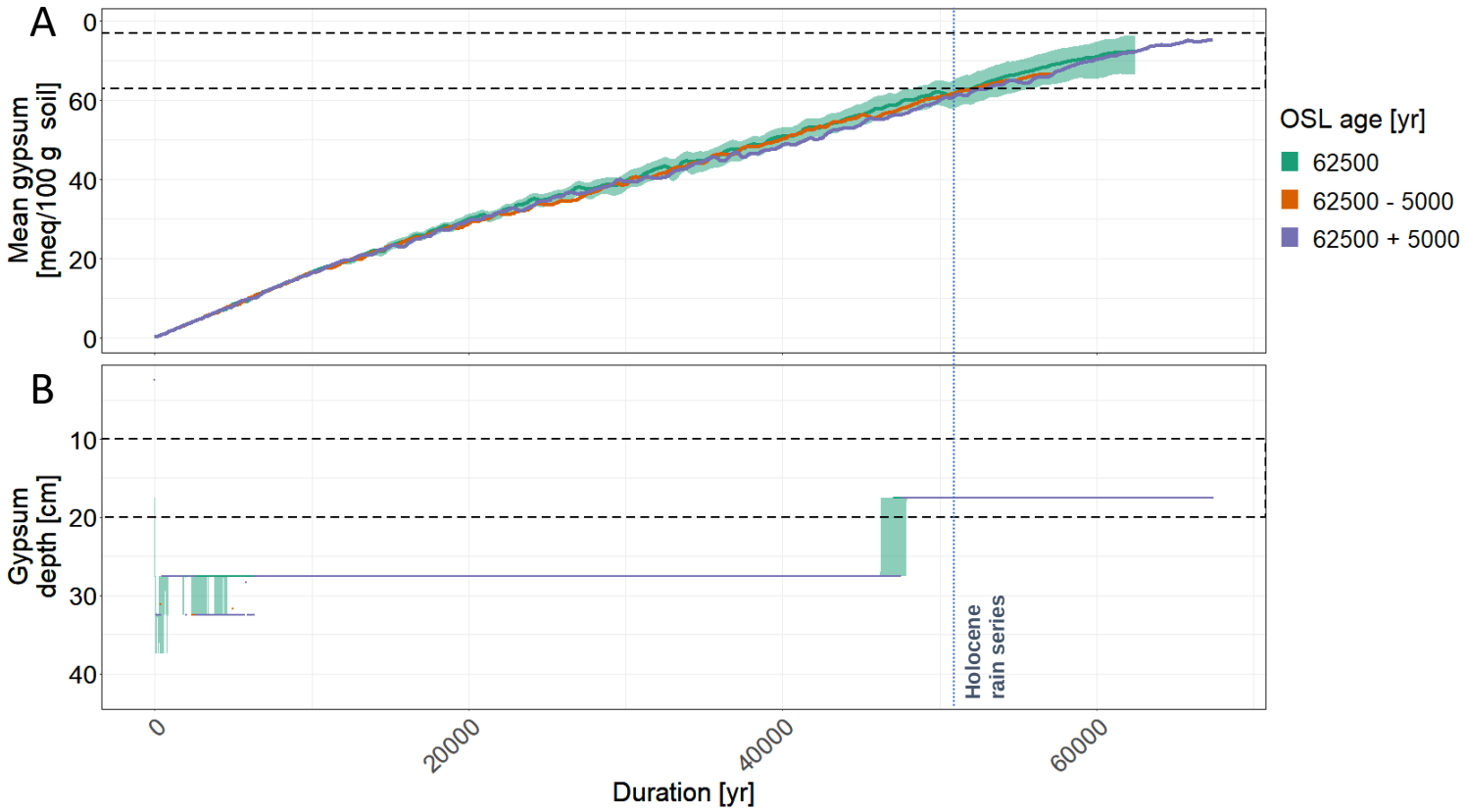

Figure 22: Gysum accumulation with time using the best fitted scenario for Elat late Plaistocene climate. (A) Mean concentration and (B) gypsic horizon depth with computation time. Curves represent different computation times to include the OSL dating uncertainty. Each curve is the median of 100 computations, green area represent the 5% and 95% percentile of all computations. Black horizontal lines represent the observed values in Qa1 surface. Blue vertical line represent the transition to Holocene rain series.

6. Discussion

In the course of this study, I modeled gypsum accumulation in soils as a response to different known controlling properties. WHC parameters (field capacity and residual water) content were calibrated to represent water distribution in Holocene reg soils. The quality of the calibration and approximation of these parameters is discussed in light of calculated parameters based on the reg soil texture. Properties that relate to sulfate sources (annual dust flux and sulfate in rainwater) were calibrated using gypsum profiles measured in Holocene reg soils. Sensitivity analyses shed light on the importance of the different properties that affect gypsum accumulation. Paleoclimate reconstruction was the final goal of the project, and numerous climate scenarios were tested to determine the most likely climatic conditions that prevailed in the study area during the late Pleistocene. These climatic conditions are further discussed and compared to previously published paleoclimate reconstructions.

6.1 *Estimating WHC parameters*

Determining the soil WHC parameters was the first and basic step in the modeling process. The accepted approach to attain field capacity (θ_{fc}), residual water content (θ_r), and other soil properties are by determining the WRC in a lab. Common values for soils with low gravel content can range from 0.00 to 0.23 $cm^3\ cm^{-3}$ for θ_r and from 0.146 to 0.644 $cm^3\ cm^{-3}$ for θ_{fc} (Assouline and Or, 2014). However, lower values are expected for gravel rich reg soils with lower retention capacity. Since no published data is available for reg soils, the parameters were roughly estimated using scarce data of soil water profiles. The results of the

calibration ($\theta_{fc} = 0.1$, $\theta_r = 0.013$) were therefore compared to values calculated using a pedotransfer function based on the texture of the soil (Schaap et al., 2001). Field capacity is in agreement with the calculated value (5% difference), On the other hand, the difference between calibrated and calculated residual water content was much higher (28%). However, sensitivity analyses showed that gypsum accumulation is not sensitive to changes in this parameter, thus even if the calibration value of residual water content is not accurate, it will not greatly affect the performance of the model.

The calculated values are given for the fine material, but since the Holocene reg soils contain at least 50% gravel (Amit et al., 1993; Gerson and Amit, 1987), the values had to be corrected before comparison. The assumption that gravel has nil water retention capacity can be tested by comparing reg soils WHC parameters to loess soils. Horowitz (2019) found the field capacity of loess soils in the northern Negev area is 0.19 $cm^3\,cm^{-3}$. Compared to Holocene reg soils, the texture of loess soils is finer and is almost entirely gravel free (Gerson and Amit, 1987). Therefore, field capacity of loess soils is expected to be around twice the value of reg soils when considering the average gravel fraction (50%) and the fine material texture, similar to the results of the calibration process.

Soil WHC is unequal along the profile, and in general, the value will decrease with depth as fine material fraction decreases (Amit, 1990). Temporal changes are also expected as dust accumulation changes the texture and bulk density of the soil (Amit and Gerson, 1986; Gerson et al., 1985). An attempt to mitigate this change was done by gradually increase the field capacity during the computation time using the field capacity module. In theory, the residual water content should also be altered with time, but since the parameter has low relative sensitivity, it was decided to keep it constant. Figure 18 demonstrates well the effect of the additional water retain by the soil as a result of the increase in field capacity: gypsic horizon depth is shallower as rain events result in shallower WD. When compared to the "no modules" curve, it is apparent that between gypsic horizon depth and gypsum concentration, the former is more susceptible to changes in soil WHC. The relation between field capacity and gypsum mean concentration is further discussed in section 6.4.

6.2 *Estimating the F_{PET} factor*

PET is supplied by the WG and is based on calculations of the Penman-Monteith equation, taking into consideration temperature, radiation and wind speed. For the PET calculations, the IMS assumes a crop coefficient of well irrigated short grass with a height of 12 cm (IMS website). The F_{PET} factor aim is to correct the values for reg soils where vegetation is scarce. The calibrated value of 1.2 for F_{pet} implies that PET for reg soils should be higher than the value supplied by the IMS for the study area. Horowitz (2019) calculate a factor of 0.6 to correct the PET values for loess soils in the northern Negev. It is reasonable that the factor of PET in loess soils is lower than in reg soils, this difference can be explained by sparse vegetation cover. Sensitivity analysis indicates that F_{PET} is the least important parameter in the model, and thus this uncertainty can be overlooked.

6.3 *Estimating sulfate fluxes*

The uncertainty introduced by calibrated soil parameters is combined with chemical module simplifications which neglects gypsum accumulation-dissolution kinetics. Since only thermodynamic constraints were taken into account, gypsum in the model is instantly dissolving while undersaturated, resulting in underestimation of gypsum accumulation at the upper horizons of the soil (top ~10 cm). This behavior causes an overestimation of the gypsic horizon depth since the entire profile is shifted down when compared to the observed profile. Since horizons are poorly distinguished in Holocene soil profiles, this uncertainty was considered minor. For late Pleistocene profiles, the use of three profiles from Q1 surface allows for a range of observed gypsic horizon depth, thus minimizes the uncertainty of the prediction.

However, the calibrated value for sulfate concentration in rainwater might be overestimated, since higher sulfate values result in a shallower gypsic horizon. Thus the model can estimate higher sulfate values to compensate the chemical module tendency to yield deeper gypsic horizons.

Another product of the simplified chemical model is an overestimation of gypsum concentration. According to the model design, additional gypsum is added to the first compartment to imitate the effect of dust accumulating on the soil surface. When rainwater are added to the profile, this gypsum is immediately dissolved and precipitates as secondary gypsum deeper in the profile. The size of dust particles measured over the Dead Sea is < 100 μm (Singer et al., 2003), whereas pedogenic gypsum crystals in reg soils are much bigger (0.25-0.5 mm) (Amit and Yaalon, 1996). Thus, gypsum in dust is likely to dissolve much faster than pedogenic gypsum since the rate of dissolution is higher for smaller crystals (Bolan et al., 1991), although not instantaneously. Still, the parameter of dust flux has a low sensitivity score and the effect of the chemical model simplification on gypsum concentration remains small.

The calibration of annual dust flux and sulfate concentration in rainwater was the initial test for the model plausibility. No separation between the study sites was taken since all profiles are of Holocene age (10.3-13.5 Ka) and only minor changes in rainwater composition and dust flux are assumed to exist between the two sites during the Holocene. The calibrated value for sulfate concentration in rainwater was 10 mg l^{-1}; it is about a half than the one measured today in Miztpe Ramon, central Negev (19 mg l^{-1}) (no value was found closer to the study sites). This difference is expected as sea spray decreases inland; the measured value was obtained from rainwater collected over 150 km north from Shehoret, and 60 km west from Ze'elim stream); In addition, modern values might be higher than the ones that prevailed during the Holocene due to anthropogenic activity (Ganor and Mamane, 1982; Herut et al., 1995, 2000). The calibrated value of annual dust flux was 2.5 g m^{-2} yr^{-1}, very similar to the annual dust flux estimated from fine sediments accumulated within Holocene reg soils in Shehoret of ~6 g m^{-2} yr^{-1} (Crouvi et al., 2017). The good agreement between the calibrated and observed values serve as an indication for the validity of the model for accurately simulating gypsum profiles in Holocene reg soils.

6.4 *What controls the depth, concentration, and rate of pedogenic gypsum?*

A relationship between mean annual rainfall and depth of gypsic horizon was noted for reg soils and other arid soils from around the world (Dan et al., 1982; Retallack and Huang, 2010). In addition, the difference in the timing and duration of storms can profoundly influence the genesis of salt horizons (Amit et al., 2010). Effect on gypsum concentration was attributed mainly to influx of airborne dust (Amit, 1990; Dan et al., 1982; Ewing et al., 2006; Gerson and Amit, 1987). Here, several factors were tested for their influence on gypsum distribution in the profile, mainly by evaluating the response of the model to changes in these factors.

Calibration and sensitivity analyses indicate that sulfate concentration in rainwater greatly influence both mean gypsum concentration and gypsic horizon depth. While past studies relate the depth mainly to rainfall characteristics and soil properties (Retallack and Huang, 2010), here sulfate concentration in rainwater is indicated to be highly influential, with high sensitivity score of 2 (Figure 14). The relationship between soluble ion influx to the soil and depth of diagnostic horizons was observed in a similar model assessing pedogenic calcite accumulation (McFadden and Tinsley, 1985). As sulfate influx increases, the available water would be insufficient to transport the increased mass of gypsum to a deeper soil horizon, and accumulation will occur at a shallower depth.

Dust flux, usually considered a major source of salts, is found to be of lesser importance compared to soluble sulfate, probably due to the small fraction of gypsum in dust at the Negev area(~1%) (Ganor and Mamane, 1982; Singer et al., 2003; Torfstein et al., 2017). Low availability of gypsum in dust can explain

the low relative sensitivity score (0.1) of the model to annual dust flux. As expected, the factor does not affect gypsum depth since it is not related to water movement in the soil (unlike WHC parameters and F_{PET}).

The high sensitivity of simulated gypsic horizon depth to changes in field capacity demonstrates the close relation between the wetting depth (WD) and salts accumulation. Increasing field capacity will lead to retention of water in the upper compartments and decrease the average WD and eventually the depth of gypsum precipitation. Since changing the parameter does not alter the amount of soluble ions infiltrating the soil, no affect is expected on the concentration and accumulation rate, however increase in field capacity slightly increases the mean concentration. As field capacity increases, soluble ions tend to concentrate in the upper compartments of the soil profile. The solution in the upper part of the soil is susceptible to higher evaporation rates, leading to high concentration of ions. The high salinity is characterized by an increased precipitation of gypsum. The correlation between field capacity and gypsum concentration is also apparent in the slightly higher accumulation rate when the field capacity module is integrated (Figure 18). Residual water content is also expected to have an affect over gypsum depth, but apparently has none. It is possible that ±20% change in the extremely low calibrated value of 0.013 $cm^3\ cm^{-3}$, is not enough to cause a meaningful difference to the model results.

F_{PET} is the factor used to correct the calculated PET to better represent the evaporation over no vegetation surface characterizing reg soils. An increase will lead to higher evaporation of water from the upper soil after rain events. In the study area, rain events are short and occur few times a year, thus most rain event will probably infiltrate a dry soil, regardless of the rate of evaporation. F_{PET} was found of lesser importance also when simulating water distribution in loessial soil of the northern Negev (T. Horowitz, 2019).

The results of this study clearly indicate that increase in rainfall will increase gypsum concentration and gypsum depth (Figure 15), mainly since rainfall is the main sulfate source, both in controlling the amount of external sulfate (i.e. sulfate concentration in rainwater) and in dissolving and transporting pedogenic gypsum to grater depths till eventually leach it to the alluvial sediments. Mean annual wet day depth is the parameter which best represent the magnitude of rain events in the model and it is correlated with gypsum accumulation depth. Therefore, a climate of high ratio between annual rainfall and frequency of rain events will yield soils with deeper horizons.

Rain event duration was not tested in this study since the WG creates rainfall series of daily resolution. In addition, no evaluation of the effect of high-intensity wet days or extreme events was tested. However, the observed stability of gypsic depth over the computation time (Figure 18, Figure 22) contributes to the assumption that singular extreme events or rainstorms hold little contribution to the long-term gypsum properties. This stability further demonstrates how the mean characteristics of the rain series determine the gypsic depth starting from the first stages of soil development. Depth stability is strengthened by the fact that in soils, gypsum is much less mobile than in the model, and therefore less affected by individual extreme rain events. Furthermore, Horowitz (2019) showed that the duration of rain events has a greater impact on By horizons depth, compared to the magnitude of singular extreme events.

6.5 *Approximating climate condition and soil age using gypsum accumulation rate*

As mean annual rainfall and sulfate concentration in rainwater are the two main factors controlling gypsum accumulation rate, these factors can be used as a generalized static model (Figure 17). Figure 17A can be divided into three general fields. The sulfate-limited field is defined by area where there is sufficient water (rainfall) to translocate soluble ions into the soil and initiate gypsum accumulation, and the rate is controlled by the availability of sulfate. The water-limited zone is defined by sufficient sulfate; gypsum accumulation rate depends on the availability of water. The upper leaching field is defined by water excess where soluble ions are constantly washed and leached from the soil and gypsum does not accumulate.

Figure 17B shows the actual flux of sulfate translocated to the soil during rain events. The two parameters are co-dependent since rainfall is the agent of the sulfate influx, and the white area demonstrates impossible combinations of the two parameters. The possible combinations indicate that the model is actually sulfate-limited, rainfall can always be supplied and the only limitation is sulfate concertation in rain water. Machette (1985) draw a similar theoretical plot for calcic soils and used it to approximate accumulation rates for soils in different regions (Figure 23), the same can be done with the generalized model for assessing soil age, paleorainfall and sulfate influx. The circles added to Figure 17, demonstrate the higher accumulation rate during the late Pleistocene.

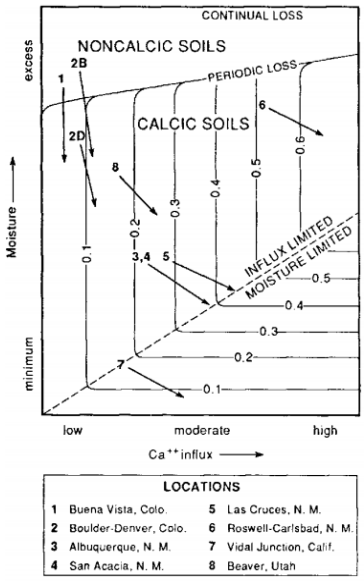

Figure 23: Long term carbonate accumulation rates under varying conditions of moisture and Calcium influx. The plot was used to approximate rates at different locations. Taken from (Machette, 1985)

6.6 *Late-Pleistocene climate scenarios*

The most probable climate scenarios for late Pleistocene conditions in both sites (62.5-10 Ka in Shehoret, 23-10 Ka in Ze'elim) are characterized by a relatively narrow range of values for sulfate concentration in rainwater and mean annual rainfall (Figure 21). This is expected following the high sensitivity of gypsum accumulation to these two parameters. The most likely values for sulfate concentrations in rainwater and mean annual rainfall during the late Pleistocene are higher than the ones that characterized current/Holocene climate. These parameters govern the influx of Ca^{2+} and SO_4^{2-} to the soil profile and greatly influence gypsum accumulation, therefore increasing their values will lead to higher gypsum concentration that is observed in late Pleistocene profiles. Dust flux is another source for gypsum, albeit least prominent and could not be narrowed to a small range of possible values. However, results still indicate higher values than those calibrated for Holocene soils, implying that dust flux was most likely higher during the late Pleistocene compared to current/Holocene time. The annual number of rain days is positively correlated with the mean annual rainfall, suggesting that an increase of one will lead to an increase of the other in order to maintain a certain gypsum depth. Annual PET is a low sensitivity parameter and cannot be evaluated precisely, the optional range was selected according to the observed current PET measured for a location proximate to the study area. Possible values are not likely to exceed the high value of 2300 mm especially if we are examining a more humid climate that existed to some extent during the late Pleistocene. Since PET is determined by several parameters that are not in the scope of this research, it can only be approximated. Overall, the results indicate an increase in rainfall and atmospheric sulfate (in rain water and dust) during 62.5 – 10 Ka.

Reg surfaces in Shehoret stream are mature and started to develop in the middle of the late Pleistocene, extending about 50,000 years into the late Pleistocene climate. High ratio between the suggested and current climate, demonstrates the range of different conditions that accompanied the development of these soils. Most scenarios are defined by relatively high rainfall and sulfate concentration, necessary to explain the high gypsum concentration. A much wetter arid to semiarid southern Negev with rainfall 50-100% more (1.5-2 times) than that of the present during the late Pleistocene, was proposed based on evidences from isotopic composition of groundwater, loess deposits and paleo-marshes in Sinai (Issar and Bruins, 1983). Pollen data associated with humid climate and archeological findings in the southern Negev are another indicator of wetter climate (A. Horowitz, 2001, 2008). However, Enzel et al.,(2008) claims that the potential source for the water cannot be explained, and no sufficient data is available for supporting substantially wetter conditions in the southern Negev. Another opposition to a scenario of arid/semiarid southern Negev is related to the spatial distribution of gypsic – saline reg soils. Under current climate conditions, calcic soils form in areas of > 80 mm yr^{-1} ; alluvial surfaces date to the last 1.2 Ma do not show any evidence of calcic horizons (Amit, Simhai, et al., 2011). The southern Negev is therefore remained hyper-arid since the middle Pleistocene with precipitation < 80 mm yr^{-1}, our results satisfy this constraint and suggesting that mean annual rainfall in this area was between 40 to 50 mm yr^{-1}.

The oldest reg surfaces in Ze'elim are relatively young, from the end of the late Pleistocene and extend only 10,000 years into the late Pleistocene climate. Reg soils in Ze'elim are thereby represents a portion of the time period represented by the Shehoret soils, in addition to different location. The results show that reg soils in Ze'elim were developed under a climate similar to that of the Holocene, which can be emphasized by the low ratio between the suggested and recent mean annual rainfall (1.8 in Ze'elim and 2 in Shehoret). Sulfate concentration in rainwater is similar to the value today. Despite the proximity to the current Holocene value, most of the scenarios are defined by higher rainfall. Wetter climate during the LGP and followed by drier Holocene climate was previously suggested for the area of the Dead Sea (Bar-Matthews et al., 1997, 2003; Sorin et al., 2010; Stein, 2001; Vaks et al., 2003, 2006). Paleorainfall estimations using speleothems from caves in the central and southern Negev imply a wet period of 300-350 mm yr^{-1} occurred at 109-142 Ka and were followed by gradual decrease in rainfall (Vaks et al., 2010). Comparison of isotopic composition in speleothems from two land caves in central Israel indicates that rainfall gradually decreased in the last 15 Ka (Bar-Matthews et al., 2003). However, these studies are focused on rainfall in the vast area of the Dead Sea catchment or the central Negev, and it is difficult to infer from these studies on local past rainfall in the southwestern shore of the Dead Sea. The results from this study are therefore instrumental in improving the paleoclimate estimation in the Negev area by suggesting an estimation for local climate regime.

According to the suggested scenarios, sulfate concentration and dust flux were much higher during the late Pleistocene. Dust influx was suggested to be higher during the LGP than the Holocene according to dust accumulation within loess soils in the northern Negev (Amit, Enzel, et al., 2011; Amit et al., 2017). The fraction of gypsum in airborne dust was not addressed in this study, but the currently small fraction (~1%) could have been higher in the past. According to ice core samples from inland Antarctica, sulfate salts (Na_2SO_4 and $CaSO_4$) flux during the LGP was much higher than in the Holocene and gypsum was the dominant salt in dust (Iizuka et al., 2008, 2012). The abundance of SO_4^{2-} in the atmosphere might have increased the concentration in rainwater since dust is the main contributor of sulfate in Negev (Herut et al., 1995, 2000). Higher flux of sulfate salts is related to removal of HCl and H_2SO_4 by reaction with dust, thereby leading to a reductive atmosphere during the LGP (Iizuka et al., 2008; Röthlisberger et al., 2003).

6.7 *Modeling pedogenic salts accumulation and paleoclimate inference*

Previous studies successfully modeled salts accumulation in soil using deterministic (Arkley, 1963; McFadden and Tinsley, 1985) and stochastic (Marion, 1994) WG. The shortcomings of these models were their inability to explore the influence of a wide range of parameters and values over salts accumulation. Interpreting paleoclimate scenarios from these models was limited only to calcic horizons; moreover, only three specific scenarios were tested using singular computations with stochastic WG (Marion, 1985). The current model undertook similar approach although higher number of parameters were calibrated and many possible climate scenarios were tested with high number of calculations. A feature presented here is the ability to run numerous calculations and decrease the uncertainty presented by the stochastic WG.

Although the strength of the current model lies in its simplicity, a major improvement can be achieved by replacing the compartment approach with a continuous physical approach. The high accuracy of simulating solutes flux through soil along with the high availability of processing abilities can render the computation task possible. Two-dimensional geochemical models like HYDRO-GEOCHEM and UNSATCHEM were widely used to simulate transport of chemicals (Šimůnek and Suarez, 1994; Suarez and Šimůnek, 1997). An interface between a stochastic WG and off-the-shelf numerical models can possibly yield an accurate analysis of climate control over salts accumulation. It will be necessary, however, to sample various reg soils of different ages and derive a WRC and other hydrological parameters necessary for numerical modeling. A further improvement would be to extend the model to operate in regional scope. Since the model is modular, upgrading the WG is relatively simple without the need to interfere with the compartment model.

7. Conclusions

The stochastic model enables gypsum accumulation simulation in reg soils as a response to a synthesized rainfall and PET daily series. The model was calibrated using gypsum and soil water profiles measured in Holocene reg surfaces in Ze'elim (southwestern shore of the Dead Sea) and Shehoret (southern Negev) alluvial fans, both located in the hyperarid region of Israel. The calibrated values are in good agreement with measured values after several assumptions and corrections, suggesting that the model simulation is plausible. Local sensitivity analysis indicate that soil field capacity and sulfate concentration in rainwater are the most influential parameters while residual water content, F_{PET} and dust flux are less so. Sensitivity analysis for climate properties further suggests that mean annual rainfall is highly correlated with gypsum concentration, and excess input of water can ultimately lead to full wash and leachate of soluble ions. Mean annual conditional daily depth can influence the gypsic horizon depth. Higher PET values cause a shallowing of the gypsic horizon depth as the mean wetting depth decreases due to increased evaporation. Overall the most influential parameters are mean annual rainfall and sulfate concentration in rainwater, and were also correlated with gypsum accumulation rate in order to estimate soil ages.

The model underestimated gypsum concentration in mature late Pleistocene profiles when supplied with rainfall series based on recent, hyperarid climate properties. Numerous climate scenarios for periods during the late Pleistocene comprised of mean annual rainfall, mean annual number of wet days, dust flux, sulfate concentration in rainwater and mean annual PET were tested to calculate gypsum profiles that best resemble the measured profiles within mature surfaces. These tests indicate that the climate in the southern Negev during the late Pleistocene (62.5-10 Ka) was wetter with mean annual rainfall of 40 to 50 mm yr^{-1} (2 – 2.5 times more than the value measured in Elat today). The climate in southwestern shore of the Dead Sea was slightly wetter during the late Pleistocene-Holocene transition with mean annual rainfall of 40 to 60 mm yr^{-1} (1.5 – 2 times more than the value measured today). Sulfate concentration in rainwater is estimated to be 20 mg l^{-1} in the southern Negev, twice the value estimated for the Holocene period. Estimation of dust flux and PET are less precise due to their low influence on the process, but the former is expected to have increased during the late-Pleistocene while the latter is expected to have decreased.

8. References

Amit, R. (1990). *Shattered gravel in desert reg soils - the effect of salts on the nature and rate of weathering processes*. Ph. D. Thesis, The Hebrew University of Jerusalem.

Amit, R., Enzel, Y., Crouvi, O., Ayalon, A. (2017). Aridisols in the Southern Levant Deserts and their Palaeoclimate Implications. In *Quaternary of the Levant* (pp. 521–530). Cambridge University Press. https://doi.org/10.1017/9781316106754.057

Amit, R., Enzel, Y., Crouvi, O., Simhai, O., Matmon, A., Porat, N., … Gillespie, A. R. (2011). The role of the Nile in initiating a massive dust influx to the Negev late in the middle Pleistocene. *Bulletin of the Geological Society of America*, *123*(5), 873–889. https://doi.org/10.1130/B30241.1

Amit, R., Enzel, Y., Grodek, T., Crouvi, O., Porat, N., Ayalon, A. (2010). The role of rare rainstorms in the formation of calcic soil horizons on alluvial surfaces in extreme deserts. *Quaternary Research*, *74*(2), 177–187. https://doi.org/10.1016/j.yqres.2010.06.001

Amit, R., Enzel, Y., Sharon, D. (2006). Permanent Quaternary hyperaridity in the Negev, Israel, resulting from regional tectonics blocking Mediterranean frontal systems. *Geology*, *34*(6), 509–512. https://doi.org/10.1130/G22354.1

Amit, R., Gerson, R. (1986). The evolution of holocene reg (gravelly) soils in deserts. *Catena*, *13*(1–2), 59–79. https://doi.org/10.1016/s0341-8162(86)80005-4

Amit, R., Gerson, R., Yaalon, D. H. (1993). Stages and rate of the gravel shattering process by salts in desert Reg soils. *Geoderma*, *57*(3), 295–324. https://doi.org/10.1016/0016-7061(93)90011-9

Amit, R., Simhai, O., Ayalon, A., Enzel, Y., Matmon, A., Crouvi, O., … McDonald, E. (2011). Transition from arid to hyper-arid environment in the southern Levant deserts as recorded by early Pleistocene cummulic Aridisols. *Quaternary Science Reviews*, *30*(3–4), 312–323. https://doi.org/10.1016/j.quascirev.2010.11.007

Amit, R., Yaalon, D. H. (1996). The micromorphology of gypsum and halite in reg soils —the negev desert, israel. *Earth Surface Processes and Landforms*, *21*(12), 1127–1143. https://doi.org/10.1002/(SICI)1096-9837(199612)21:12<1127::AID-ESP656>3.0.CO;2-G

Arkley, R. J. (1963). Calculation of carbonate and water movement in soil from climatic data. *Soil Science*, *96*(4), 239–248. https://doi.org/10.1097/00010694-196310000-00003

Assouline, S., Or, D. (2014). The concept of field capacity revisited: Defining intrinsic static and dynamic criteria for soil internal drainage dynamics. *Water Resources Research*, *50*(6), 4787–4802. https://doi.org/10.1002/2014WR015475

Bar-Matthews, M., Ayalon, A., Gilmour, M., Matthews, A., Hawkesworth, C. J. (2003). Sea - land oxygen isotopic relationships from planktonic foraminifera and speleothems in the Eastern Mediterranean region and their implication for paleorainfall during interglacial intervals. *Geochimica et Cosmochimica Acta*, *67*(17), 3181–3199. https://doi.org/10.1016/S0016-7037(02)01031-1

Bar-Matthews, M., Ayalon, A., Kaufman, A. (1997). Late Quaternary Paleoclimate in the Eastern Mediterranean Region from Stable Isotope Analysis of Speleothems at Soreq Cave, Israel. *Quaternary Research*, *47*(2), 155–168. https://doi.org/10.1006/qres.1997.1883

Bolan, N. S., Syers, J. K., Sumner, M. E. (1991). Dissolution of various sources of gypsum in aqueous solutions and in soil. *Journal of the Science of Food and Agriculture*, *57*(4), 527–541. https://doi.org/10.1002/jsfa.2740570406

Bresler, E. (1967). A model for tracing salt distribution in the soil profile and estimating the efficient combination of water quality and quantity under varying field conditions. *Soil Science*, *104*(4), 227–233. https://doi.org/10.1097/00010694-196710000-00001

Bresler, E., Hanks RJ. (1969). Numerical Method for Estimating Simultaneous Flow of Water and Salt in Unsaturated Soils, *33*(6), 827–832.

Crouvi, O., Amit, R., Ben Israel, M., Enzel, Y. (2017). Loess in the Negev Desert: Sources, Loessial Soils, Palaeosols, and Palaeoclimatic Implications. In *Quaternary of the Levant* (pp. 471–482). Cambridge University Press. https://doi.org/10.1017/9781316106754.053

Crouvi, O., Amit, R., Enzel, Y., Porat, N., Sandler, A. (2008). Sand dunes as a major proximal dust source for late Pleistocene loess in the Negev Desert, Israel. *Quaternary Research*, *70*(2), 275–282. https://doi.org/10.1016/j.yqres.2008.04.011

Dan, J., Yaalon, D. H. (1982). Automorphic saline soils in Israel. *Aridic Soils and Geomorphic Processes*, 103–115.

Retrieved from http://agris.fao.org/agris-search/search.do?recordID=US201302533902

Dan, J., Yaalon, D. H., Moshe, R., Nissim, S. (1982). Evolution of reg soils in Southern Israel and Sinai. *Geoderma*, *28*(3–4), 173–202. https://doi.org/10.1016/0016-7061(82)90002-7

Davies, C. W., Shedlovsky, T. (1964). Ion Association. *Journal of The Electrochemical Society*, *111*(3), 85C. https://doi.org/10.1149/1.2426129

Dunn, P. K. (2004). Occurrence and quantity of precipitation can be modelled simultaneously. *International Journal of Climatology*, *24*(10), 1231–1239. https://doi.org/10.1002/joc.1063

Enzel, Y., Amit, R., Dayan, U., Crouvi, O., Kahana, R., Ziv, B., Sharon, D. (2008, February 1). The climatic and physiographic controls of the eastern Mediterranean over the late Pleistocene climates in the southern Levant and its neighboring deserts. *Global and Planetary Change*. Elsevier. https://doi.org/10.1016/j.gloplacha.2007.02.003

Eswaran, H., Zi-Tong, G. (1991). Properties, genesis, classification, and distribution of soils with gypsum. *Occurrence, Characteristics, and Genesis of Carbonate, Gypsum, and Silica Accumulations in Soils. Proc. Symposium, Anaheim, CA, 1988*, (26), 89–119. https://doi.org/10.2136/sssaspecpub26.c6

Ewing, S. A., Sutter, B., Owen, J., Nishiizumi, K., Sharp, W., Cliff, S. S., … Amundson, R. (2006). A threshold in soil formation at Earth's arid-hyperarid transition. *Geochimica et Cosmochimica Acta*, *70*(21), 5293–5322. https://doi.org/10.1016/j.gca.2006.08.020

Ganor, E. (1975). *Atmospheric dust in Israel—sedimentological and meteorological analysis of dust deposition*. *Unpublished Ph. D. thesis*. Hebrew University, Jerusalem.

Ganor, E., Foner, H. A. (1996). The Mineralogical and Chemical Properties and the Behaviour of Aeolian Saharan Dust Over Israel (pp. 163–172). Springer, Dordrecht. https://doi.org/10.1007/978-94-017-3354-0_15

Ganor, E., Mamane, Y. (1982). Transport of Saharan dust across the eastern Mediterranean. *Atmospheric Environment (1967)*, *16*(3), 581–587. https://doi.org/10.1016/0004-6981(82)90167-6

Garfunkel, Z. (1998). Constrains on the origin and history of the Eastern Mediterranean basin. *Tectonophysics*, *298*(1–3), 5–35. https://doi.org/10.1016/S0040-1951(98)00176-0

Gerson, R., Amit, R. (1987). Rates and modes of dust accretion and deposition in an arid region—the Negev, Israel. *Geological Society, London, Special Publications*, *35*(1), 157–169. https://doi.org/10.1144/gsl.sp.1987.035.01.11

Gerson, R., Amit, R., Grossman, S. (1985). *Dust avilability in desert terrains*. Retrieved from https://apps.dtic.mil/dtic/tr/fulltext/u2/a166447.pdf

Ginat, H., Opitz, S., Ababneh, L., Faershtein, G., Lazar, M., Porat, N., Mischke, S. (2018). Pliocene-Pleistocene waterbodies and associated deposits in southern Israel and southern Jordan. *Journal of Arid Environments*, *148*, 14–33. https://doi.org/10.1016/j.jaridenv.2017.09.007

Greenbaum, N. (1986). Infiltration and Runoff in an extremely Arid Region: Infiltration Experiments in Small Plots in the Southern Arava Valley and Their Hydrological, Pedological and Paleomorphological Implications [M. Sc. thesis].

Greenbaum, N., Mushkin, A., Porat, N., Amit, R. (2020). Runoff generation, rill erosion and time-scales for hyper-arid abandoned alluvial surfaces, the Negev desert, Israel. *Geomorphology*, *358*. https://doi.org/10.1016/j.geomorph.2020.107101

Herut, B., Spiro, B., Starinsky, A., Katz, A. (1995). Sources of sulfur in rainwater as indicated by isotopic δ34S data and chemical composition, Israel. *Atmospheric Environment*, *29*(7), 851–857. https://doi.org/10.1016/1352-2310(94)00307-7

Herut, B., Starinsky, A., Katz, A., Rosenfeld, D. (2000). Relationship between the acidity and chemical composition of rainwater and climatological conditions along a transition zone between large deserts and Mediterranean climate, Israel. *Atmospheric Environment*, *34*(8), 1281–1292. https://doi.org/10.1016/S1352-2310(99)00291-5

Horowitz, A. (2001). *The Jordan Rift Valley at Present*. *The Jordan Rift Valley*. https://doi.org/10.1201/9781439834244.ch3

Horowitz, A. (2008). The Quaternary of Israel. *Boreas*, *9*(4), 306–306. https://doi.org/10.1111/j.1502-3885.1980.tb00709.x

Horowitz, T. (2019). *Control of climate properties on long term soil water distributions in semi-arid and arid soils with implications on pedogenic salts*. Unpublished M.Sc, Thesis, The Hebrew University of Jerusalem.

Iizuka, Y., Horikawa, S., Sakurai, T., Johnson, S., Dahl-Jensen, D., Steffensen, J. P., Hondoh, T. (2008). A relationship between ion balance and the chemical compounds of salt inclusions found in the Greenland Ice Core Project and Dome Fuji ice cores. *Journal of Geophysical Research*, *113*(D7), D07303. https://doi.org/10.1029/2007JD009018

Iizuka, Y., Uemura, R., Motoyama, H., Suzuki, T., Miyake, T., Hirabayashi, M., Hondoh, T. (2012). Sulphate-climate coupling over the past 300,000 years in inland Antarctica. *Nature*, *490*(7418), 81–84. https://doi.org/10.1038/nature11359

Issar, A. S., Bruins, H. J. (1983). Special climatological conditions in the deserts of Sinai and the Negev during the latest Pleistocene. *Palaeogeography, Palaeoclimatology, Palaeoecology*, *43*(1–2), 63–72. https://doi.org/10.1016/0031-0182(83)90048-2

Lehmann, P., Assouline, S., Or, D. (2008). Characteristic lengths affecting evaporative drying of porous media. *Physical Review E - Statistical, Nonlinear, and Soft Matter Physics*, *77*(5), 1–16. https://doi.org/10.1103/PhysRevE.77.056309

Machette, M. N. (1985). Calcific soils of the southwestern United States. *Soils and Quaternary Geology of the Southwestern United States: Geological Society of America Special Paper*, *203*, 1–21.

Marani, M., Ignaccolo, M. (2015). A metastatistical approach to rainfall extremes. *Advances in Water Resources*, *79*, 121–126. https://doi.org/10.1016/j.advwatres.2015.03.001

Marion, G. M. (1994). CALGYP : A Simulation Model for Precipitation-Dissolution in Soils. *COLD REGIONS RESEARCH AND ENGINEERING LAB HANOVER NH*, 40.

Marion, G. M., Schlesinger, W. H., Fonteyn, P. J. (1985). Caldep: A regional model for soil CaCo3(Caliche) deposition in southwestern deserts. *Soil Science*. https://doi.org/10.1097/00010694-198505000-00014

Marra, F., Armon, M., Adam, O., Zoccatelli, D., Gazal, O., Rostkier-edelstein, D., … Morin, E. (2020). Local constraints reduce uncertainty in the projection of precipitation extremes. *Unpublished Article*.

Marra, F., Nikolopoulos, E. I., Anagnostou, E. N., Morin, E. (2018). Metastatistical Extreme Value analysis of hourly rainfall from short records: Estimation of high quantiles and impact of measurement errors. *Advances in Water Resources*, *117*, 27–39. https://doi.org/10.1016/J.ADVWATRES.2018.05.001

Marra, F., Zoccatelli, D., Armon, M., Morin, E. (2019). A simplified MEV formulation to model extremes emerging from multiple nonstationary underlying processes. *Advances in Water Resources*, *127*, 280–290. https://doi.org/10.1016/J.ADVWATRES.2019.04.002

Mcfadden, L. D., Amundson, R. G., Chadwick, O. A. (1991). Numerical modeling, chemical, and isotopic studies of carbonate accumulation in soils of arid regions. In *Occurrence, characteristics, and genesis of carbonate, gypsum, and silica accumulations in soils. Proc. symposium, Anaheim, CA, 1988* (Vol. sssaspecia, pp. 17–35). Soil Science Society of America. https://doi.org/10.2136/sssaspecpub26.c2

McFadden, L. D., Tinsley, J. C. (1985). Rate and depth of pedogenic-carbonate accumulation in soils: formation and testing of a compartment model. *Special Paper, Geological Society of America Vol. 203*, 23–41. https://doi.org/10.1130/spe203-p23

Nettleton, W. D., Nelson, R. E., Brasher, B. R., Derr, P. S. (1982). Gypsiferous soils in the Western United States. *SSSA Special Publication*, *10*, 147–168. https://doi.org/10.2136/sssaspecpub10.c9

Penman, H. L. (1948). Natural Evaporation from Open Water, Bare Soil and Grass. *Proceedings of the Royal Society of London. Series A, Mathematical and Physical Sciences*, *193*(1032), 120–145.

Porat, N., Amit, R., Enzel, Y., Zilberman, E., Avni, Y., Ginat, H., Gluck, D. (2010). Abandonment ages of alluvial landforms in the hyperarid Negev determined by luminescence dating. *Journal of Arid Environments*, *74*(7), 861–869. https://doi.org/10.1016/j.jaridenv.2009.10.018

Retallack, G. J. (2005). Pedogenic carbonate proxies for amount and seasonality of precipitation in paleosols. *Geology*, *33*(4), 333–336. https://doi.org/10.1130/G21263.1

Retallack, G. J., Huang, C. (2010). Depth to gypsic horizon as a proxy for paleoprecipitation in paleosols of sedimentary environments. *Geology*, *38*(5), 403–406. https://doi.org/10.1130/G30514.1

Reznik, I. J., Ganor, J., Gal, A., Gavrieli, I. (2009). Gypsum saturation degrees and precipitation potentials from Dead Sea - seawater mixtures. *Environmental Chemistry*, *6*(5), 416. https://doi.org/10.1071/EN09038

Richardson, C. W. (1981). Stochastic simulation of daily precipitation, temperature, and solar radiation. *Water Resources Research*, *17*(1), 182–190. https://doi.org/10.1029/WR017i001p00182

Röthlisberger, R., Mulvaney, R., Wolff, E. W., Hutterli, M. A., Bigler, M., de Angelis, M., … Udisti, R. (2003). Limited dechlorination of sea-salt aerosols during the last glacial period: Evidence from the European Project for Ice Coring in Antarctica (EPICA) Dome C ice core. *Journal of Geophysical Research: Atmospheres*, *108*(16), 1–6. https://doi.org/10.1029/2003jd003604

Schaap, M. G., Leij, F. J., Van Genuchten, M. T. (2001). Rosetta: A computer program for estimating soil hydraulic parameters with hierarchical pedotransfer functions. *Journal of Hydrology*, *251*(3–4), 163–176. https://doi.org/10.1016/S0022-1694(01)00466-8

Semenov, M., Brooks, R. (1999). Spatial interpolation of the LARS-WG stochastic weather generator in Great Britain. *Climate Research*, *11*(2), 137–148. https://doi.org/10.3354/cr011137

Šimůnek, J., Suarez, D. L. (1994). Two-dimensional transport model for variably saturated porous media with major ion chemistry. *Water Resources Research*, *30*(4), 1115–1133. https://doi.org/10.1029/93WR03347

Singer, A. (1994). The Chemistry of Precipitation in Israel. *Israel Journal of Chemistry*, *34*(3–4), 315–326. https://doi.org/10.1002/ijch.199400035

Singer, A., Ganor, E., Dultz, S., Fischer, W. (2003). Dust deposition over the Dead Sea. *Journal of Arid Environments*, *53*(1), 41–59. https://doi.org/10.1006/jare.2002.1023

Sorin, L., Anton, V., Miryam, B. M., Roi, P., Amos, F. (2010). Late Pleistocene palaeoclimatic and palaeoenvironmental reconstruction of the Dead Sea area (Israel), based on speleothems and cave stromatolites. *Quaternary Science Reviews*, *29*(9–10), 1201–1211. https://doi.org/10.1016/j.quascirev.2010.01.018

Stein, M. (2001). The sedimentary and geochemical record of neogene-quaternary water bodies in the Dead Sea basin - Inferences for the regional paleoclimatic history. *Journal of Paleolimnology*, *26*(3), 271–282. https://doi.org/10.1023/A:1017529228186

Suarez, D. L., Šimůnek, J. (1997). UNSATCHEM: Unsaturated Water and Solute Transport Model with Equilibrium and Kinetic Chemistry. *Soil Science Society of America Journal*, *61*(6), 1633–1646. https://doi.org/10.2136/sssaj1997.03615995006100060014x

Thornthwaite, C. W. (1948). An Approach toward a Rational Classification of Climate. *Geographical Review*, *38*(1), 55. https://doi.org/10.2307/210739

Torfstein, A., Teutsch, N., Tirosh, O., Shaked, Y., Rivlin, T., Zipori, A., … Erel, Y. (2017). Chemical characterization of atmospheric dust from a weekly time series in the north Red Sea between 2006 and 2010. *Geochimica et Cosmochimica Acta*, *211*, 373–393. https://doi.org/10.1016/j.gca.2017.06.007

Tsakiris, G. (1988). Daily potential evapotranspiration modelling. *Agricultural Water Management*, *13*(2–4), 393–402. https://doi.org/10.1016/0378-3774(88)90169-2

Vaks, A., Bar-Matthews, M., Ayalon, A., Matthews, A., Frumkin, A., Dayan, U., … Schilman, B. (2006). Paleoclimate and location of the border between Mediterranean climate region and the Saharo-Arabian Desert as revealed by speleothems from the northern Negev Desert, Israel. *Earth and Planetary Science Letters*, *249*(3–4), 384–399. https://doi.org/10.1016/j.epsl.2006.07.009

Vaks, A., Bar-Matthews, M., Ayalon, A., Schilman, B., Gilmour, M., Hawkesworth, C. J., … Matthews, A. (2003). Paleoclimate reconstruction based on the timing of speleothem growth and oxygen and carbon isotope composition in a cave located in the rain shadow in Israel. *Quaternary Research*, *59*(2), 182–193. https://doi.org/10.1016/S0033-5894(03)00013-9

Vaks, A., Bar-Matthews, M., Matthews, A., Ayalon, A., Frumkin, A. (2010). Middle-Late Quaternary paleoclimate of northern margins of the Saharan-Arabian Desert: Reconstruction from speleothems of Negev Desert, Israel. *Quaternary Science Reviews*, *29*(19–20), 2647–2662. https://doi.org/10.1016/j.quascirev.2010.06.014

van Genuchten, M. T. (1980). A Closed-form Equation for Predicting the Hydraulic Conductivity of Unsaturated Soils. *Soil Science Society of America Journal*, *44*(5), 892–898. https://doi.org/10.2136/sssaj1980.03615995004400050002x

Warrick, A. W., Biggar, J. W., Nielsen, D. R. (1971). Simultaneous Solute and Water Transfer for an Unsaturated Soil. *Water Resources Research*, *7*(5), 1216–1225. https://doi.org/10.1029/WR007i005p01216

Yaalon, D. H., Ganor, E. (1979). East Mediterranean trajectories of dust-carrying storms from the Sahara and Sinai. *Saharan Dust*, 187–193.

Zeng, W., Xu, C., Wu, J., Huang, J. (2014). Soil salt leaching under different irrigation regimes: HYDRUS-1D modelling and analysis. *Journal of Arid Land*, *6*(1), 44–58. https://doi.org/10.1007/s40333-013-0176-9

9. Appendix – source code

Full code at https://github.com/liorstov/evapocalc

```
class CSM
{
public:
     CSM();
    Rcpp::List Calculate(Rcpp::DoubleVector, Rcpp::DoubleVector, int years, int Depth, int nthick,
 double WieltingPoint,int FieldArea, double FieldCapacity, double DustSO4, double AETFactor, bool verbose, double dustFlux, double
rainCa, double rainSO4,bool withFC);
    std::vector<Compartment>* GetCompartments();
    Rcpp::NumericMatrix output2Matrix(Rcpp::DoubleVector & inputVector, bool verbose);
    double meqSoil2molar(double, double,double);
    double mol2meqSoil(double mol, double);
    double moistcm2Litre(double);

    ~CSM();
    double GetPrecision(double);
    //Rcpp::List GetResults();
    int nNumOfDays;
    float nDepth;
    float thick;
    int nNumOfCompatments;
    float nArea;
    float nTotalCaDust;
    float nTotalRain;
    float nTotalCaLeachate;
    float nTotalSO4Leachate;
    float nTotalLeachate;
    float nTotalMoist;
    float nTotalWP;
    float nTotalAet;
    float nTotalWhc;
    float BulkDensity;
    float accumolateDustDays;

    Rcpp::List results;
    void InitCompartments();
    void initVector(Rcpp::DoubleVector & inputVector);
    inline bool firstDayInYear(int day) {
        return(!((day + 1) % 365));
    }

//holocene profile have 0.1 FC and plesitocene profiles have 0.19 FC. a linear function updates the fc every year
    inline int updateFieldCapacity(int year) {
        if (year > 10000) {
            int CompDuration = 12500;
            int DustComp = (year-10001)/ (int)CompDuration;
            float yearsInProcess = (year - 10001) % CompDuration;
            //x is yearsinprocess and 0.01 is b and
            Compartments[DustComp].nFieldCapacity = ((yearsInProcess)*0.09/ (float)CompDuration +0.1)*thick;

            updateTotalWHC();

            //Rcout << year <<"    " <<DustComp <<"  "<< Compartments[DustComp].nFieldCapacity/thick<<"   WHC" << nTotalWhc << endl;
            return(DustComp);
        }
    }

    inline void updateTotalWHC() {
        nTotalWhc = 0.0;
        for (std::vector<Compartment>::iterator it = Compartments.begin(); it != Compartments.end(); ++it) {
            nTotalWhc += (it->nFieldCapacity - it->nThetaWeildingPnt);
        }

    }



    std::vector<Compartment> Compartments;
    Rcpp::NumericVector RainArr;
    float AET;


    float nDailyDustCa;
    float nDailyDustGyp;
    float wieltingPoint;
    float nFieldCapacity;
    float CCa;
    float CSO4;
    float nCaco3less;


    float nTemp;
    float nLeachate;

    double TempArr[12] = { 20,21,24.7,29.7,31.4,37.6,39.4,39.4,36.5,32,26.5,27.1};
};

RCPP_EXPOSED_CLASS(CSM);
#endif
```

```
CSM::CSM()
{
    nTotalWhc = 0;
    nTotalCaDust = 0;
    nTotalRain = 0;
    nTotalCaLeachate = 0;
    nTotalSO4Leachate = 0;
    nTotalLeachate = 0;
    nTotalMoist = 0;
    nTotalAet = 0;
    nTotalWP = 0;
    nTemp = 0;
    accumolateDustDays = 0.0F;

    nLeachate = 0;

    AET = 0;
    printf("csm Const\n");
}

//flux is gram/cm2/day
//dust concentration is mg/gram; rain concentration is mg/l
Rcpp::List CSM::Calculate(Rcpp::DoubleVector rain, Rcpp::DoubleVector PET, int years, int Depth, int nthick, double
WieltingPoint,
    int FieldArea, double FieldCapacity, double DustGyp, double AETFactor, bool verbose, double dustFlux, double
rainCa, double rainSO4,bool withFC)
{
    Rcpp::Rcout << "years: " << years << endl <<
        "Depth: " << Depth << endl <<
        "thick: " << nthick << endl <<
        "WieltingPoint: " << WieltingPoint << endl <<
        "FieldArea: " << FieldArea << endl <<
        "FieldCapacity: " << FieldCapacity <<  endl <<
        "DustGyp: "  << DustGyp<< endl << "AETFactor: " << AETFactor << endl << "verbose: " << verbose << endl
        << "dustFlux: " << dustFlux<< endl<< "rainCa: " << rainCa << endl << "rainSO4: " << rainSO4<< endl;

    double nTemp = 25;
    double nDailyPET = 0;
    double nDailyAET = 0;
    double nDailyRain = 0;
    double DailySO4Rain;
    double DailyCaRain;
    double inputCa = 0;
    double outputCa = 0;
    double GypAgg = 0;
    int year = 0;
    int nWDComp = 0;
    int nRainEvents = 0;
    int nRainVecLength = rain.length();
    float fDailyMaxGyp = 0;
    int nCurrentMaxGyp = 0;
    nTotalWhc = 0;
    nTotalRain = 0;
    nTotalCaLeachate = 0;
    nTotalSO4Leachate = 0;
    nTotalLeachate = 0;
    nTotalMoist = 0;
    nTotalAet = 0;
    nTotalWP = 0;
    accumolateDustDays = 0.0F;

    nLeachate = 0;

    nNumOfDays= years*365;
    nDepth = Depth;
    thick = nthick;
    nArea = FieldArea;
    nNumOfCompatments = nDepth / thick;
    wieltingPoint = WieltingPoint*thick ;//in cm
    nFieldCapacity = FieldCapacity*thick;
    RainArr = rain;
    nTotalWhc = (nFieldCapacity - wieltingPoint) * nNumOfCompatments;//in cm


    // flux is gram/cm2/day multiple by concentration % convert to mol/cm2/day
    nDailyDustGyp = dustFlux * DustGyp  / 172.172F; //gypsum molar waight  172.172
    nTotalMoist = wieltingPoint * nNumOfCompatments;///[cm]
    nTotalWP = nTotalMoist;
    InitCompartments();

    CCa =0; // molar
    CSO4 = 0; // molar


    // create list with all compartment
    Rcpp::DoubleVector vect = Rcpp::DoubleVector::create();
```

```
    Rcpp::DoubleVector Gypsum = Rcpp::DoubleVector::create();
    Rcpp::DoubleVector GypsumDay = Rcpp::DoubleVector::create();
    Rcpp::DoubleVector Ca = Rcpp::DoubleVector::create();
    Rcpp::DoubleVector SO4 = Rcpp::DoubleVector::create();
    Rcpp::DoubleVector moisture = Rcpp::DoubleVector::create();
    Rcpp::DoubleVector CompWash = Rcpp::DoubleVector::create();
    Rcpp::DoubleVector floodComp = DoubleVector::create();
    Rcpp::DoubleVector AETLoss = DoubleVector::create();
    Rcpp::DoubleVector dayRain = DoubleVector::create();
    Rcpp::DoubleVector WD (nNumOfDays);
    Rcpp::DoubleVector YearGyp (years);
    Rcpp::DoubleVector YearMeanGyp (years);
    Rcpp::DoubleVector YearMaxGyp (years);
    Rcpp::DoubleVector gypDepth (years);
    Rcpp::DoubleVector YearCa(years);
    Rcpp::DoubleVector YearSulfate(years);
    initVector(YearGyp);
    initVector(YearMeanGyp);
    initVector(YearMaxGyp);
    initVector(gypDepth);
    initVector(YearCa);
    initVector(YearSulfate);

    Gypsum.erase(0, Gypsum.length());

    Rcout.precision(10);
    /*std::ofstream myfile;
    myfile.open("example.csv");
    myfile << "day,compartment, daily rain [L], dialy AET[L],moistutre [L], input Ca [mol/L], input SO4 [mol/L], input
gyp [mol/L], output Ca [mol/L], output SO4 [mol/L], output gyp [mol/L].\n";
*/
    nNumOfDays =   std::min(nNumOfDays, nRainVecLength);
    Rcpp::Rcout << nNumOfDays << endl;
    //main loop over days
    for (int day = 0; ((day < nNumOfDays)); day++)
    {
        year = day / 365;
        int DustComp;
        //field capacity increased with time
        if (firstDayInYear(year) && withFC) {
            DustComp = updateFieldCapacity(year);
        }

        nDailyPET = PET[day]/10;
        nDailyRain = RainArr[day]/10;
        DailySO4Rain = nDailyRain * 0.001*rainSO4 / 1000 / 96.06F;// convert cm3 to littre and multiple with
concentration to get mg sulfate, convert to gram and multiply by atomic mass, to get mol
        DailyCaRain = nDailyRain * 0.001*rainCa / 1000 / 40.078F;// convert cm3 to littre and multiple with
concentration

        inputCa += DailyCaRain;

        /*nTotalCaDust += nDust;
        nTotalCaRain += RainArr[day] * CCa*40.0 / 1000.0;*/
        if (nTotalMoist >= (0.546*nTotalWhc)) // according to Marion et al. (1985), for the upper 45% of the total whc
the actual evapotranspiration (AET) is the potential evapotranspiration (pet)
            AET = nDailyPET;        // in case of 10 compartments of 10 cm each, if total moistute > 8.465
                                                    //AET=PETdaily[monthperday[day]];
        else if ((nTotalMoist > nTotalWP*1.001) && (nTotalMoist < 0.546*nTotalWhc))
{                                   // the lower 55% of the total whc are according to modifeid Thornthwaite-
Mather model
            AET = (nTotalMoist / nTotalWhc)*nDailyPET;
        }
        else{// in case the soil is at WP, no evaporation
            AET = 0;
        }
        //if (AET == 0 && nDailyRain == 0) continue;
        //Rcpp::Rcout << nTotalMoist << endl << nTotalWP << endl << nTotalWhc<<endl<<AET<<endl;
        nTotalMoist = 0;
        AET *= AETFactor;

        nDailyAET = AET;
        //AET = AET * 10;
        nTotalAet += nDailyAET;

        nTotalRain += nDailyRain;
        Compartments[0].nMoist += nDailyRain;   // set the moiture of the 1st compartment to the intial moisture plus
the daily rainfall. rainfall is added only the 1st compartment


        //accumolate dust and relaese when its raining
        if (nDailyRain > 0) {
            Compartments[0].C_Ca +=  DailyCaRain;
            Compartments[0].C_SO4 += DailySO4Rain;
            Compartments[0].C_CaSO4 += accumolateDustDays * nDailyDustGyp;
            YearSulfate[year] += DailySO4Rain;
```

```
            accumolateDustDays = 0;
        }
        else
        {
            accumolateDustDays++;
        }

        //Initiate counter for gypsum depth
        fDailyMaxGyp = 0;
        nCurrentMaxGyp = 0;

        // This is the second loop that runs through the soil profile
        for (int CurrentComp = 0; CurrentComp < nNumOfCompatments; CurrentComp++)
        {

            //WASHING
            if (Compartments[CurrentComp].nMoist > Compartments[CurrentComp].nFieldCapacity)
            {
                // determines the leachate by substracting the field capacity from the moisture content
                nLeachate = Compartments[CurrentComp].nMoist - Compartments[CurrentComp].nFieldCapacity;
                Compartments[CurrentComp].nFloodedCount++;
                nWDComp = CurrentComp+1;
            }
            // in case the comp is floated without leaching
            else if(Compartments[CurrentComp].nMoist == Compartments[CurrentComp].nFieldCapacity)          {

                Compartments[CurrentComp].nFloodedCount++;
                nLeachate = 0.0;
            }
            else
            {
                nLeachate = 0.0;
            }

            Compartments[CurrentComp].fTotLeachate += nLeachate;

            // subtract the leachate from the moisture of the  compartment
            Compartments[CurrentComp].nMoist -= nLeachate;


            // EVAPORATING
            //  taking into account the AET for this current compartment, and updating the AET value
            // moist - wieltingPOint is the water available for evaporation
            if (Compartments[CurrentComp].nMoist - (Compartments[CurrentComp].nThetaWeildingPnt) < AET)
            {
                AET -= (Compartments[CurrentComp].nMoist - (Compartments[CurrentComp].nThetaWeildingPnt));
                Compartments[CurrentComp].fAETLoss += Compartments[CurrentComp].nMoist -
Compartments[CurrentComp].nThetaWeildingPnt;
                Compartments[CurrentComp].nMoist = Compartments[CurrentComp].nThetaWeildingPnt;
            }
            else
            {
                Compartments[CurrentComp].nMoist -= AET;
                Compartments[CurrentComp].fAETLoss += AET;
                AET = 0.0;
            }


            //CHEMISTRY
            //calculating gypsum concentration and ion available for washing
            // only if moist change since yesterday
            if (Compartments[CurrentComp].nMoist != Compartments[CurrentComp].nLastMoist) {
                Compartments[CurrentComp].nLastMoist = Compartments[CurrentComp].nMoist;
                GypAgg = Compartments[CurrentComp].solubility(nTemp);
                YearGyp[year] += mol2meqSoil(GypAgg, thick);

            }


            if (Compartments[CurrentComp].C_CaSO4 > fDailyMaxGyp) {
                fDailyMaxGyp = Compartments[CurrentComp].C_CaSO4;
                nCurrentMaxGyp = CurrentComp;
            }


            if (firstDayInYear(day)) {
                YearMeanGyp[year] += mol2meqSoil(Compartments[CurrentComp].C_CaSO4, thick)/nNumOfCompatments;
                YearCa[year] += mol2meqSoil(Compartments[CurrentComp].C_Ca, thick);;
                //YearSulfate[year] += mol2meqSoil(Compartments[CurrentComp].C_SO4, thick);
                // get gypsum horizon of the year
                if (Compartments[CurrentComp].C_CaSO4 > YearMaxGyp[year])
                {
                    YearMaxGyp[year] = mol2meqSoil(Compartments[CurrentComp].C_CaSO4,thick);
                }
```

```
            }


            //LEACHATE
            //  examin if we reached saturation
            if (nLeachate > 0)
            {
                //wash to next compartment or to leachete
                // ion are in mol
                if (CurrentComp != nNumOfCompatments - 1) {
                    //adding the fractional quantitiy of matter
                    Compartments[CurrentComp + 1].C_Ca += Compartments[CurrentComp].C_Ca*
nLeachate/((Compartments[CurrentComp].nFieldCapacity - wieltingPoint) +nLeachate);
                    Compartments[CurrentComp + 1].C_SO4 += Compartments[CurrentComp].C_SO4* nLeachate /
((Compartments[CurrentComp].nFieldCapacity - wieltingPoint) + nLeachate);
                    Compartments[CurrentComp + 1].nMoist += nLeachate;
                }
                else
                {
                    //adding the fractional quantitiy of matter
                    nTotalCaLeachate += Compartments[CurrentComp].C_Ca* nLeachate /
((Compartments[CurrentComp].nFieldCapacity - wieltingPoint) + nLeachate);
                    nTotalSO4Leachate += Compartments[CurrentComp].C_SO4* nLeachate /
((Compartments[CurrentComp].nFieldCapacity - wieltingPoint) + nLeachate);
                    nTotalLeachate += nLeachate;
                    nWDComp = CurrentComp;
                }
                //leaving  the fractional quantitiy of matter
                Compartments[CurrentComp].C_Ca *= (Compartments[CurrentComp].nFieldCapacity - wieltingPoint) /
((Compartments[CurrentComp].nFieldCapacity - wieltingPoint) + nLeachate);
                Compartments[CurrentComp].C_SO4 *= (Compartments[CurrentComp].nFieldCapacity - wieltingPoint) /
((Compartments[CurrentComp].nFieldCapacity - wieltingPoint) + nLeachate);
                nLeachate = 0;
            }

            nTotalMoist += Compartments[CurrentComp].nMoist;
        }

        //nnual avarege gyp depth
        gypDepth[year] += (((float)nCurrentMaxGyp+0.5)*thick/365.0);

        // Write to output

        if (verbose == 1)
        {
            GypsumDay.push_back(day);
            GypsumDay.push_back(nDailyRain);
            GypsumDay.push_back(nDailyAET);
            GypsumDay.push_back(nTotalMoist);
            GypsumDay.push_back((nWDComp + 0.5)*nthick);

            WD.push_back(day);
            WD.push_back(nDailyRain);
            WD.push_back(nDailyAET);
            WD.push_back(nTotalMoist);
            WD.push_back((nWDComp + 0.5)*nthick);
            for (std::vector<Compartment>::iterator it = Compartments.begin(); (it - Compartments.begin()) < 15 ;
++it) {
                WD.push_back(it->nMoist);
                GypsumDay.push_back(it->C_CaSO4);
            }

        }
        else if (nDailyRain > 0)
        {
            nRainEvents++;
            Compartments[nWDComp].nWetCount++;
            WD[day]=((nWDComp + 0.5)*nthick);
        }

        nWDComp = 0;

        if (fmod(double(day)/ double(nNumOfDays), 0.1 )  == 0) {
            Rcout << double(day) / double(nNumOfDays) * 100 << "%; ";
        }
    }

    for (std::vector<Compartment>::iterator it = Compartments.begin(); it != Compartments.end(); ++it) {
        vect.push_back(it->nWetCount);
        CompWash.push_back(it->fTotLeachate);
        AETLoss.push_back(it->fAETLoss);
        floodComp.push_back(it->nFloodedCount);
        Gypsum.push_back(mol2meqSoil(it->C_CaSO4,thick));
        Ca.push_back(mol2meqSoil(it->C_Ca, thick));
        SO4.push_back(mol2meqSoil(it->C_SO4, thick));
```

```
        moisture.push_back(it->nMoist);

        outputCa += it->C_Ca + it->C_CaSO4;
    }

    outputCa += nTotalCaLeachate;
    Rcpp::Rcout << WD.length() << verbose<< endl;


    results = Rcpp::List::create(_["gypsum"] = Gypsum, _["gypsumDay"] = output2Matrix(GypsumDay, verbose),
        _["Ca"] = Ca,
        _["SO4"] = SO4,
        _["WD"] = WD,
        _["moist"] = moisture,
        _["WetZone"] = floodComp,
        _["AET"] = nTotalAet,
        _["AETLoss"] = AETLoss,
        _["totalRain"] = nTotalRain,
        _["CompWash"] = CompWash,
        _["Leachate"]= nTotalLeachate,
        _["inputCa"]= inputCa,
        _["outputCa"]= outputCa,
        _["YearGyp"] = YearGyp,
        _["YearMeanGyp"] = YearMeanGyp,
        _["YearMaxGyp"] = YearMaxGyp,
        _["gypDepth"] = gypDepth,
        _["YearSulfate"] = YearSulfate,
        _["YearCa"] = YearCa);

    return results;
}

std::vector<Compartment>* CSM::GetCompartments()
{
    return &Compartments;
}

Rcpp::NumericMatrix CSM::output2Matrix(Rcpp::DoubleVector & inputVector, bool verbose)
{
    Rcpp::NumericMatrix outputMat;
    if (verbose == 1)
    {
        inputVector.attr("dim") = Dimension(20, inputVector.length() / (20));
        outputMat = transpose(as<NumericMatrix>(inputVector));
        Rcpp::colnames(outputMat) = CharacterVector::create("day", "rain[cm]", "AET", "soilMoisture",  "WD","1", "2",
"3", "4", "5", "6", "7", "8", "9", "10", "11", "12", "13", "14", "15");
    }
    else
    {
        inputVector.attr("dim") = Dimension(3, inputVector.length() / (3));
        outputMat = transpose(as<NumericMatrix>(inputVector));
        Rcpp::colnames(outputMat) = CharacterVector::create("day","rain[cm]", "WD");
    }
    Rcpp::Rcout << outputMat.nrow() << " " << outputMat.ncol() << endl;
    return(outputMat);
}

//input meq/100g return mol/Litre
double CSM::meqSoil2molar(double fMeq, double SoilVolume, double moisture)
{
    //fmeq is meq/100g soil . multiply by bukl denisty[g/cm3] divide by 100[gr soil ] mult by soilVolume [cm3] mult by
0.5[mmol/meq] mult by 0.001 [mol/mmol] divide by moisture
    return(fMeq * 1.44* SoilVolume/100  *0.5* 0.001 / moisture );
}

//input mol and multiply by 2000 [meq/mol] divide by compartment soil wight and multiply to represent 100 g soil
double CSM::mol2meqSoil(double mol, double SoilVolume)
{
    double inMeq = mol * 2000;
    return (( inMeq * 100/(SoilVolume*1.44))  );
}

double CSM::moistcm2Litre(double moist_cm) {
    return(moist_cm*0.001F);
}

CSM::~CSM()
{
    //Compartments.~vector();
    //Months.~vector();
    printf ("csm destructor\n");
}

double CSM::GetPrecision(double x)
{
    return(((int)(x*10000.0)) / 10000.0F);
```

```
}

//Rcpp::List CSM::GetResults()
//{
//  return results;
//}

void CSM::InitCompartments()
{
    if (Compartments.size() > 0) {
        Compartments.clear();
    }
    Compartment *newCompartment;
    for (int i = 0; i < nNumOfCompatments; i++)
    {
        newCompartment = new Compartment(i, nArea, wieltingPoint, nFieldCapacity, thick, CCa, CSO4);
        Compartments.push_back(*newCompartment);
    }
}

void CSM::initVector(Rcpp::DoubleVector & inputVector)
{
    for (R_xlen_t i = 0; i < inputVector.length(); i++)
    {
        inputVector[i] = 0;
    }
}



// [[Rcpp::plugins(cpp11)]]
RCPP_MODULE(CSM_MODULE) {
    using namespace Rcpp;
    class_<CSM>("CSMCLASS")
    .constructor()

    .method("Calculate", &CSM::Calculate,
        "Docstring for stats")


    .field("RainArr", &CSM::RainArr, "rain array")
    ;
}
```

תקציר

קרקעות מדבריות היפר-ארידיות מתאפיינות באופקי מלחים (גבס והליט) המצטברים כתוצאה ממיעוט משקעים. ברוב המדבריות, מקור המלחים בקרקע הינו אבק ויונים מומסים במי גשם. יחסי הגומלין בין מאפייני אקלים כמו תדירות ועוצמת אירועי גשם, הרכבם הכימי של מי הגשם, שטף האבק וקצבי ההתאדות, מכתיבים את עומק הצטברות המלחים וריכוזם. הבנת היחסים בין רכיבים אלו עשויה לשפר את יכולתנו להעריך את התנאים הסביבתיים ומאפייני האקלים הקדומים באזור הנחקר. נכון להיום, קיימת הערכה אמפירית בלבד של הקשר בין גשם שנתי ממוצע לאופקי המלחים בקרקע.

מטרות המחקר: 1) הדמית תהליך ארוך טווח של הצטברות גבס בקרקע, 2) כימות קצב הצטברות הגבס בקרקע כפונקציה של גורמי אקלים נבחרים, 3) הערכת התרחיש הסביר ביותר שהוביל ליצירת אופקי הגבס במניפות סחף בנגב החל מתקופת הפלייסטוקן המאוחר (22.9 – 62.5 Ka). בכדי להשיג מטרות אלו, פותח מודל תאים המדמה את תהליך הצטברות הגבס בקרקע ומעריך את רגישותו למגוון שינויים במאפיינים אקלימיים ארוכי טווח. המודל חוזה את ריכוז המלחים ועומק ההצטברות בפרופיל הקרקע על פני משכי זמן של אלפי שנים ויותר. משתני הקלט הם סדרות סטוכסטיות של גשם ואידוי יומי, שטף אבק וריכוז הסולפט (SO_4^{2-}) במי הגשם. המודל נבדק וכויל באמצעות נתוני גבס מדודים במניפות סחף מגיל הולוקן (10.3 – 13.5 Ka), בהנחה שהאקלים במהלך ההולוקן אינו שונה משמעותית מהאקלים כיום (ממוצע גשם שנתי < 50 מ״מ). על פי בדיקות הרגישות, ריכוז הגבס בקרקע רגיש ביותר לכמות הגשם השנתית ולריכוז הסולפט בגשם. פרופילים סינטטיים של גבס חושבו באמצעות תרחישי אקלים שונים והושוו לפרופילים מדודים של קרקעות מתקופת הפלייסטוקן המאוחר. התוצאות מראות כי: א) הארכת זמן ההצטברות בלבד תוך שמירה על מאפייני האקלים הנוכחיים, אינה מסבירה את כמות הגבס בקרקעות מהפלייסטוקן המאוחר. ב) התרחיש הסביר ביותר לפלייסטוקן המאוחר, חייב לכלול כמות גשם גבוהה יותר (פי 1.5 – 2 מהיום) וריכוז גבוה יותר של סולפט במי הגשם (פי 2 – 2.5 מהיום) על מנת לשחזר בהצלחה את הצטברות הגבס הנמדד כיום בקרקעות הבוגרות (22.9 – 62.5 Ka).

המכון הגיאולוגי
משרד האנרגיה

הערכת השפעתם של גורמי אקלים על הצטברות מלחים בקרקעות היפר-ארידיות באמצעות מודל סטוכסטי

ליאור סימן-טוב

עבודה זו הוגשה כחיבור לקבלת תואר "מוסמך" באוניברסיטה העברית, ירושלים.

העבודה נעשתה בהדרכתם של:

ד"ר און כרובי, המכון הגיאולוגי, ירושלים.

פרופ' אפרת מורין, האוניברסיטה העברית, ירושלים

דוח מס' GSI/04/2021 אדר תשפ"א פברואר 2021